Restriction of Rho signaling by the RhoGAP STARD13 integrates growth and morphogenesis in the pancreas

D i s s e r t a t i o n

zur Erlangung des akademischen Grades

d o c t o r r e r u m n a t u r a l i u m

(Dr. rer. nat.)

im Fach Biologie

eingereicht an der

Mathematisch-Naturwissenschaftlichen Fakultät I

der Humboldt-Universität zu Berlin

von

Dipl. Biol. M. Sc. Kristin M. Petzold

Präsident der Humboldt-Universität zu Berlin

Prof. Dr. Jan-Hendrik Olbertz

Dekan der Mathematisch-Naturwissenschaftlichen Fakultät I

Prof. Stefan Hecht, PhD

Gutachter/innen:

1. Prof. Dr. Harald Saumweber
2. Dr. Salim Seyfried
3. Prof. Dr. Kai Schmidt-Ott

Tag der mündlichen Prüfung: 08.11.2012

Die vorliegende Arbeit wurde unter der Anleitung von Frau Dr. Francesca M. Spagnoli am Max-Delbrück-Centrum für Molekulare Medizin (MDC) in Berlin-Buch angefertigt.

Summary

The development of functional organ architecture relies on coordinated morphogenesis and growth. In the developing pancreas, the branching epithelium is organized in discrete domains that delineate one specific domain of progenitor cells at the tip of the branches. Very little is known about branching morphogenesis in the pancreas and how it is coordinated with proliferation.

This thesis presents the first analysis of the RhoGAP-domain-containing protein STARD13 and its role as an essential regulator of pancreas tissue architecture in the mammalian embryo. It is shown that *Stard13* is expressed in the pancreatic endoderm and enriched at the distal tip of the branching epithelium. Conditional ablation of *Stard13* expression in the mouse pancreas disrupts epithelial morphogenesis and tip domain organization, resulting in hampered proliferation of pancreatic progenitors and subsequent organ hypoplasia. *Stard13* acts by regulating Rho signaling spatially and temporally during pancreas development. This thesis provides new insights into the mechanisms that shape pancreatic epithelium to create a mature organ and establishes a functional link between Rho-mediated control of epithelial remodeling and organ size determination, involving reciprocal interaction of actin-MAL-SRF and MAPK signaling.

The results of this thesis are submitted as manuscript for publication:

Petzold KM, Naumann H, Spagnoli FM: Rho signaling restriction by the RhoGAP *Stard13* integrates growth and morphogenesis in the pancreas. *DEVELOP_2012_082701v1*. Under review.

The pancreatic explant culture system are published in JoVE:

Petzold KM, Spagnoli FM: A system for *ex vivo* culturing of embryonic pancreas. Journal of Visualized Experiments. 2012 Aug 27;(66),e3979.

Zusammenfassung

Die Koordination von Morphogenese und Proliferation ist bei der Entwicklung einer funktionellen Organarchitektur von essentieller Bedeutung. Während der Embryonalentwicklung verzweigt sich das Epithel der Bauchspeicheldrüse, wobei jeder Zweig in zwei Domänen unterteilt wird, die man als “Epithelspitzen” und “Epithelstamm” bezeichnet. In den “Epithelspitzen” befinden sich schnell proliferierende Vorläuferzellen. Bisher ist nicht viel darüber bekannt, wie diese Domänen entstehen und wie dieser morphogenetische Prozess mit der Proliferation der Pankreaszellen koordiniert wird.

Diese Dissertation analysiert zum ersten Mal STARD13, ein Protein mit einer RhoGAP-Domäne, und dessen Rolle als essentiellen Regulator der Pankreasarchitektur im Mausembryo. Es wird gezeigt, dass *Stard13* anfangs im pankreatischen Endoderm exprimiert wird und später in den “Epithelspitzen” angereichert ist. Konditionelle Ablation von *Stard13* im Mauspankreas beeinflusst die normale Epithelmorphogenese und die Organisation der “Epithelspitzen”. Das beeinträchtigt die Proliferation der Pankreasvorläuferzellen und führt zu Organhypoplasie. Dabei reguliert STARD13 örtlich und zeitlich Rho-Signale, die für die Morphogenese essentiell sind. Desweiteren werden die Mechanismen, die für die Entwicklung des Pankreasepithels in ein funktionierendes Organ notwendig sind, neu beleuchtet. Es wird zum Beispiel eine funktionelle Verbindung zwischen Rho-vermittelter Kontrolle der Epithelumgestaltung und der Determinierung der Organgröße hergestellt. Dabei spielt die reziproke Interaktion von actin-MAL-SRF and MAPK Signalen eine wichtige Rolle.

Die Ergebnisse dieser Dissertation wurden als Manuskript eingereicht:

Petzold KM, Naumann H, Spagnoli FM: Rho signaling restriction by the RhoGAP *Stard13* integrates growth and morphogenesis in the pancreas. *DEVELOP_2012_082701v1*. Under review.

Die Methode der *ex vivo* Pankreaskultivierung sind in JoVE veröffentlicht:

Petzold KM, Spagnoli FM: A system for *ex vivo* culturing of embryonic pancreas. Journal of Visualized Experiments. 2012 Aug 27;(66),e3979.

Table of Contents

Table of Figures

1 Introduction

1.1 The Pancreas

1.1.1 The Adult Pancreas Tissue Architecture and Function

The adult pancreas controls vital functions of our body, including the digestion and blood sugar levels. The name pancreas derives form the Greek roots ‘pan’ meaning ‘all’ and ‘creas’ meaning ‘flesh’ [**1**]. The organ is located in proximity to the stomach and connected to the duodenum via the ampulla of Vater. In humans, the pancreas is divided in anatomical segments, namely the head, neck, body and tail [**1**]. In mice, the shape of the organ is less well defined, being partitioned into gastric and splenic lobes [**2**]. The adult pancreatic tissue consists of two main components with distinct organization and function: the exocrine and the endocrine tissues (Figure 1) [**3**] [**4**]. The exocrine pancreas is a lobulated, branched, acinar gland. The pyramidal secretory cells are grouped into acinar structures that are interconnected through a tree-like branched network of bicarbonate- and mucin-depositing cuboidal duct cells. Duct cells line the ducts that drain secreted digestive enzymes from the acini into the duodenum [**5**] [**1**] [**6**]. The digestive enzymes, including Amylase, Trypsin, Carboxypeptidase, promote nutrient absorption in the gut [**7**]. The endocrine portion, also called islets of Langerhans, is organized in globular clusters, which are scattered among the exocrine branches and intermingled with blood vessels, neurons and mesodermally-derived stromal components (Figure 1) [**5**]. Through intimate interaction between endocrine and vascular cells, the islets regulate nutrient metabolism and glucose homeostasis [**8**]. The islets consist of five different hormone-secreting cell types: Insulin-producing β-cells, which reside in the islet core; Glucagon-secreting α-cells; Somatostatin-releasing δ-cells; Pancreatic Polypeptide-secreting PP-cells and the very minor population of Ghrelin-releasing ε-cells. These different pancreatic islet hormones are necessary for a fine-tuned regulation of glucose levels [**9**].

Glucose serves as primary source of energy for all cells in living organisms. It is derived from digestion of dietary carbohydrates, breakdown of glycogen in the liver (glycogenolysis) and production of glucose from amino acid precursors in the liver and, to a lesser extent, in the kidney (gluconeogenesis) [**10**]. The most important hormone involved in glucose metabolism is Insulin. It is secreted by pancreatic β-cells, which represent the majority of cells (>80%) within an islet (Figure 1) [**1**] [**9**] [**7**]. By inhibiting the production of glucose (gluconeogenesis), stimulating glucose digestion (glycolysis) and stimulating storage of glucose as glycogen

(glycogenesis), Insulin is the only hormone in the body that decreases blood glucose levels [**9**] [**11**]. The antagonistic endocrine hormone Glucagon promotes glycogenolysis and gluconeogenesis as the level of glucose in the blood decreases. The hormones Somatostatin and Pancreatic Polypeptide are inhibitory effectors of both endocrine and exocrine secretion [**9**].

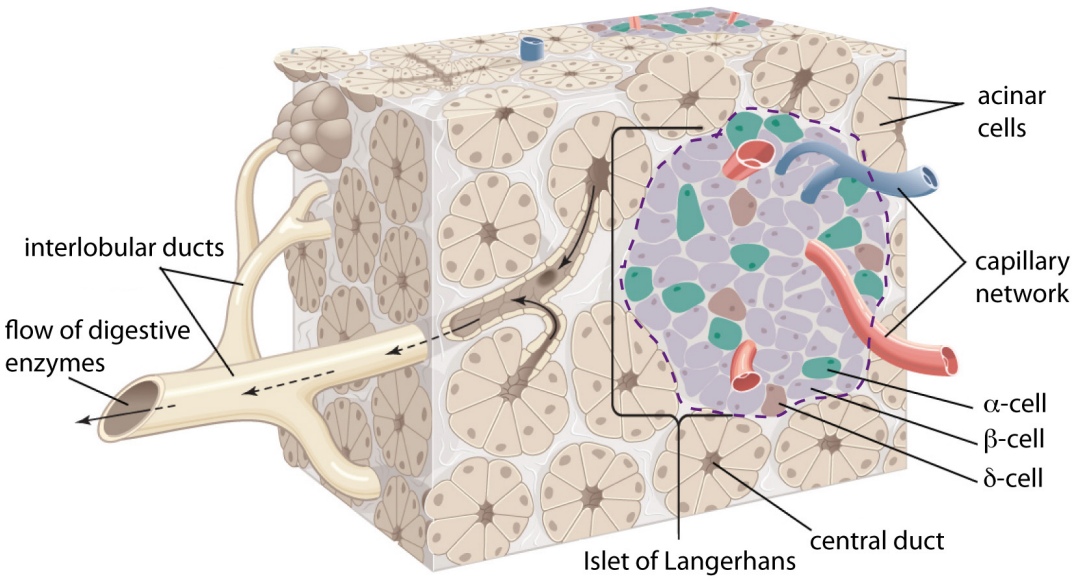

Figure 1: Cell types of the adult pancreas

The adult pancreas contains exocrine and endocrine tissue. Exocrine tissue is a branching network of ducts and acini. Acinar cells release digestive enzymes into the central ducts, which drain them into the duodenum. The endocrine tissue is organized in islets of Langerhans. The islets are connected to the capillary network of the blood system and consist of hormone-producing cell types, such as Insulin-producing β-cells and Glucagon-producing α-cells. Adapted from [**12**].

High blood glucose level (hyperglycemia) is the common feature of all forms of the disease diabetes mellitus. The endocrine β-cells and their secretory product Insulin are central in the pathophysiology of diabetes mellitus [**13**]. In type I diabetes, β-cells are destroyed by autoimmunological response and consequently Insulin is not produced leading to hyperglycemia. Type II diabetic patients develop Insulin resistance and the normal function of β-cells (e.g. Insulin secretion) is lost. This results in hampered glucose uptake in muscle, fat and liver cells and, consequently, hyperglycemia. One of the forms of type II diabetes is the Maturity onset diabetes of the young (MODY) [**14**]. MODY are monogenic forms of diabetes due to mutations in genes, which are required for the embryonic development of the endocrine pancreas. The mutations are inherited in an autosomal dominant mode and cause

a primary defect in the development and function of β-cells at the onset of adolescence [**13**] [**14**].

Diabetes mellitus is still an incurable metabolic disease. A potential cure for diabetes is to replace the lost or destroyed β-cells [**15**]. Due to shortage of human pancreatic islets or β-cells, a conceivable strategy is to generate *in vitro* a renewable source of β-cells, e.g. by differentiating embryonic stem cells (ESC) specifically into β-cells [**9**]. To attain this goal, we still need to understand each single step of pancreas development. Studying pancreas development in animal models will help us in this quest.

1.1.2 The Embryonic Pancreas Epithelium

In vertebrate embryos, the pancreas arises from two distinct embryonic thickenings of the dorsal and ventral regions of the foregut endoderm [**1**] [**9**]. In the mouse embryo, the dorsal pancreatic rudiment is specified at embryonic day (E) 9.5 and the ventral rudiment at E10 (Figure 2A). Pancreas organ formation is generally described in two overlapping waves of development: the **primary transition** between E9.5 and E12.5 and the **secondary transition** starting from E13.5 (Figure 2A-C) [**7**].

During the primary transition, the pancreas epithelium undergoes dramatic morphogenetic changes and growth. This stage is characterized by high proliferation of pancreatic progenitor cells, by which the pancreatic buds grow to form a stratified epithelium (Figure 2A-B) [**7**]. During this "protodifferentiated stage", progenitor cells start to express a set of transcription factors, such as the *Pancreas duodenal homeobox factor 1 (Pdx1), Pancreatic transcription factor 1 (Ptf1a), SRY (sex determining region Y)-box 9 (Sox9)* and *Hepatocyte nuclear factor 1 β (Hnf1β)* (Figure 3). Lineage tracing studies has shown that cells expressing these factors during early pancreatogenesis give rise to all three pancreatic lineages [**16**] [**17**] [**18**] [**19**]. At E11.5, the gut tube starts to undergo its first coiling movements, which bring dorsal and ventral buds into close proximity to form the definitive pancreas by fusion of the buds [**7**]. Concomitantly, from E11.5 onwards, some epithelial pancreatic cells begin to aquire apico-basal polarity and scattered microlumina form throughout the tissue (Figure 2B, Figure 4B) [**2**]. These microlumina subsequently fuse to form the so-called primitive ducts [**20**]. Between E11.5 and E12.5, the pancreatic stratified epithelium undergoes extensive epithelial remodeling (see Chapter 1.2.5) and rearranges into a monolayer of polarized cells surrounding coalescing lumina (Figure 2B-C) [**20**]. By E12.5, primary epithelial branches are formed and start to elongate into the surrounding mesenchyme. Within the epithelial branches, two typical domains can be recognized: a **tip domain** at the distal edge of the branches and a **trunk domain** residing in the center of the

tissue (Figure 2C-D) [**1**] [**21**]. Cells located in the trunk are committed to the endocrine fate, being positive for *Neurogenin 3 (Ngn3)* or Glucagon (Figure 2D) [**22**] [**23**] [**21**]. On the other hand, tip cells are devoid of differentiation markers and proliferate much faster than trunk cells [**24**] [**7**]. At this stage, these tip cells co-express *Pdx1, Ptf1a, c-myc* and *Carboxypeptidase A1 (Cpa1)* [**21**]. Lineage tracing experiments have shown that the tip cells are multipotent and give rise to pancreatic endocrine, exocrine and ducts cells (Figure 2E) [**21**]. Furthermore, it has been shown that these multipotent progenitor cells (MPCs) at the branching tip self-renew, possibly, leaving behind daughter cells; but this self-renewal is limited [**21**].

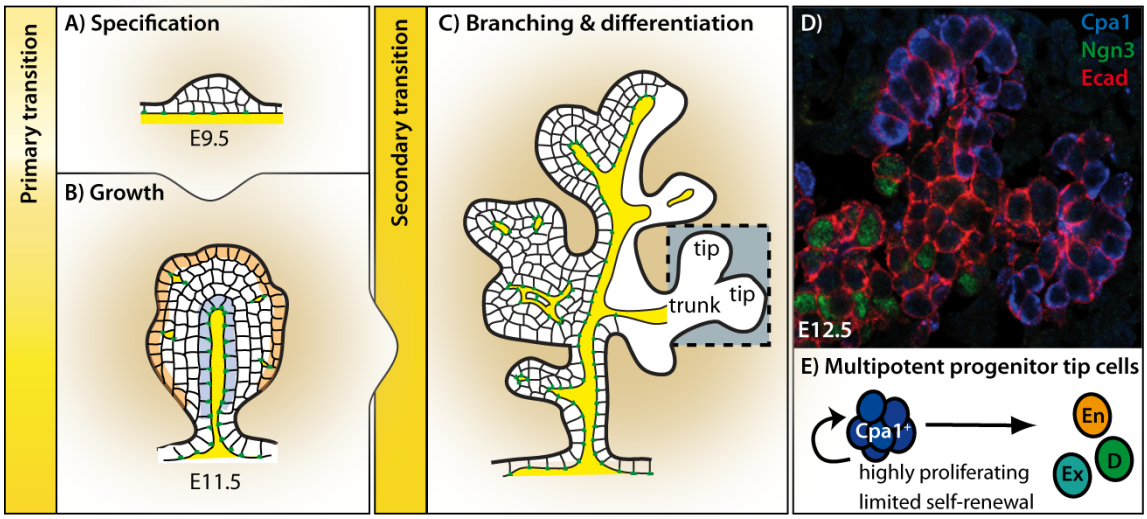

Figure 2: Development of the embryonic pancreas

During pancreatic development, a progression from a stratified into a monolayered epithelium occurs. (A) The primary transition starts with the specification of pancreatic cells within the foregut endoderm. (B) At E11.5, the first microlumina appear. Cells with apical cell junctions (green dots) are facing the center of the microlumina or surround the central lumen derivative of the gut primitive tube, also described as primary lumen (in yellow). Cap and inner cells are demarcated in orange and blue, respectively. (C) Between E12.5 and E14.5, branching morphogenesis progresses resulting in a tree-like tissue with branches consisting of tip and trunk domains (grey box). These branches are interconnected by coalescing microlumina forming a network of ducts. (D) The pancreatic epithelium can be visualized by immunofluorescence staining against the epithelial membrane marker Ecadherin (Ecad), depicting the tip and trunk domains shown in the schematic micrograph in C. At E12.5, $Cpa1^+$ multipotent progenitor cells are located at the branch tips, whereas $Ngn3^+$ endocrine progenitor cells are located in the trunk. (E) $Cpa1^+$ multipotent progenitor cells (dark blue) are highly proliferating, have a limited self-renewal and can differentiate into the exocrine (Exo), endocrine (En) and duct (D) pancreatic lineages. Abbr.: Cpa1, Carboxypeptidase 1; Ngn3, Neurogenin 3; A-C: Adapted from [**20**].

By conditional ablation of pancreatic progenitors, Stanger et al. showed that the number of progenitor cells allocated to the pancreatic primordium between E9.5 and E12.5 determines the final size of the organ [**25**]. These findings indicate that the initial number of tip MPCs in the developing pancreas and the maintenance of their progenitor potential is important for

the establishment of the final organ size; and compensatory growth in pancreas is limited or does not occur [**25**].

During the primary transition, differentiation of Glucagon-producing α-cells, a small number of Insulin$^+$ β-cells and Glucagon$^+$ Insulin$^+$ double positive cells occurs, whereas differentiation of exocrine or duct cells is not obvious yet [**7**]. Indeed, the main wave of cell differentiation and lineage allocation with amplification of exocrine and endocrine cell number starts at E13.5 during the secondary transition [**3**] [**7**].

During the secondary transition, the tip cells of the epithelial branches undergo a developmental switch, becoming committed to the exocrine lineage, and cluster into so-called acinar structures. At this stage, *Cpa1* and *Ptf1a* expression become restricted to the exocrine lineage and protein synthesis of exocrine enzymes, such as Amylase, starts [**21**] [**26**]. By contrast, epithelial trunk cells give rise to endocrine and duct cell lineages [**25**].

By E15.5, fate specification of all pancreatic cell types has occurred. From E16.5 onwards, further expansion of the pancreas epithelium is mainly driven by acinar proliferation [**6**] [**7**]. Exocrine cells are well-polarized displaying an apical pole that faces a secretory duct, while the basal region faces the mesenchymal tissue, which provides nutrients. Compared to exocrine cells, endocrine cells are found in a non-polarized configuration and they typically go through an epithelial exit process that is thought to involve epithelial to mesenchymal transition, referred to as **delamination** [**5**] [**27**] [**28**]. During late gestation and in the first weeks after postnatal life, endocrine cells cluster into islets, which are interspersed within the exocrine gland, and stay in proximity to ducts (Figure 1) [**6**] [**7**].

1.1.3 Extrinsic Regulators of Pancreas Development

Commitment of endodermal cells towards a pancreatic fate is a multistep process involving continuous crosstalk between the endoderm and surrounding tissues [**4**] [**7**]. Soluble or membrane-bound factors released from the surrounding tissues, such as the notochord, mesenchyme, dorsal aorta and vitelline veins, control growth, morphogenesis and differentiation of the developing pancreas [**3**] [**4**] [**6**] [**7**] [**9**] [**29**]. For example, it has been shown that when E11.5 pancreas explants are cultured *ex vivo* without the mesenchyme, they fail to grow [**9**].

Important signaling pathways, including members of the bone morphogenetic protein/ transforming growth factor β (BMP/TGFβ), fibroblast growth factor (FGF), epidermal growth factor (EGF), vascular endothelial growth factor A (VEGF-A), Wingless/Integration (Wnt), Retinoic acid (RA), Hedgehog and Notch families play dynamic and multiple stage-specific

roles during endoderm patterning, cell fate specification and later pancreas development [**9**] [**3**] [**4**] [**7**] [**29**].

During broad anterior-posterior (a-p) patterning of the endoderm, RA released from the mesoderm is required for pancreas organ specification and later to promote endocrine progenitor fate and further differentiation into β-cells (Figure 3) [**7**] [**30**]. Before budding, the prospective dorsal pancreatic endoderm is associated with the notochord. FGF2 and Activinβ2 released from the notochord suppress Sonic hedgehog (Shh) in the dorsal endoderm to establish the dorsal pre-pancreatic domain at E8.0 [**31**]. At E8.5, the dorsal aortae fuse and thus place the notochord distant from the dorsal endoderm, establishing direct contact with the pancreas territory. VEGF signals from the dorsal aorta and ventral vitelline veins promote *Pdx1* and *Ptf1a* expression in the pre-pancreatic endoderm (Figure 3).

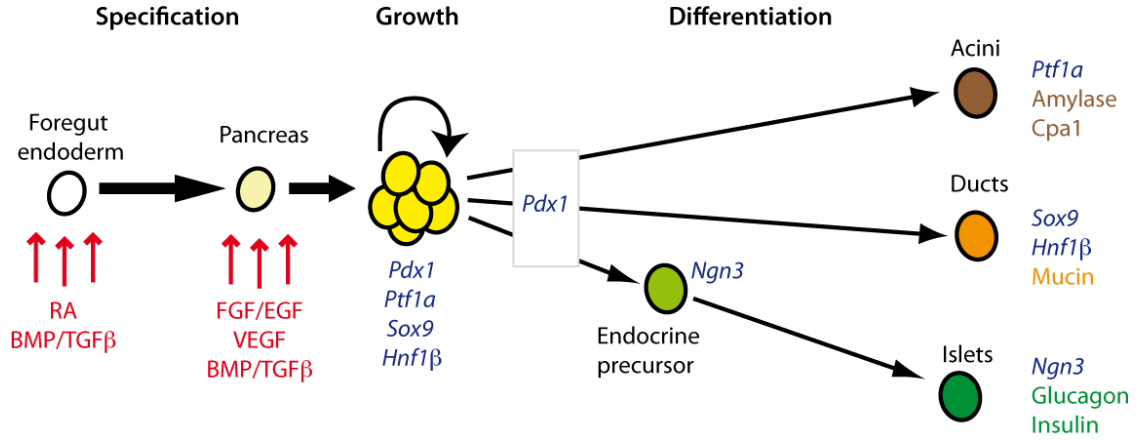

Figure 3: Pancreatic extrinsic and intrinsic regulators

An armada of extrinsic soluble signaling factors (depicted in red) controls pancreas specification from the foregut endoderm and later influences growth and differentiation of the pancreas. In parallel, a cascade of pancreas-specific transcription factors is activated (indicated in blue). Acinar, duct and islet cell markers identify differentiated cells. Adapted from [**32**].

Instead, ventral pancreatic cells arise from a presumptive bipotential progenitor population in the ventral foregut endoderm next to the hepatic domain [**33**]. The “default fate” of the ventral foregut endoderm appears to be pancreas. Surrounding BMP and FGF signals in the ventral foregut endoderm would direct the fate of the endoderm into liver [**34**] [**35**]. Thus, BMP and FGF signal inhibition promotes ventral pancreas and suppresses liver formation.

Around stage E10, mesenchyme condenses around the pancreatic anlagen and FGF10 stimulates bud outgrowth [**7**]. Evidences exist that EGF and FGF signaling in the pancreas are important for organ growth and morphogenesis, acting potentially in concert on early pancreatic progenitors to stimulate proliferation [**9**].

Furthermore, the Notch signaling pathway plays a crucial role during pancreas development. Multiple Notch ligands and receptors and downstream mediators, including *Notch1-4, Recombination signal binding protein for immunoglobulin kappa J (RBP-J)* and *Hairy-and-Enhancer-of-split 1 (Hes1),* are expressed in the early pancreatic epithelium and in the mesenchyme during budding [**7**]. Mice devoid of various Notch pathway components show a hypoplastic pancreas and accelerated differentiation towards the endocrine lineage that causes progenitor pool depletion [**36**] [**37**] [**38**].

These examples underscore the importance of surrounding tissue and the mesenchyme during pancreas development. Future studies will have to investigate how these extrinsic signals are connected to the activation of the intrinsic factors in the pancreas.

1.1.4 Intrinsic Regulators of Pancreas Development

Specification of pancreatic tissue in the endoderm is characterized by the activation of pancreatic transcription factors (Figure 3) [**4**]. The earliest known pancreatic transcription factor expressed just prior to organogenesis is *Pdx1* [also known as *Insulin-promoter factor 1 (IPF1)* in human], being expressed at E9.0-9.5 in pancreatic buds [**7**]. *Pdx1/Ipf1* was shown to be required for the earliest steps of pancreas formation both in mice and humans, indicating a clear evolutionarily conserved function [**39**] [**40**] [**41**]. Genetic lineage tracing experiments in the mouse showed that *Pdx1*-expressing progenitors produce acini, ducts and endocrine cells of the mature pancreas (Figure 3) [**16**]. In humans, a homozygous deletion of the *IPF1* gene causes pancreas agenesis [**40**]. Similarly, in homozygous $Pdx1^{-/-}$ mutant mice pancreas growth and cell differentiation are arrested and embryos die shortly after birth, however the pancreatic bud is formed [**39**] [**41**].

Another important pancreatic progenitor cell transcription factor is *Ptf1a*. It is expressed as early as E9.5 in most of the nascent pancreatic bud cells, which potentially can produce all pancreatic lineages (Figure 3) [**17**]. Studies in different vertebrate species, such as frog, zebrafish and mouse, suggest that both *Pdx1* and *Ptf1a* are required to act together to induce pancreatic fate [**42**] [**43**]. However, in $Pdx1^{-/-}/Ptf1a^{-/-}$ double homozygous null mutant mice, a dorsal pancreatic bud forms, suggesting an additional role for other factors upstream of *Pdx1* and *Ptf1a,* which direct initial allocation of endodermal cells to the pancreatic fate [**7**] [**43**].

Both the *Sox* gene family and the Notch-pathway have been implicated in preserving progenitor cells in a pluripotent state in many tissues. *Sox9* was identified as being important for proliferation, survival and maintenance of pancreatic progenitors [**44**] [**45**]. *Sox9* expression in the pancreas starts at E10.5 and lineage tracing studies showed that pancreas

cells expressing *Sox9* produce all pancreatic lineages (Figure 3) [**45**]. After E12.5 *Sox9* expression is confined to centrally located epithelial cord cells, and later, *Sox9* additionally marks centroacinar cells [**45**]. Ablation of *Sox9* in the developing pancreas causes tremendous organ hypoplasia and newborn pups are smaller in body size and die of dehydration and elevated blood glucose levels [**45**]. It has been shown that *Sox9* regulates the downstream mediator of Notch signaling *Hes1* in the pancreas [**45**]. In the developing pancreas, Notch signaling controls the choice between progenitor fate and endocrine differentiation. Indeed, blocking Notch-receptor activation in early pancreatic progenitors promotes endocrine cell differentiation [**36**] [**46**].

Another factor playing a role in the expansion of the pancreas progenitor pool is *Hnf1β* [also known as *Transcription factor 2 (TCF2)* in human] [**19**]. Heterozygous mutations of *TCF2* in humans are associated with Type II diabetes disease MODY5 (see Chapter 1.1.1) and in the mouse embryo ablation of *Hnf1β* leads to pancreatic agenesis [**47**]. *Hnf1β* is expressed in the pancreas starting from E9.5 and lineage tracing showed that *Hnf1β*$^+$ cells give rise to duct, acinar and endocrine cells (Figure 3) [**19**] [**47**]. From E16.5 onwards, *Hnf1β* transcription factor expression becomes confined within the pancreatic tissue, being localized to central epithelial cords that contain endocrine/duct bipotent progenitor cells [**19**] [**45**].

The transcription factor *Ngn3* is the initiator of the endocrine developmental program and starts to be expressed as early as E9.5 in the pancreas (Figure 3). *Ngn3* knockout mice fail to generate any endocrine cell and die postnatally of diabetes [**22**] [**23**]. At E12.5, *Ngn3* is expressed in cells localized in the trunk of the epithelial branches, whereas tip cells keep a multipotent progenitor identity, co-expressing *Pdx1*, *Ptf1a*, *c-myc* and *Cpa1* (Figure 2D) [**22**] [**23**] [**21**]. *Ngn3* induces the expression of pro-endocrine transcription factors, including *NK6 homeobox 1 (Nkx6.1)*, *Islet1*, *Paired box gene 4 (Pax4)* and *Paired box gene 6 (Pax6)* [**7**]. Newly differentiated endocrine cells are marked by their secretion products such as the hormone Glucagon in α-cells and Insulin in β-cells (Figure 3) [**3**] [**7**].

Even though an entire cascade of pancreatic transcription factors has been characterized, early steps of pancreas development are still poorly understood and, in particular, which factors act upstream of *Pdx1* and *Ptf1a* is still an open question. Future analysis will hopefully identify early pancreatic regulators, as these are crucial components for any protocol suited to specifically differentiate ESCs into Insulin-producing β-cells in order to cure patients suffering from diabetes.

1.2 Morphogenesis of the Pancreas

1.2.1 Morphogenesis

Morphogenesis is a biological process that allows an organism and/or its organs to develop their three-dimensional (3D) shape over time. Many epithelial organs, including the pancreas, lung, mammary gland, salivary gland and kidney, form in an embryo from a simple bud or placode or tube and, subsequently, branch and ramify into complex tree-like structures [**48**] [**49**] [**50**]. Each of these organs displays a physiological architecture of branched tubular systems that is tailored to the organ's physiological function. Branching morphogenesis and tubulogenesis are crucial for the generation of functionally efficient, complex, but well-ordered tissue architecture proper to the aforementioned epithelial organs. Indeed, these processes increase the total cellular area for metabolic processes, whereas the distance over which substances have to travel is reduced [**48**]. Branching morphogenesis involves a series of interdependent events, including reiterative events of branch point formation, duct formation and elaboration that eventually give rise to networks of tubes opening into a single outlet [**49**] [**48**]. Although different regulatory mechanisms are employed temporally and spatially by each organ, common mechanisms are also shared by multiple branched organs [**49**]. The next chapters will give an insight into different aspects of branching morphogenesis, tubulogenesis and underlying morphogenetic mechanisms.

1.2.2 Branching Morphogenesis of Epithelial Organs

The first sign of branching morphogenesis is the invagination of a placode or evagination of a primary bud. Invagination or evagination processes are then followed by branch outgrowth and reiteration of the branching.

Two ways of branch point formation have been described and they can happen independently or concomitantly: 1) **side branching**, or 2) **bifurcation** (Figure 4A).

Side branching is mainly driven by localized cell proliferation and is characterized by local outgrowths of branches or budding of duct epithelium. During **bifurcation** a tip expands and ramifies by formation of clefts in the basement membrane that subdivide the epithelia into buds or lobules. The mechanism of cleft formation is poorly understood. One currently accepted model for cleft formation involves the local loss of epithelial cell-cell adhesions and their subsequent replacement by cell-extracellular matrix (ECM) adhesions [**51**]. The extracellular matrix protein fibronectin (FN), for example, is required for cleft formation in the submandibular salivary gland (SMG) and is focally expressed by the epithelial cells adjacent to forming clefts [**51**]. Rho kinase (ROCK) 1-mediated actinomyosin contraction is the

upstream signal that drives FN assembly during SMG cleft progression [**51**]. Furthermore, in lung and salivary glands a characteristic of cleft formation is the differential accumulation of collagen, being denser at the stalks and clefts of the branches and thinner around the expanding lobules [**52**].

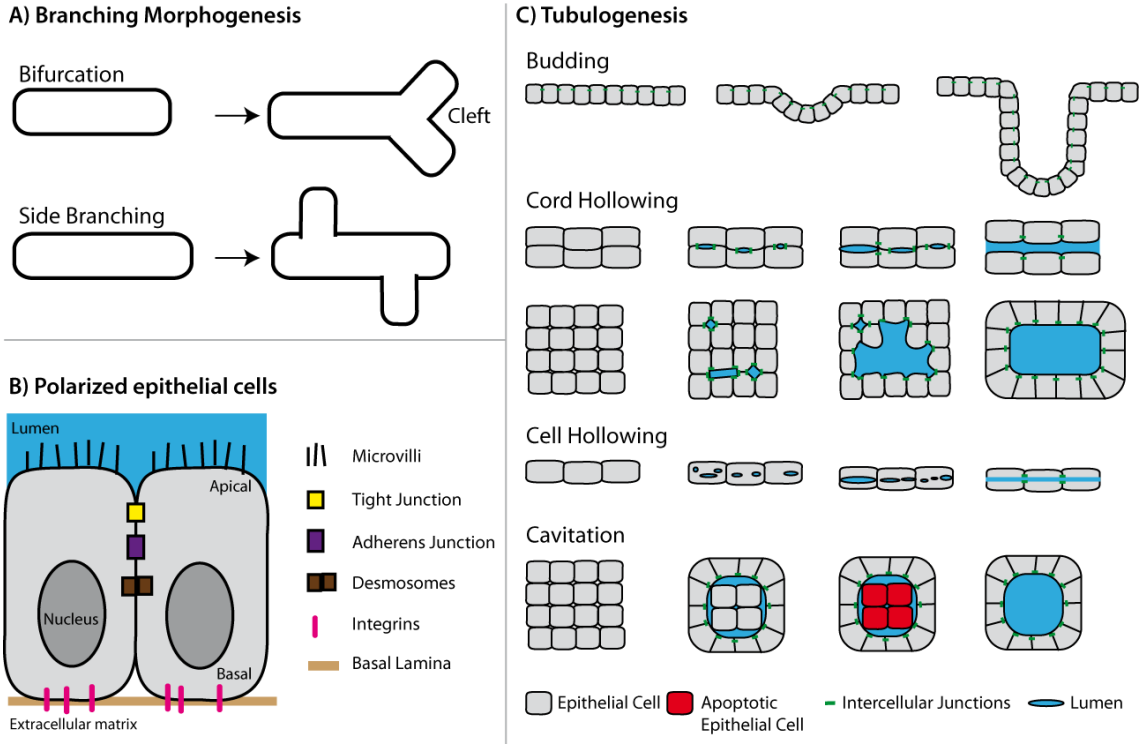

Figure 4: Branching morphogenesis and tubulogenesis of polarized epithelia

A) Branches establish through bifurcation, in which the end of the tube splits into two new tubes, or side branching, in which new tubes form on the side of the main tube. B) Schematic of polarized epithelial cells. Apical cell surfaces contain microvilli and are in contact with lumina. Cells are interconnected through intercellular junctions (tight junctions, adherens junctions, desmosomes). The basal membranes interact with the basal lamina and the ECM. C) Tube formation can start by budding of an already polarized epithelium. Tubes can be also formed from unpolarized epithelium through cord hollowing, cell hollowing or cavitation (see Chapter 1.2.3). Adapted from [**53**] [**54**].

Both modes, side branching and bifurcation, are described in the lung, whereas kidney only forms through side branching, and the submandibular salivary gland only by bifurcation [**49**] [**51**] [**55**] [**56**] [**57**].

After branch point formation, a finger of epithelium (also called the tip) expands into the surrounding tissue developing an epithelial trunk or stalk. Thereby, cells at the branching tip are exposed much more to surrounding signals than trunk cells (Figure 2D). Moreover, undifferentiated cells and/or MPCs are often found at the tips in different epithelia [**48**].

Finally, the size of the branches increase by extensive cell proliferation of evaginated cells especially in the branching tips and by additional shifting of cells, for example through convergent extension or oriented cell divisions, and/or by progression of clefts [**5**] [**58**] [**48**].

1.2.3 Tubulogenesis of Epithelial Organs

The formation of tubes occurs in concert with branching morphogenesis, generating the basic “plumbing” for the secretion and transport of cell products. Tubulogenesis is fundamental for organ function [**53**]. For example, the mammary gland tubes allow secretion and transport of milk, whereas the pancreas tubes are needed for enzyme transport and secretion into the duodenum. Tubes start to form when epithelial sheets rearrange into a single layer of cells, lining lumina, which must then be sealed and unobstructed [**53**]. Tubulogenesis or tube formation in organs such as the mammary gland, salivary gland and pancreas initiate within anlagen of unpolarized cells closely packed together. Two important aspects for initiation of tubulogenesis in non-polarized tissue are 1) the *de novo* establishment of polarity and 2) the elaboration of intercellular connections through junctional complexes [**48**]. Cell polarity is acquired when intracellular organelles, cytoskeleton components and cell surfaces of a cell are asymmetrically organized, generating an apical and a basal side (Figure 4B) [**53**]. Cells lining tubes are polarized displaying an apical cell membrane that faces a central lumen and a basal membrane in contact with the ECM. Once the cells are polarized and organize around microlumina, cell junctions are formed. Junctional complexes at the apical membrane between neighboring cells strongly limit random diffusion of molecules between the lumen and the ECM [**5**]. Cells excluded from the newly polarized tissue during tubulogenesis become pyknotic and die [**48**].

Different basic strategies underlay the formation of lumina during tubulogenesis, including 1) **budding,** 2) **cavitation,** 3) **cord hollowing** and 4) **cell hollowing** (Figure 4C) [**48**] [**53**] [**54**] [**59**].

Budding is described as evagination of polarized epithelial sheets into the ECM (Figure 4C), like in the vertebrate kidney, lung, mammary gland, and/or invagination into the lumen of a tube, like in the *Drosophila melanogaster* salivary gland and trachea. **Cavitation** is the formation of a lumen between moderately polarized cells by apoptosis of the inner most cells that are not in contact with the ECM (Figure 4C), as described in mammary end buds [**53**]. **Cord hollowing** involves *de novo* lumen formation between cells in a cylindrical cord without any cell loss (Figure 4C). This occurs for example during the development of the zebrafish gut [**60**]. **Cell hollowing** is the formation of lumen within individual cells (Figure 4C). This is due to the formation of vesicular structures, which move toward the cell apical surface and

coalesce to produce intracellular lumina, and, eventually, fuse with the plasma membrane to generate lumenized structures [**53**].

1.2.4 Morphogenetic Mechanisms Involved in Branching Tubules

Branching morphogenesis and tubulogenesis are complex processes and occur in slightly different ways in each branching organ. Recent observations have suggested that each organ utilizes a specific spatial and temporal configuration of common basic cellular and molecular programs to achieve organ-specific branching patterns [**49**] [**55**] [**56**]. Therefore, understanding the mechanism of morphogenesis of one type of branched organ can provide significant insight into that of another one. Effective morphogenetic mechanisms for the generation of a branched organ *in vivo* involve cell shape changes, cell growth, cell rearrangement, migration, adhesion and interaction between the epithelium and the mesenchyme [**24**] [**48**] [**49**] [**52**] [**55**] [**56**].

Whereas cell size changes, like swelling or shrinking, are not known to play a direct role in branching morphogenesis, it is conceivable that coordinated cell-shape changes in an epithelium could lead to branch formation. For example, cell shape changes can confer the overall shape of an epithelium by changing the local curvature [**48**] [**54**]. Also, when cuboidal cells in an epithelium change their aspect ratio (ratio of the width to the height) in a coordinated fashion, the final result will be a squamous or columnar epithelium [**61**]. The cytoskeletal machinery, including intracellular microfilaments and microtubules, plays an important role in cell shape changes. For example, the actinomyosin cytoskeleton promotes apical constriction of cells, by which a tissue can change its morphology as observed in bottle cells during blastopore invagination in *Xenopus laevis* [**62**].

One building block of branching morphogenesis is growth, which is regulated by reciprocal epithelial and mesenchymal tissue interactions. Surrounding mesenchymal cues promote cell proliferation, for example the FGF signaling in organs like the lung, kidney, mammary gland and pancreas, while the epithelium is also capable to release factors that influence these proliferation signals to enforce localized proliferation, for example at the tips of the branches [**9**] [**24**] [**63**]. Localized cell proliferation can trigger bud formation and branching in some epithelia. For instance, in the embryonic mouse lung a continuous basal lamina surrounds most of the epithelium except at the tips [**48**]. This might help tip cells to sense gradients of mesenchymal derived ligands, for example, proliferation signals. Apoptosis, the counterpart of growth, does not play a key role in branch point formation, but is important in lumen formation through cavitation (see Chapter 1.2.3) [**53**] [**61**].

In the process of active cell migration, cells interact with the ECM through the establishment of focal adhesions (FAs) [**49**] [**64**] [**51**]. FAs are points of cell-ECM connection and represent highly dynamic macromolecular assemblies of an armada of proteins, including focal adhesion kinase (FAK), heterodimeric Integrins, Talin, Vinculin and Paxillin [**64**]. The central core proteins of FAs are heterodimeric Integrins, which consist of α and β subunits. Integrins can bind to extracellular proteins, such as Fibronectin, Laminin or Collagen, and are linked to the cytoskeleton by intracellular adaptor proteins, such as Talin, Vinculin and Paxillin [**65**]. Talin contains multiple binding sites for Vinculin and can also recruit Paxillin [**64**]. FA formation is dependent on non-muscle Myosin type II activity. Rho-mediated contractility has also been directly implicated in the formation and maturation of such cell-matrix contacts [**66**] [**51**] [**67**] [**65**] [**64**].

Cell-ECM interactions may consist primarily of cells migrating actively into the ECM or, also, rearrangement of the ECM through digestion by enzymes [**52**]. For example, during *Drosophila melanogaster* trachea branching the matrix metalloproteinase-2 (MMP2) restricts FGF signaling in the ECM by its proteolytic activity in the trunk of the branches [**63**].

1.2.5 Pancreas Branching Morphogenesis

While considerable progress has been made in understanding branching morphogenesis in organs like the lung or kidney, comparatively very little is known about how this process occurs and is regulated in the developing mammalian pancreas. Only recent reports started to shed some light on these complex processes in the pancreas [**68**] [**20**] [**69**] [**2**].

The pancreas arises as two buds from a polarized single layered foregut epithelium. As the buds undergo growth and cell proliferation, the epithelium displays transient stratification, acquiring multiple layers of cells, which partially lose polarity. At E10.5, pancreatic cells maintain epithelial identity, as they express E-cadherin, but only the inner cells, which surround the central primary lumen (PL), and the outer layer (so called cap cells), display apical or basal polarity, respectively (Figure 2B). For example, inner cells express Mucin apically and cap cells Laminin and Collagen-IV basally [**2**]. The cells inside the stratified bud do not show any sign of apico-basal polarity and lack proper junctional complexes [**20**]. Starting from E11.5, branching events initiate through remodeling of the epithelium in a stereotypical manner [**20**] [**69**] [**2**]. Gradually, epithelial cells re-acquire complete apical and basal polarity, express tight-junction proteins, such as Zonula occludens (ZO)-1, and resolve into a monolayered branched epithelium. The first individual branches are established by E12.5 and are referred to as **primary buds or primary branches**. Interestingly, in the pancreas there is no progressive tubular and perpendicular extension of the epithelial

primary buds through bifurcation, as described in the developing lung and salivary glands [**3**]. The pancreatic primary buds rather expand by longitudinal growth, sending new tips into the surrounding mesenchyme through side branching [**2**] [**68**].

At E12.5, the epithelial branches are well formed and compartmentalized into two distinct domains, referred to as **tip** and **trunk domains** (Figure 2D, see Chapter 1.1.2). Cell division occurs at higher rate at the tips than in trunks of the branches [**24**]. In addition, the highly proliferating tip MPCs have been shown to contribute to all pancreatic lineages (Figure 2E) [**21**]. Previous work in pancreatic *ex vivo* organ cultures addressed the question whether cell division is the major force for budding and branch outgrowth in the pancreas [**24**]. Even though inhibition of DNA synthesis results in extreme inhibition of branching, this study could not determine whether "localized" growth is the only mechanism driving morphogenesis. The mesenchyme is necessary for this typical morphogenetic process, apparently not only controlling cell proliferation, but also other unknown aspects [**24**]. Indeed, the addition of mitogenic factors, such as FGF, which are normally released by the surrounding mesenchyme, is not sufficient to induce supernumerary buds [**24**]. MPCs at the pancreatic tips are in close proximity to this special mesenchyme supporting environment that possibly promotes MPC proliferation rate and, as a result, outgrowth of the branches.

Branching morphogenesis in the pancreas occurs concomitantly with tubulogenesis [**20**]. At E11.5, microlumina form throughout the epithelium and are surrounded by polarized cells (Figure 2B). Dramatic cell shape changes occur in the developing pancreas, for example the arrangement of clusters of bottle-shaped epithelial cells in **"rosette-like"** structures, which surround the microlumina, has been described and these are reminiscent of rosette structures in the *Drosophila melanogaster* germband epithelium [**2**] [**70**] [**71**]. Multiple microlumina start to coalesce (approx. E12.5), and, at the same time, the tissue undergoes complex cell rearrangements and matures into an extensive network of independently organized luminal structures that are surrounded by monolayers of polarized epithelial cells (approx. E15.5) [**20**]. At this stage, cells are well polarized, displaying a basal pole contacting the basal lamina and an apical pole facing a luminal network [**20**] [**2**]. E-cadherin is restricted to the basolateral membrane and absent from the apical pole [**20**]. β–catenin, which is a well-known cell-cell adhesion molecule binding to the cytoplasmic domain of type 1 cadherins and linking them through α-catenin to the actin cytoskeleton, mimics E-cadherin localization [**72**] [**2**]. Atypical Protein Kinase C (aPKC), Mucin and F-actin are all expressed at the apical membrane of polarized pancreatic cells [**2**][**69**].

The ECM is the supporting environment for the pancreas organ growth, because it sends growth factor signals to the epithelium, but it may also serve as matrix for cell attachment and cell movements. Cell-ECM adhesion mediated by Integrins has been suggested to play a role in pancreas branching morphogenesis in mouse embryos [**73**]. Integrins mediate cell-ECM adhesion within the FA plaques and in pancreas cells the $\beta1$-subunit of Integrins is the primary receptor for basement membrane. The $\beta1$-subunit interacts with various α-subunits to mediate cell-ECM adhesion in different compartments of the pancreas adult tissue, e.g. $\alpha6\beta4$ heterodimers in duct cells, $\alpha6\beta1$ both in acinar and duct cells and $\alpha3\beta1$ in acinar, duct and islet cells [**74**]. Conditional gene ablation of $\beta1$-Integrin in the pancreas leads to age-dependent degeneration of the organ, suggesting a role in preserving the pancreas organ architecture [**75**]. Ablation of both $\alpha3$- and $\alpha6$-Integrins causes a decrease of pancreas branching [**73**]. All this shows that cell-ECM adhesion is necessary for pancreas organ development and also its normal branching morphogenesis.

Importantly, branching morphogenesis in the pancreas is coupled with growth and differentiation [**4**] [**6**] [**7**] [**46**]. During the same window of time between E11.5 and E14, morphogenetic branching events occur and the final size of the organ is defined [**25**]. However, the molecular mechanisms underlying the coordinated action of these different events (branching, proliferation, differentiation) are largely unknown in the pancreas.

1.2.6 Rho GTPases During Embryonic Pancreas Development

Rho GTPases are well-known regulators of essential cellular processes, including cytoskeletal dynamics, cell polarity, adhesion, migration and cell proliferation, and, thereby, control morphogenesis in a variety of tissues [**69**] [**76**] [**77**]. Rho GTPases comprise a family of numerous proteins that are well-conserved across species from plants and yeast to mammals. In mammals, 20 distinct Rho GTPase molecules have been identified and characterized. The best-studied members of this family are the Ras homolog gene family member A (**RhoA**), Cell division control protein 42 (**Cdc42**) and Ras-related C3 botulinum toxin substrate 1 (**Rac1**) [**76**] [**77**].

Rho is a well-known regulator of stress-fiber formation and contraction and formation of focal adhesions, on which stress fibers are coupled via Integrin proteins to the extracellular matrix [**76**] [**77**]. Cdc42 and Rac1 are better known for their role in determining cell polarity and regulating cell migration [**77**].

Because of their broad range of activities in cell biology and cytoskeleton dynamics, Rho GTPases control morphogenesis and branching in a variety of epithelia, including the

pancreas. For example, the small GTPases Cdc42 and Rac1 have been shown to control different aspects of pancreatic morphogenesis [**78**] [**69**]. Cdc42 has been indicated as a molecular player connecting cell polarity and fate specification in the developing pancreas. In particular, Cdc42 plays a role in the initiation of microlumen formation and the failure of tubulogenesis in the pancreas of Cdc42-null mice affects pancreatic cell differentiation [**69**]. By contrast, Rac1 has been shown to play a role at later stages in pancreas development, controling islet cell migration through modulation of E-cadherin mediated cell-cell adhesion [**78**].

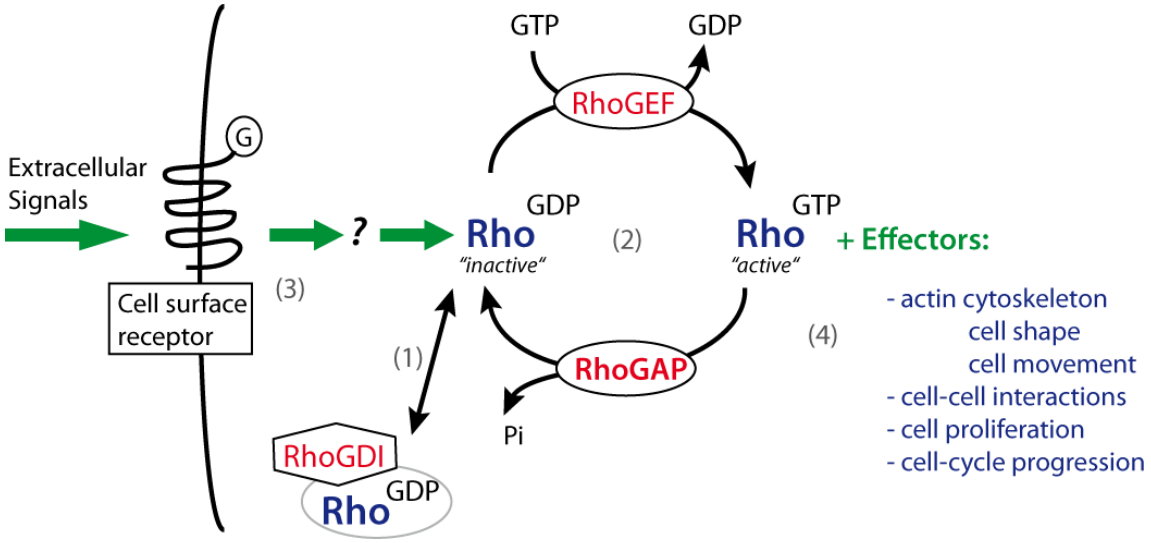

Figure 5: Schematic of Rho GTPase cycling and function

Regulation of Rho proteins occurs at the levels of GDP/GTP cycling and of translocation between cytoplasm and plasma membrane. (1) Rho proteins are inactive when localized in the cytoplasm and bound to guanine-nucleotide dissociation inhibitors (RhoGDI). By phosphorylation of Rho-GDI, RhoGTPases are released, bind to the plasma membrane and enter GDP-to-GTP-cycling. (2) RhoGTPases cycle between an inactive GDP-bound stage and an active GTP-bound stage. This is controlled by guanine-nucleotide exchange factors (RhoGEF) and GTPase-activating proteins (RhoGAP). (3) Intracellular and/or extracellular signals transmitted through G-protein coupled receptors (GPCRs) or Integrins modulate the activation/inactivation of RhoGTPases. (4) Through hydrolysis of GTP by Rho-GAPs, downstream effectors are activated and important cell processes are regulated.

GTPases function as molecular switches, cycling between an active GTP-bound and an inactive GDP-bound state (Figure 5) [**79**]. This cycling is tightly regulated by three classes of proteins: the GDP-dissociation inhibitors (**GDI**), the guanine-nucleotide exchange factors (**GEF**) and the GTPases-activating proteins (**GAP**) (Figure 5) [**79**]. Specifically, the GDIs keep the Rho proteins in an inactive state by stabilizing their GDP-bound state in the cytoplasm. The GEFs activate small GTPases by catalyzing the exchange of GDP for GTP, whereas GAPs inactivate small GTPases by accelerating their intrinsic GTPase activity and converting them into the inactive GDP-bound form (Figure 5) [**79**] [**80**]. A preferential tissue expression of these regulatory proteins is critical for precisely timed and localized activity of

Rho-GTPases. The numerous roles and ubiquitous nature of small GTPases raise questions concerning their spatio-temporal regulation. Specifically, how are they regulated within the pancreatic tissue?

1.2.7 STARD13, a Pancreas-Specific Rho GTPase-Regulator

So far, over 70 Rho-GTPases-activating proteins (Rho-GAPs) have been identified in eukaryotes, but very few show a tissue-preferential expression and tissue-specific activity [**79**] [**81**] [**82**].

Through an expression cloning screening in *Xenopus laevis*, the pancreatic RhoGAP *Shirin* was identified [**83**]. The *Shirin* full-length gene encodes a 1001-amino acid (aa) protein with two conserved domains: a Rho-GTPase-activating protein (Rho-GAP) and a StAR-related lipid transfer (START) domain. In *Xenopus* embryos, *Shirin* is expressed in the endoderm and future pancreatic rudiments from gastrulation onwards [**83**]. Remarkably, *Shirin* 3'UTR is sufficient to induce pancreatic fate and *Insulin* expression in the frog embryo. The *Shirin* 3'UTR mRNA sequence has an important function in binding *trans*-activating factors, including Vg1-RNA binding protein (Vg1RBP), which was shown to be required for pancreatic fate within the frog endoderm [**83**].

A significant conservation of early pancreatic development events exists across different vertebrate species, including *Xenopus*, zebrafish, amniotes and mammals. The *Xenopus Shirin* shows high similarity to the human *Deleted in Liver Cancer 2 (DLC2)* gene, which is a paralog of *DLC1*, a known tumor suppressor gene commonly deleted in hepatocellular carcinoma [**84**] [**85**] [**86**] [**87**]. The Rho-GAP domain of DLC2 has GAP specific activity for RhoA *in vitro* and with less affinity for Cdc42 [**88**] [**85**] [**89**]. DLC2 is a cytoplasmic protein and like DLC1 has been shown to localize to focal adhesions through its N-terminal domain in HeLa cells [**90**] [**91**].

Most RhoGAPs have a number of functional domains and are thought to mediate cross talk between Rho GTPases and other signaling pathways [**79**]. In addition to its RhoGAP domain, DLC2 also contains two other functional domains, a START domain and a sterile alpha motif (SAM) [**81**] [**85**]. The RhoGAP and START domain locate closer to the C-terminus of DLC2, wheras the SAM domain is located at the N-terminus. There are nearly 1000 proteins in eukaryotes and some bacteria containing a SAM domain, but no common functional theme exists for this domain [**92**] [**93**]. In general, the SAM motif has been shown to promote homodimerization of proteins and it can also bind RNA or lipid domains [**92**] [**94**].

The mouse homolog of *Shirin* is called *Stard13 (Steroidogenic acute regulatory protein-related lipid transfer (START) domain containing protein 13)* and contains the three conserved domains described above: SAM, RhoGAP and START (Figure 6). Thorsell et al. analyzed the crystal structure of the START domain of the mouse *Stard13* and proposed as possible ligands for this protein negatively charged small lipids, such as phosphatidylcholine and fatty acids [**95**]. Intriguingly, it has been shown that phospholipids can influence the GTPase substrate preference and regulate the catalytic activity of GAPs [**96**]. A potential lipid ligand of *Stard13* and interacting partners of the different functional domains of STARD13/DLC2 protein have yet to be identified. Also, understanding whether the START domain of STARD13/DLC2 might serve as a molecular switch to regulate RhoGAP activity upon binding with lipids remains an open questions [**84**].

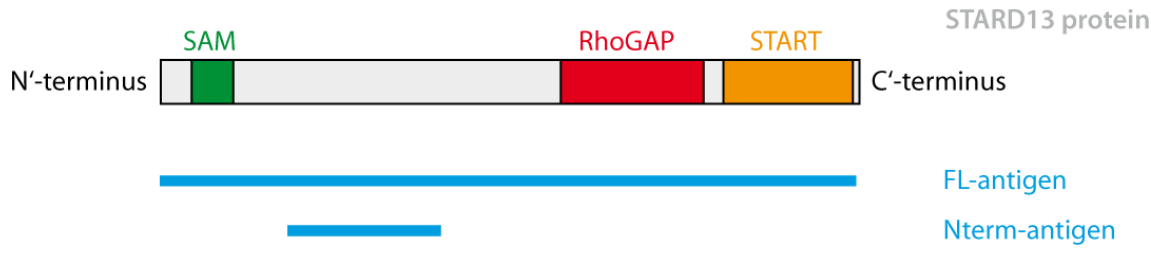

Figure 6: STARD13 protein

Schematic representation of the mouse STARD13 protein. The protein is 1113 amino acids (aa) long and consists of three conserved domains: the SAM (aa 57-129; in green), RhoGAP (aa 657-874; in red) and START domain (aa 901-1104; in orange). For the antibody generation (described in Chapter 2.2) I selected as antigens the full-length protein (FL-antigen; in blue) and a fragment (from aa 208-449) of the protein at the N-terminus without any conserved domains (Nterm-antigen; in blue).

Little is known about the biological function of *Stard13* and no embryological function has been assigned to it. To investigate the biological function of *Stard13* and, in particular, a potential conserved role in pancreatic development, a conditional knockout mouse of *Stard13* was generated in our laboratory (Chapter 2.3, Figure 9).

1.3 Aim of the Study

During embryonic development, the pancreas undergoes branching morphogenesis, which occurs concomitantly with growth and differentiation. The formation of a typical tip and trunk domain organization in the branched pancreas epithelium is a prerequisite to place proliferating and differentiating cell types to distinct regions in the tissue. For example, recent observations showed that MPCs localize at the distal tips of the branches [**21**]. Importantly, it has been shown that the initial number of progenitor cells predetermines the final pancreas organ size [**25**]. Thus, establishment of a proper progenitor pool size during branching phase

is critical to normal pancreas formation and function, including digestion and blood sugar regulation. The molecular mechanisms underlying coordinated tissue branching and proliferation are largely unknown.

The main aim of my PhD study was to investigate the role of the RhoGAP STARD13 during mammalian embryonic development and, in particular, during pancreas organogenesis. Preliminary studies in the Spagnoli laboratory showed that *Stard13* is expressed in the mouse pancreatic rudiments from E10.5 onwards, suggesting an evolutionarily conserved function across species [**83**]. To investigate *Stard13* biological function, I took advantage of the *Cre*-Lox system in the mouse and used the *Stard13* floxed allele, which was previously generated in the laboratory, to ablate its gene expression in a temporal- and spatial-controlled fashion.

By using a *Pdx1-Cre* transgenic strain I achieved conditional ablation of *Stard13* from E10.5 onwards specifically in the pancreas tissue and, subsequently, analyzed the pancreatic phenotype at different developmental stages. First, I observed a hypoplastic pancreas that showed branching defects throughout embryonic development. Second, I found that the loss of the typical pancreatic branches included mislocalization of MPCs within the epithelium. The proliferative activity of progenitor cells and the size of the progenitor pool were reduced, resulting in the primarily observed organ hypoplasia in *Stard13*-ablated pancreata. Third, I presented evidences for a role of STARD13 protein in regulating Rho signaling via its RhoGAP domain, by which it controls actin cytoskeletal dynamics during pancreas morphogenesis. Finally, this study defined a reciprocal interaction between the actin-Megakaryoblastic leukemia 1 (MAL)-serum response factor (SRF) and the Mitogen-activated-protein-kinase (MAPK) signaling to regulate progenitor cell proliferation in the pancreas.

In summary, this thesis represents the first *in vivo* study of the pancreas-specific Rho-GTPase regulating protein STARD13. I showed that STARD13 acts as a molecular integrator of growth and branching morphogenesis by restricting Rho-signaling in the developing mouse pancreas.

2 Results

2.1 *Stard13* Is Expressed in the Mouse Pancreas Throughout Embryogenesis

In order to characterize *Stard13* expression pattern during mouse embryonic development, *in-situ* hybridization was performed on cryosections of mouse embryos with a probe against *Stard13* mRNA. We found *Stard13* expression in the mouse endoderm from gastrulation onwards (data not shown). At E10.5, *Stard13* transcript was detected in the dorsal pancreatic rudiment, overlapping with the domain of expression of *Pdx1*, one of the earliest pancreatic transcription factors (Figure 7A-A') [**3**] [**6**]. Subsequently, at E12.5 and E14.5, *Stard13* was detected in both ventral and dorsal pancreas (Figure 7B-C). Importantly, at E14.5 the transcript of *Stard13* was enriched at the tips of the branching epithelium, which contain pancreatic MPCs at this stage (Figure 7C) [**21**]. Later in development (E18.5), the transcript became restricted to the endocrine compartment of the pancreas (Figure 7D-D'). In addition to its expression in the pancreas, we could detect *Stard13* in the neural crest territory and muscle progenitors in the mouse embryo (Figure 7A, B).

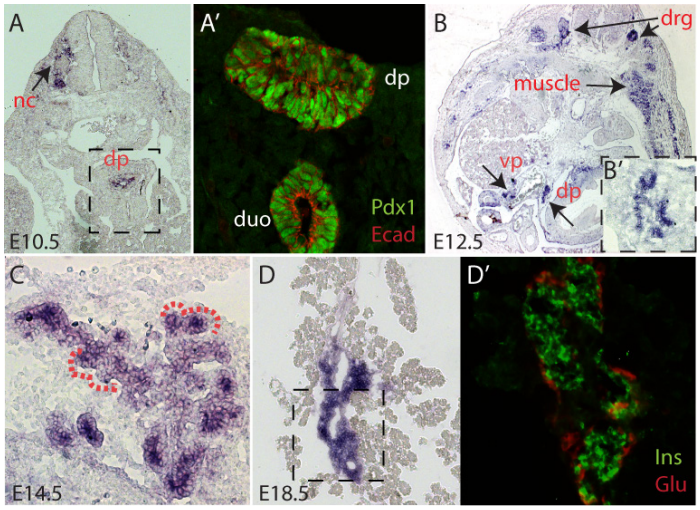

Figure 7: *Stard13* expression during pancreatogenesis

In situ hybridization analysis of *Stard13* on cryosections of mouse embryos. (A-A') At E10.5, *Stard13* expression was visible in the budding pancreas, which coexpressed *Pdx1* and E-cadherin (Ecad) (A'), as seen by immunofluorescence staining on a serial section (inset in A). (B-B') *Stard13* expression was visible in the dorsal pancreas and ventral pancreas at E12.5. (C) The transcript of *Stard13* accumulated at the branching tips (red outline). (D-D') At E18.5, *Stard13* expression was restricted to the islet cells that co-expressed Insulin (Ins) and Glucagon (Glu), as see by immunofluorescence analysis (D', inset of D). Abbr.: dorsal and ventral pancreas (dp, vp); dorsal root ganglion (drg); duodenum (duo); neural crest (nc).

2.2 Generation of STARD13 Antibody

Currently, three commercial antibodies against STARD13 are available and they were all generated against synthetic peptide immunogens (anti-Stard13 from Sigma: S9573 and S9698; anti-Stard13 from Santa Cruz: sc-67843). I tested all three antibodies and found that they detected the over-expressed STARD13 protein by Western blot (WB) and immunofluorescence (IF) analyses, but not the endogenous STARD13 protein (data not

shown, Figure 8A-C). This suggests that the synthetic peptides used did not contain the best epitope for immunization, possibly due to the absence of natural 3D structure. For this reason, I decided to generate a homemade antibody against the recombinant STARD13 protein.

To this aim, I used as antigen the full-length STARD13 protein (NCBI: NP_666370.3) and an N-terminal STARD13 protein fragment (NCBI: NP_666370.3: from aa 208 to aa 449), which lacks the two evolutionarily conserved C-terminal domains, Rho-GAP and START. Since these two domains are in common with many other proteins, I reasoned that eliminating them from the antigen would increase the specificity of the immunoreaction against STARD13. First, I cloned the full length *Stard13* cDNA (NM_146258.2; referred to as ***Stard13-fl***; see Figure 6) and a 737-bp cDNA fragment of *Stard13* (corresponding to nucleotides 721 to 1458; referred to as ***Stard13-Nterm***; see Figure 6) into the pGEX-4T-1 bacterial expression vector. The cloning of the inserts in-frame resulted into Glutathione-S-Transferase (GST)-tagged proteins (referred to as **GST-STARD13-FL** and **GST-STARD13-Nterm**). Second, I transfected both constructs into BL21-E.coli cells. By Isopropyl β-D-1-thiogalactopyranoside (IPTG) induction, I accelerated the expression of the GST-STARD13 fusion proteins. Subsequently, both GST-STARD13 recombinant proteins were immunoprecipitated with Protein G-Sepharose, analyzed by SDS-PAGE and Coomassie staining.

Because of the low yield recovery after pull-down of the large **GST-STARD13-FL** construct, I decided to produce the antibody only against the **GST-STARD13-Nterm** construct. The **GST-STARD13-Nterm** recombinant protein was sent to the Davids Biotechnology GmbH (Regensburg) for immunization of rabbit and chicken, as host species. GST was depleted and the sera purified. The antibody was called **STARD13-Nterm.**

To verify that **STARD13-Nterm** antibody detects STARD13 antigen, I tested its detection potential by Western blot and by immunofluorescence. Importantly, in Western blot analysis, the **STARD13-Nterm** antibody generated in rabbit strongly detected endogenous mouse STARD13 (mSTARD13) on WT E14.5 pancreas lysates, while the signal in E17.5 pancreatic lysates was weak (Figure 8D). This discrepancy might be due to the restricted expression of *Stard13* to the islets at E17.5 and later stages (Figure 7D). The **STARD13-Nterm** antibody detected overexpressed mSTARD13 protein upon transfection in Human embryonic kidney (HEK) cell lysates too (Figure 8D), whereas no signal was detected in non-transfected HEK cells (negative control) (Figure 8D). Furthermore, the **STARD13-Nterm** antibody recognized endogenous mSTARD13 in cell lysates of E14.5 wildtype (WT) mouse embryonic fibroblasts (MEFs), while the protein was not detectable in cell lysates of E14.5 MEFs, which were

isolated from *Stard13* gene knockout embryos (referred to as *Stard13*$^{\Delta/\Delta}$; see Chapter 4.2.1 for further detail).

Immunofluorescence staining was performed on pancreatic tissue cryosections with the **STARD13-Nterm** antibodies produced in either rabbit or chicken. So far, the immunofluorescence protocols tested did not allow detection of the endogenous protein. Ongoing experiments are aimed at improving the experimental conditions for immunolocalization analysis with the **STARD13-Nterm** antibody and to perform immunoprecipitation experiments to identify potential interacting partners of STARD13.

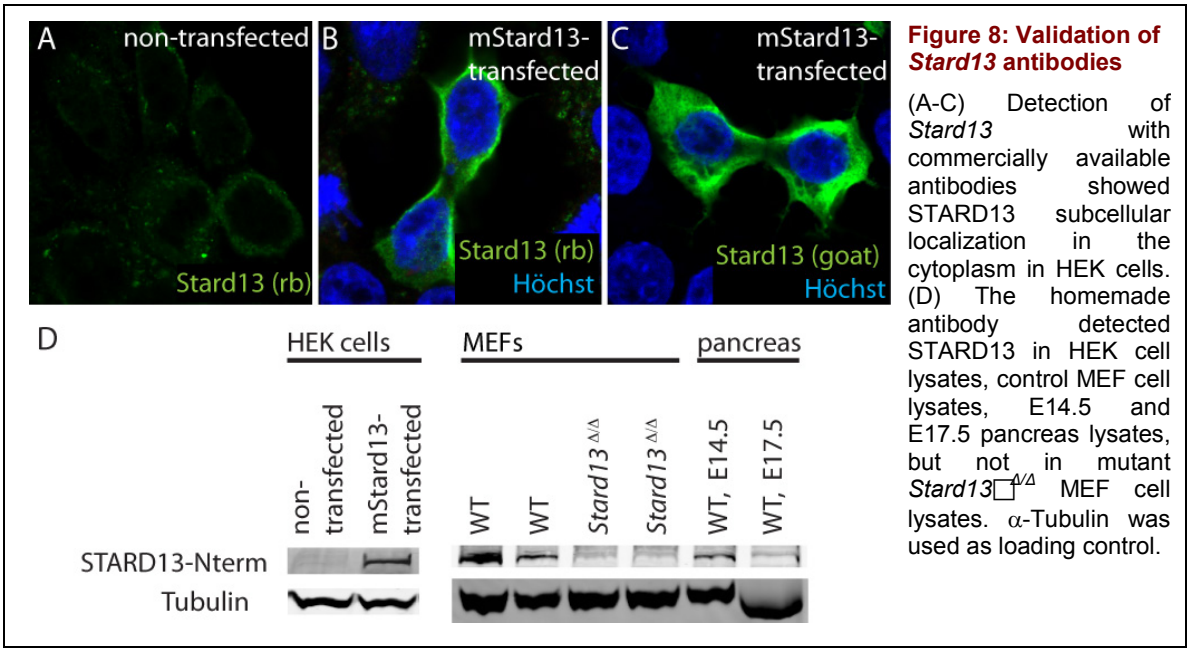

Figure 8: Validation of *Stard13* antibodies

(A-C) Detection of *Stard13* with commercially available antibodies showed STARD13 subcellular localization in the cytoplasm in HEK cells. (D) The homemade antibody detected STARD13 in HEK cell lysates, control MEF cell lysates, E14.5 and E17.5 pancreas lysates, but not in mutant *Stard13*$^{\Delta/\Delta}$ MEF cell lysates. α-Tubulin was used as loading control.

2.3 Generation of Pancreas-Specific *Stard13* Mutant Mice

To investigate the role of *Stard13* in pancreatogenesis, we undertook a conditional knock-out approach and deleted *Stard13* gene expression specifically in the pancreas. A floxed allele of the mouse *Stard13 (Stard13*^{lox}*)* was generated by flanking exon5 of the gene with LoxP sites (Figure 9A). We showed that deletion of the exon5 by *Cre*-recombinase transgenic mouse strains led to a frame-shift and incorporation of an early stop-codon, which resulted in a truncated non-functional protein (Figure 8D, Figure 9A). Pancreas tissue-specific ablation was achieved by intercrossing floxed *Stard13* homozygous mice (*Stard13*$^{lox/lox}$) with *Pdx1-Cre* transgenic mice. *Pdx1* is the earliest known pancreatic transcription factor being expressed in all pancreatic lineages [**41**][**16**]. The *Pdx1-Cre* transgenic mouse is known to promote DNA recombination at LoxP sites starting from E10.5-E11.5 [**16**]. Occasionally, *Pdx1-Cre* mouse transgenic strain showed inconsistent recombination efficiency in standard

tests with the ROSA26R lacZ reporter line [**80**], resulting in a variable percentage of pancreatic cells that escaped recombination. To reduce this variability and increase recombination efficiency, we interbred *Stard13*$^{lox/lox}$ with *cytomegalovirus (CMV)-Cre* mice [**97**] to generate mice carrying a germline-deleted allele of *Stard13* (*Stard13*$^{\Delta}$). Subsequently, these mice were bred with *Pdx1-Cre* transgenic mice to generate the *Stard13*$^{\Delta/+}$*; Pdx1-Cre* line (see methods Chapter 4.2.1). Finally, for conditional ablation of *Stard13* in the pancreas *Stard13*$^{lox/lox}$ and *Stard13*$^{\Delta/+}$*; Pdx1-Cre* mice were interbred resulting in progeny with four different genotype variants (Figure 9B). From here on, *Stard13*$^{lox/\Delta}$*; Pdx1-Cre* mice are either referred to as mutants or as *Stard13*$^{PA\text{-}deleted}$ (*Stard13*$^{pancreas\text{-}deleted}$) mice. Being *Stard13*$^{lox/+}$ or *Stard13*$^{lox/\Delta}$ wildtype mice indistinguishable from *Stard13*$^{lox/+}$*; Pxd1-Cre* heterozygous mice, hereafter they are all referred to as WT control mice.

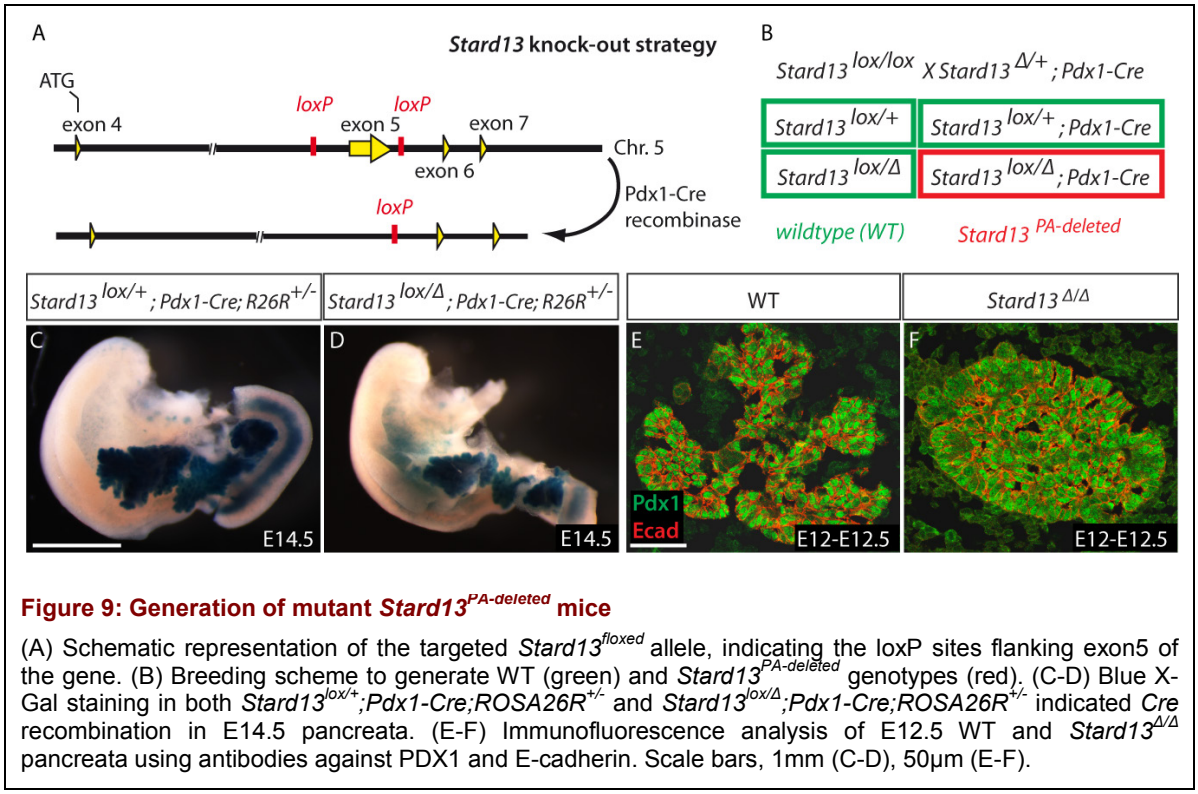

Figure 9: Generation of mutant *Stard13*$^{PA\text{-}deleted}$ mice

(A) Schematic representation of the targeted *Stard13*^{floxed} allele, indicating the loxP sites flanking exon5 of the gene. (B) Breeding scheme to generate WT (green) and *Stard13*$^{PA\text{-}deleted}$ genotypes (red). (C-D) Blue X-Gal staining in both *Stard13*$^{lox/+}$*;Pdx1-Cre;ROSA26R*$^{+/-}$ and *Stard13*$^{lox/\Delta}$*;Pdx1-Cre;ROSA26R*$^{+/-}$ indicated *Cre* recombination in E14.5 pancreata. (E-F) Immunofluorescence analysis of E12.5 WT and *Stard13*$^{\Delta/\Delta}$ pancreata using antibodies against PDX1 and E-cadherin. Scale bars, 1mm (C-D), 50µm (E-F).

X-Gal staining in both heterozygous *Stard13* ablated (*Stard13*$^{lox/+}$*; Pdx1-Cre; ROSA26R*$^{+/-}$) and homozygous *Stard13* ablated (*Stard13*$^{lox/\Delta}$*; Pdx1-Cre; ROSA26R*$^{+/-}$) pancreata indicated efficient *Cre* recombination, showing almost uniform blue staining in the E14.5 pancreas. Pancreatic size difference was evident between heterozygous and mutant pancreata (Figure 9C-D).

2.4 *Stard13* Is Required for Pancreatic Branching Morphogenesis

To investigate the consequences of *Stard13* deletion during pancreatic development, I started by performing immunofluorescence analysis using antibodies against the transcriptional factors *Pdx1* or *Sox9* at different stages of embryonic development. The epithelial basolateral marker E-cadherin (Ecad) was used together with these transcription factors to visualize the whole pancreatic epithelium.

The first remarkable difference that I recognized between WT and $Stard13^{PA\text{-}deleted}$ pancreas was in the architecture of the pancreatic tissue. This could be observed starting from E10.5. The WT dorsal bud displayed a “T-like“ shape and the ventral bud was round, both surrounding narrow primary lumina, whereas mutant dorsal and ventral bud cells did not define these typical shapes, but spread in an unordered fashion with wide open primary lumina (Figure 10A-D).

At E11.5, the WT pancreas was a stratified unpolarized epithelium, which just started to expand by sending “protrusions” into the surrounding mesenchyme, while in the mutant the epithelial “protrusions” and clefts were not visible and the surface stayed smooth (Figure 10E-F). Primary branches of pancreatic epithelium became evident at E12.5 in WT pancreata, displaying cells that gradually organize into a monolayer to surround future luminal structures (Figure 10G). At E14.5, the tips of the primary branches further divided to generate new tips (Figure 10I). By contrast, the mutant tissue failed to form primary branches at E12.5 and, at later stages, cell proliferation resulted into larger and disorganized acini structures, consisting of multiple stratified cell layers and lacking a typical duct-like organization (Figure 10H,J). Finally, mutant tissue defects were still visible in E16.5 mutant pancreata, including larger and discontinuous ducts and disorganized cell groups at their edge (Figure 10L). In contrast, the WT tissue at this stage matured into an interconnected tubular network with acinar structures at their end that consist of a monolayer of cells surrounding common lumina (Figure 10K).

The *CMV-Cre* transgenic strain ensures Cre-recombinase expression in all tissues from pre-implantation stages onwards [**97**]. Therefore, ubiquitous *Stard13* ablation in all tissues ($Stard13^{\Delta}$) using the *CMV-Cre* transgenic strain corresponds to the generation of a null allele. Homozygous ubiquitous *Stard13* deletion ($Stard13^{\Delta/\Delta}$) led to a pancreas-specific phenotype displaying problems in tissue morphogenesis similar to those observed in the $Stard13^{PA\text{-}deleted}$ pancreata, suggesting that the activity of *Stard13* is tissue-specific (Figure 9E-F).

Altogether these results indicate that *Stard13* affects the morphogenesis of the pancreas, resulting in branching defects and overall disorganization of the pancreatic tissue.

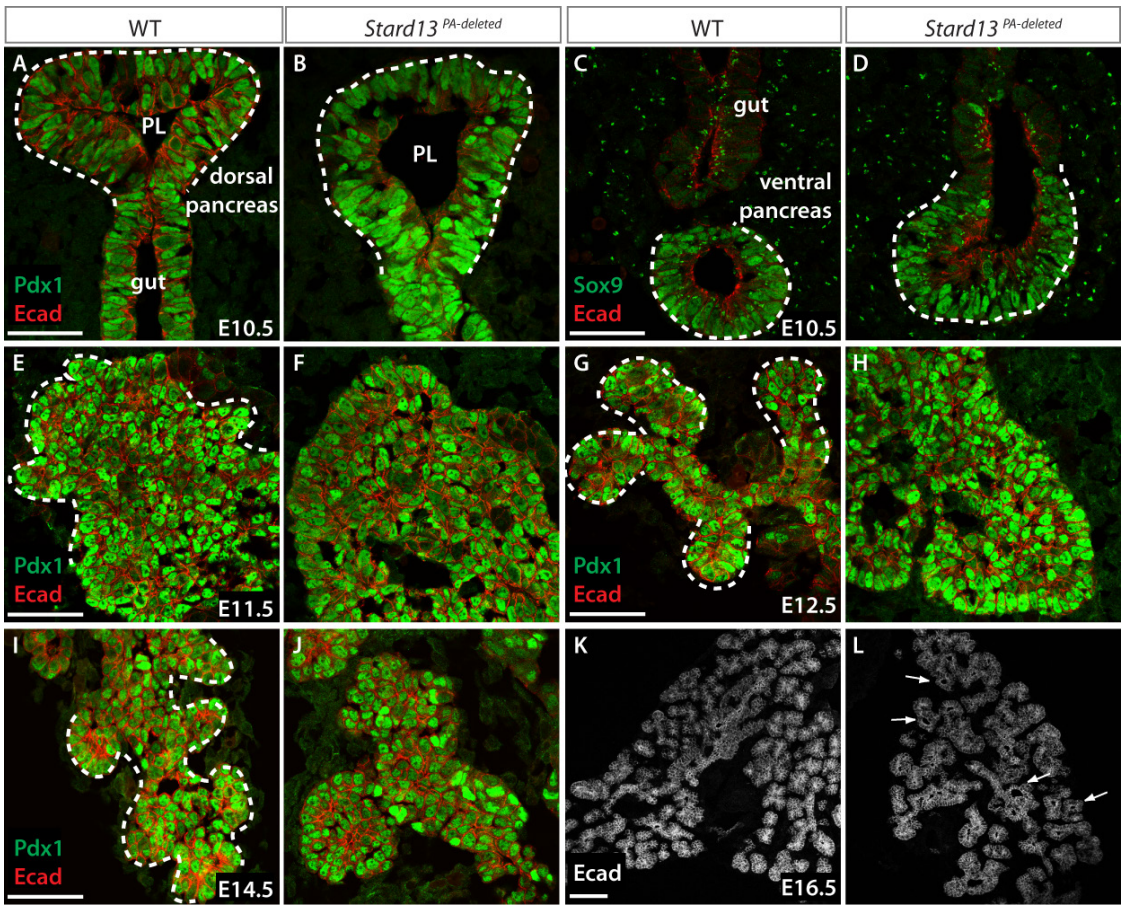

Figure 10: *Stard13* ablation causes disorganization of pancreatic tissue

Immunostaining analysis with antibodies against *Pdx1*, *Sox9* and E-cadherin (Ecad) on cryosections of WT and mutant pancreatic tissue. (A-B) The mutant dorsal tissue grew, displaying a wide open primary lumen (PL), lacking typical "T-shape" as seen in the WT (see white outline). (C-D) The ventral WT tissue protruded as a round bud, whereas in the mutant the bud was irregularly shaped. (E-F) At E11.5, epithelial protrusions (white outline) were sent out from the WT pancreatic tissue, but were absent from the mutant tissue. (G-H) E12.5 WT tissue showed typical primary branches (white outline), while branches were absent in *Stard13*$^{PA\text{-}deleted}$ mutants. (I-J) E14.5 WT branching tips further divided to generate new tips. Mutant pancreas tips were composed of disorganized multiple cell layers. (K-L) At E16.5, typical tree-like branching epithelium was formed, whereas mutant embryos showed wide open ducts and disorganized cell groups at their distal ends. Scale bars, 50 µm (A-H), 100 µm (K-L).

2.5 Localization and Proliferation of Multipotent Progenitor Tip Cells Are Perturbed in *Stard13*-Deficient Mice

At E14.5, the transcript of *Stard13* was enriched at the tip of the pancreatic epithelial branches (Figure 7C). I therefore tested whether *Stard13* gene ablation affects the tip and trunk tissue-organization that is typical of the developing pancreas [**21**]. To this aim, I analyzed the expression of *Cpa1*, which has been previously described as a marker of

pancreatic progenitors located at the tip of the branches [**21**]. Tip progenitors are highly proliferative, undergo limited self-renewal and give rise to the three pancreatic cell types, endocrine, exocrine and duct cells (Figure 2C-D) [**21**] [**24**]. Around E14.0 in the mouse embryo, tip progenitor cells undergo a developmental switch and become committed toward the exocrine cell lineage [**21**]. By immunostaining analysis at E12.5, I detected $Cpa1^+$ cells in both WT and *Stard13*$^{PA\text{-}deleted}$ embryos at E12.5. However, only in the WT the $Cpa1^+$ cells were confined to the tips of the branches (Figure 11A,C), while in the mutant I detected a disorganized distribution of $Cpa1^+$ cells either at the periphery or inside the tissue (Figure 11B,D). $Ngn3^+$ endocrine-progenitor cells are normally located in the "trunk" of the pancreatic branches and did not show an altered localization at E12.5 or E14.5 in mutant tissue compared to WT controls (Figure 11C-F).

Taken together, these results show that the typical tip and trunk tissue architecture is lost in the *Stard13* mutant pancreas and, in particular, progenitor cells are not properly localized to the tip of the branches. Finally, the malformed acini and tubular structures observed at later stages (E14.5-E16.5) might be a consequence of the altered tip and trunk organization in the early mutant tissue (Figure 10J,L).

At birth, *Stard13* mutant pups showed a remarkable pancreatic hypoplasia (Figure 11H), which was recognizable by gross morphological observation starting from embryonic stage E14.5 (Figure 9C-D). Morphometric analyses confirmed this size difference, being the pancreatic sectional volume of the mutant about one third smaller than the WT (Figure 11I).

We hypothesized that pancreatic hypoplasia in *Stard13*-ablated pancreata might be due to:

(1) defects in apoptosis,

(2) defects in cell proliferation and/or

(3) a size reduction of the progenitor pool.

To address the reasons behind the observed pancreatic hypoplasia in *Stard13* mutants, we first tested apoptosis and proliferation on pancreatic sections. Apoptosis was measured using a TdT-mediated dUTP-biotin nick end labeling (TUNEL) assay and cell proliferation was assessed by IF analysis against the mitotic marker, phospho-Histone H3 (pHH3) and incorporation of Bromodeoxyuridin (BrdU) (see methods Chapter 4.4.4). Whereas the levels of apoptosis on sections of E14.6 and E16.5 pancreata showed no difference between WT and mutant (data not shown), a clear reduction in the number of proliferating cells of *Stard13* mutant pancreata was observed from embryonic stage E12.5 onwards (Figure 11J). In particular, we measured a one third decrease in average of the number of proliferating

pHH3$^+$ cells at E12.5 in the mutant epithelium compared to the WT counterpart (Figure 11J), suggesting that size reduction of the mutant pancreas tissue was due to a decrease in cell proliferation during embryogenesis.

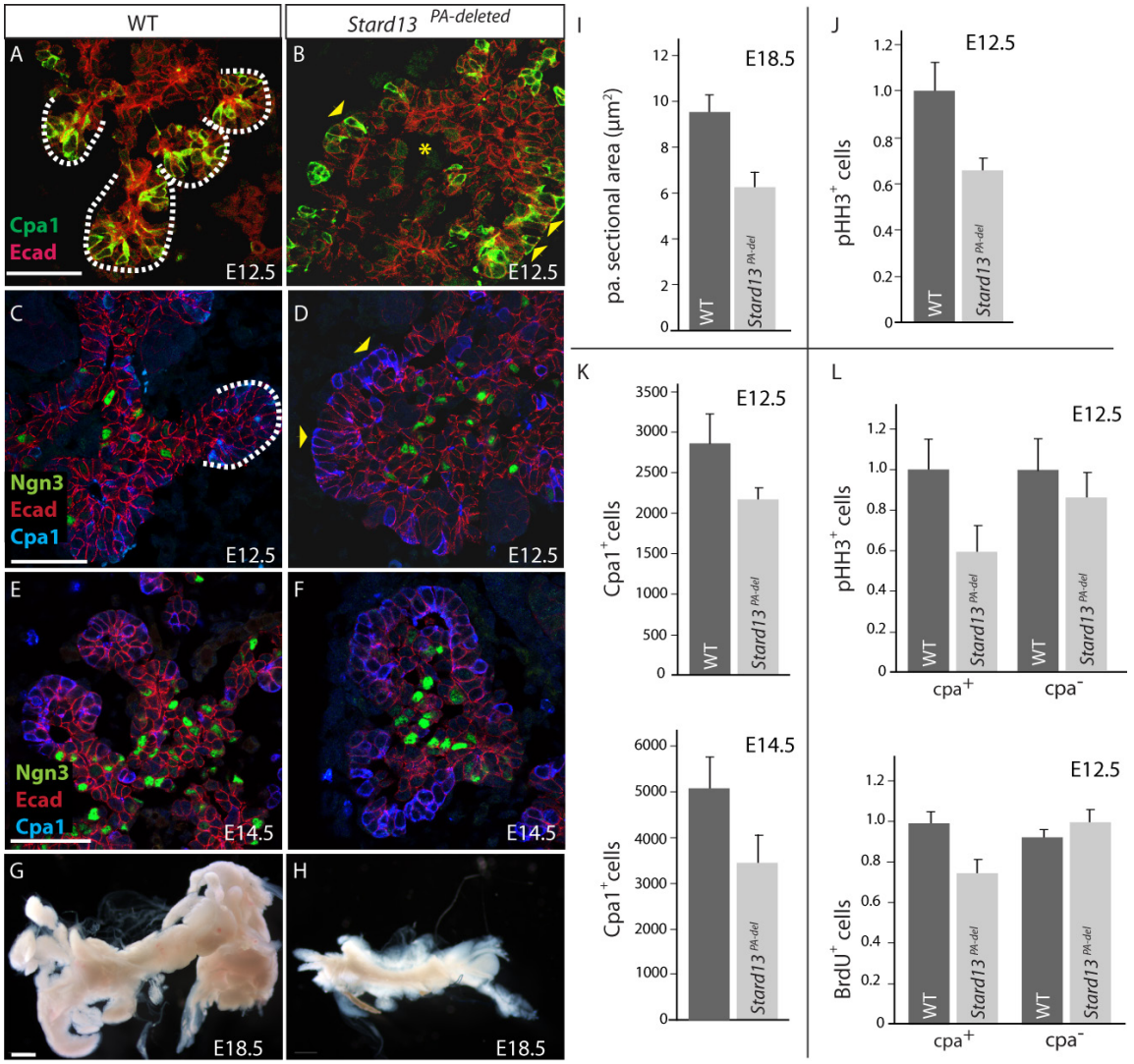

Figure 11: *Stard13* controls the size of the progenitor pool in the developing pancreas

(A-F) Immunostaining analyses of tip- and trunk-specific domains, using Cpa1 and Ngn3 antibodies, respectively. Cpa1$^+$ tip cell distribution was altered in mutant (B) versus WT pancreas (A), but Ngn3$^+$ endocrine progenitor marker location in the trunk was maintained (C-F). (G-H) At E18.5 mutant pancreata showed a tremendous pancreatic hypoplasia. (I) Morphometric analyses of pancreatic sectional area (µm^2) comparing E18.5 WT (n=5) and mutant sections (n=6). (J) Relative number of pHH3$^+$ cells/Ecad$^+$ area (µm^2) showed reduction of proliferating cells in E12.5 *Stard13*$^{PA\text{-}deleted}$ pancreas. n=5. (K) Quantification of progenitor Cpa1$^+$ cells/Ecad$^+$ area (mm^2) showed reduction in *Stard13*$^{PA\text{-}deleted}$ at E12.5 and E14.5. (L) The relative number of pHH3$^+$ Cpa1$^+$ proliferating progenitors versus E-cad$^+$ E12.5 pancreatic areas (µm^2) was reduced, whereas pHH3$^+$ Cpa1$^-$ cells were unchanged, n=4. *Stard13*$^{PA\text{-}deleted}$ epithelium showed reduced numbers of Cpa1$^+$ cells incorporating Bromodeoxyuridine (BrdU) at E12.5 compared to BrdU$^+$/Cpa1$^-$ cells. n=3. All results are expressed as means ± SEM. White dashed lines highlight the tip of branches and arrowheads altered distribution of Cpa1$^+$ cells. Scale bars, 50 µm (A-F), 1mm (G-H).

Since MPCs at the tips have been shown to be highly proliferative [**24**], we addressed if the reduction in overall proliferation could be attributed to the loss or decrease in the number of proliferating progenitor cells in the absence of *Stard13*. To this aim, we measured the rate of MPC proliferation at E12.5 using the marker pHH3, which stains proliferating cells in all mitotic phases from prophase to telophase, and the tip progenitor marker CPA1 ($pHH3^+Cpa1^+$ cells). Interestingly, we detected a reduction of one third in the number of double $pHH3^+Cpa1^+$ pancreatic cells in *Stard13* mutant when compared to WT pancreata, whereas the number of proliferating $pHH3^+Cpa1^-$ cells was not significantly different (Figure 11L). Similar results were also obtained upon *in vivo* labeling E12.5 pancreata with the proliferation marker BrdU, which stains proliferating cells in the S-phase of cell cycle, and quantification of double $BrdU^+Cpa1^+$ cells (Figure 11L).

Importantly, it was previously shown that the pancreas organ size is limited by the number of embryonic progenitor cells, which is established before E14.5 in the developing pancreas [**25**]. The reduction in size of the pancreatic progenitor pool could be therefore a cause of the hypoplastic phenotype observed in *Stard13* mutants. We counted the number of multipotent $Cpa1^+$ progenitor cells [**21**] and detected an average reduction of 25% of the $Cpa1^+$ cells in the mutant pancreas at E12.5 (Figure 11K). Later at E14.5, the number of $Cpa1^+$ cells showed further reduction in $Stard13^{PA\text{-}deleted}$ pancreata, which is consistent with their decreased proliferative activity at E12.5 (Figure 11K).

In summary, the hypoplastic pancreatic phenotype in the *Stard13* mutant is not due to an increase in apoptosis, but to a decrease in cell proliferation, in particular of the $Cpa1^+$ multipotent progenitors. The decreased proliferative activity of $Cpa1^+$ progenitors results into an overall depletion of the pancreatic progenitor pool, which in turn would be responsible for the smaller size of the *Stard13*-ablated pancreas (Figure 11G-I) [**25**] [**21**]. Taken together, these results suggest *Stard13* being responsible for maintaining $Cpa1^+$ progenitor pool at the tip of the pancreatic branches in order to sustain its proliferative self-renewing potential. Finally, this underscores the importance of establishing proper tissue architecture in order to set up the final pancreas organ size.

2.6 Analysis of *Sox9, Hes1* and *p63* as Markers of the Tip Progenitor Pool

At E12.5, multipotent $Cpa1^+$ progenitor cells are preferentially localized to the pancreatic tips, being more exposed to the surrounding mesenchyme than the cells inside the tissue, such as the endocrine $Ngn3^+$ progenitors. This preferred tip localization is suggestive of the existence of a "**niche"** that might sustain proliferation of undifferentiated progenitor cells. The presumptive "niche" could be defined through pancreas-mesenchyme cell interactions and/or

through signals released from the mesenchyme, which in turn influence transcription factor expression within the tip cells [**9**].

Transcription factors that might define a "stem cell-like niche" during pancreas development are *Sox9, Hes1* and *p63*, which are known to keep cells in an undifferentiated state in various epithelia [**7**] [**98**] [**32**] [**99**]. I analyzed the expression of these transcription factors in the normal pancreatic epithelium and whether they are mislocalized following perturbation of tip morphogenesis in *Stard13* mutants.

Sox9 is first detected around E10.5 in early mitotically active/Notch-responsive/PDX1$^+$ pluripotent progenitors, which give rise to all three pancreatic lineages (Figure 10C-D) [**45**]. I showed that *Sox9* is present in all pancreas epithelial cells at E12.5 in the WT and mutant pancreas, which is in line with previous observations (Figure 12A,B) [**45**]. Interestingly, I found that the intensity of SOX9 protein expression varied among cells in both WT and mutant tissues (Figure 12A'-B'). However, the differences in intensity did not account for a typical area (e.g. the tip cells) and not for a specific pattern. In addition, preliminary results did not reveal any significant difference in the number of *Sox9*$^+$ cells at E12.5 between WT and mutant tissue (Figure 12C).

Notch signaling influences early pancreas development by preserving or maintaining *Pdx1*$^+$ cells in an undifferentiated state and *Sox9* possibly regulates Notch-signaling [**32**] [**45**] [**98**]. The downstream Notch target and transcription factor *Hes1* has a widespread expression pattern during pancreas primary transition, but it becomes enriched in pancreas progenitors following Notch activation [**100**]. At the onset of the secondary transition (~E13.5 onward), downregulation of *Hes1* expression occurs and it becomes exclusively detectable in duct and centroacinar cells, where activated Notch promotes duct differentiation [**100**]. Since downregulation of Notch signaling and, in particular, *Hes1* knockout results into a poorly branched pancreatic epithelium, which is reduced in size, I asked if Notch signaling plays a role in preserving Cpa1$^+$ cells in a multipotent progenitor state at the branching tips [**36**]. To this aim, I analyzed the expression of *Hes1* in the developing pancreas before secondary transition. I observed a widespread expression of *Hes1* without any preferential tissue regionalization in both WT and mutant pancreas epithelium at E12.5 (Figure 12D-E). Both Cpa1$^+$Hes1$^+$-double positive cells, as well as Hes1$^+$-single positive cells, were present in WT and mutant pancreata, suggesting that HES1 does not mark exclusively tip progenitor cells (Figure 12D-E). At E14.5, immunostaining for *Hes1* was more intense in cells located in the trunk and ductal compartments in both WT and mutant tissue, but still detectable at the tips (Figure 12F-G).

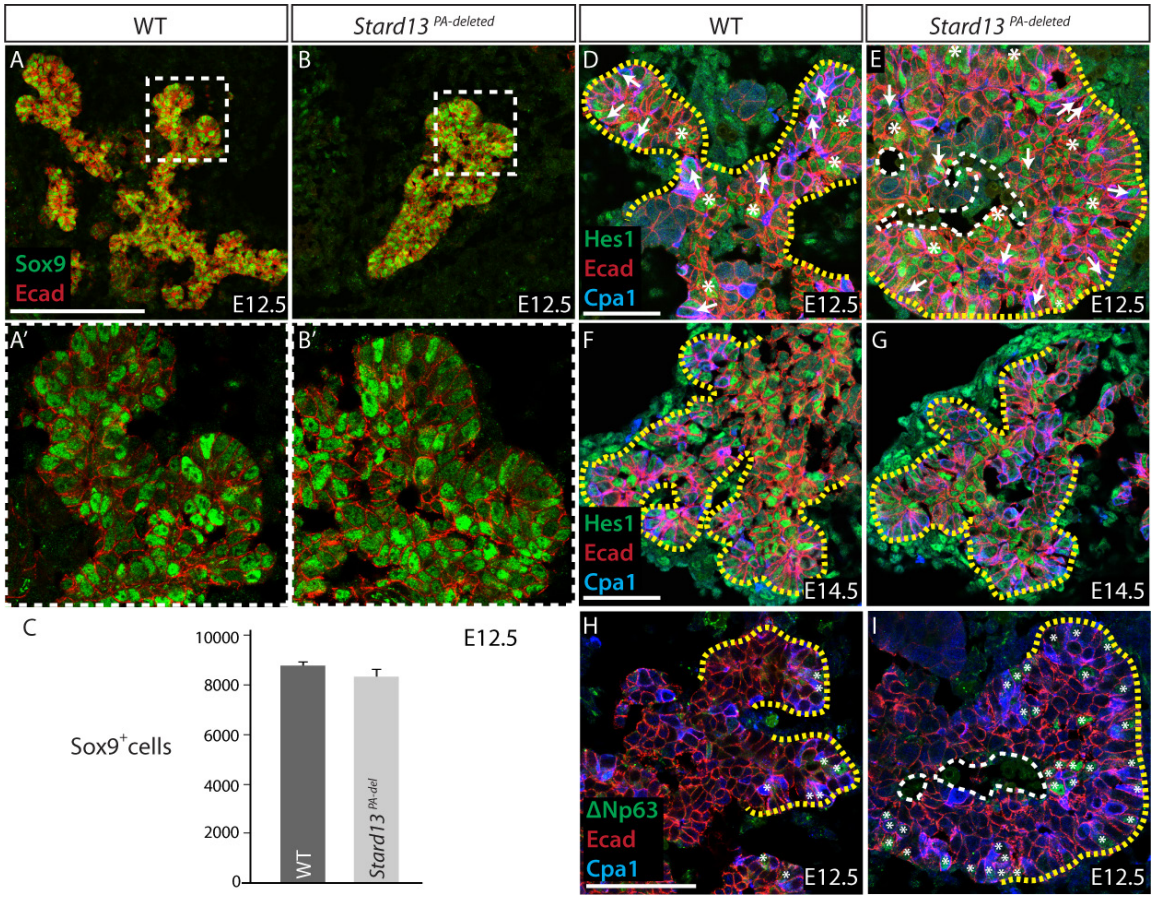

Figure 12: Analysis of *Sox9, Hes1* and *p63* as markers for the tip progenitor pool

(A, B) Immunostaining for SOX9 in E12.5 pancreatic cells of WT and mutant embryos. A' and B' are higher magnifications of micrographs in A and B sections, respectively. Differences in SOX9 staining intensities were visible (C) Quantification of progenitor Sox9^{+} cells versus total Ecad^{+} area (mm^{2}) showed no difference in numbers between WT and *Stard13*$^{PA\text{-}deleted}$ pancreas at E12.5. Results are expressed as means ± SEM. (D-E) Immunostaining for HES1 in WT and *Stard13*$^{PA\text{-}deleted}$ pancreata. Hes1^{+}-single positive cells are indicated by white asterisks and Cpa1^{+}Hes1^{+}-double positive cells are marked by white arrows. In the mutant they were localized to the tissue periphery, as well as within the tissue. (F-G) At E14.5, *Hes1* expression was most intense in cento-acinar cells and ductal compartments. (H) ΔNp63 staining (white asterisks) was detectable at the tips in E12.5 WT tissue, partially overlapping with CPA1. (I) In mutant tissue, ΔNp63 was detected not only at the tissue border, but inside the epithelium. Borders between pancreas and mesenchyme are demarcated by yellow dotted line. Note luminal spaces within tissue marked by white dashed lines. Scale bars, 200 µm (A, B), 100µm (D-E), 50 µm (F-I).

The transcription factor *p63* has been described to be essential for the proliferative potentials of stem cells in different stratified epithelia and, as such, for the development of stratified epithelial tissues, including the epidermis, mammary gland and prostata [**101**] [**102**] [**99**]. Genetic ablation of *p63* in the mouse results in the lack of stratified squamous epithelia [**103**] [**104**] [**105**]. Furthermore, *p63* regulates extracellular matrix adhesion molecules in mammary gland and other stratified epithelia tissues [**106**]. *ΔNp63*, one of two isoforms of *p63*, has been reported as a reliable marker of squamous differentiation in human adult pancreas and, particularly, valuable in distinguishing squamous/transitional metaplasia from pancreatic

intraepithelial neoplasia [**107**]. However, a potential role for *p63* in the pancreatic epithelium formation has not been investigated so far.

I was interested in testing the hypothesis whether *p63* might have a potential conserved role in stem-cell proliferation and be a pancreas progenitor pool marker. I started by analyzing *ΔNp63* expression in the developing pancreas and testing a possible overlap with the progenitor pool at branching tips before secondary transition. Furthermore, I was interested in investigating if *ΔNp63* expression is changed in *Stard13* mutant pancreata.

Preliminary immunostaining analysis of E12.5 WT pancreata revealed ΔNp63 staining mainly in cells that are located at the tips and in contact with the mesenchyme (Figure 12H-I, white stars). Interestingly, I detected an overlap between Cpa1$^+$ and *ΔNp63*$^+$ tip cells, though single positive Cpa1$^+$ and ΔNp63$^+$ cells were also visible (Figure 12H-I). In the mutant epithelium, *ΔNp63* expression was maintained, but ΔNp63$^+$ cells were mislocalized and detected mostly inside of the pancreatic tissue (Figure 12J, white stars). These defects are reminiscent of those previously described for Cpa1$^+$ tip cells (Figure 11B,D).

In summary, the transcription factors *Sox9* and *Hes1* did not show a tip-restricted tissue-localization in the WT pancreatic epithelium and were not affected by the ablation of *Stard13*. This suggests that *Sox9* and *Notch*-signaling do neither define an assumptive progenitor "niche" for Cpa1$^+$ cells nor account for the phenotype observed in the mutant tissue. In contrast, I found that p63 is an additional marker of pancreatic tip cells and very likely marks a larger progenitor population than CPA1. Lineage tracing studies of *p63*$^+$ cells would be necessary to define p63 as true progenitor marker. Moreover, *p63* transcription factor expression was maintained in mutant epithelial cells, even though the loss of the typical tip and trunk organization mislocalized *ΔNp63*$^+$ cells. It is likely that non-cell autonomous extrinsic localization signals coming from the mesenchyme act as signals promoting *p63* and *Cpa1* expression in the tip of the pancreatic branch and thus localize MPCs to this region in the pancreas.

2.7 All Pancreatic Cell Lineages Are Specified in *Stard13*$^{PA\text{-}deleted}$ Pancreata

The mature pancreas contains distinct cell types, which perform exocrine and endocrine functions. These different cell types can be identified by a set of transcription factors and exocrine or endocrine products after the secondary transition (see Chapters 1.1.2 & 1.1.4). To address whether all different pancreatic cell lineages were specified in *Stard13* mutant pancreas, I performed a set of immunofluorescence analyses on pancreatic tissue at E14.5 and E16.5 and measured the relative cell numbers of different cell types.

Amylase was used as marker of the exocrine lineage. Both WT and mutant pancreata showed similar numbers of Amylase-positive cells (Figure 13A-B,G). Similarly, differentiated endocrine cells, stained by Insulin and Glucagon, were detected in both WT and mutant pancreas from E12.5 throughout development (Figure 13C-D). Measurement of Glucagon^{+} cells did not reveal any difference between WT and mutant (Figure 13H). Finally, the duct cell lineage was analyzed at E16.5, stage at which all duct-lining epithelial cells are positive for the transcription factor *Sox9* [**23**]. Even though pancreatic duct SOX9^{+} cells were found in both WT and mutant embryos and in similar number (Figure 12C), the duct architecture was severely disrupted in the mutant (Figure 13E-F). Specifically, the ducts displayed aberrant organization in mutant pancreata, showing variations in diameter and discontinuity (Figure 13F).

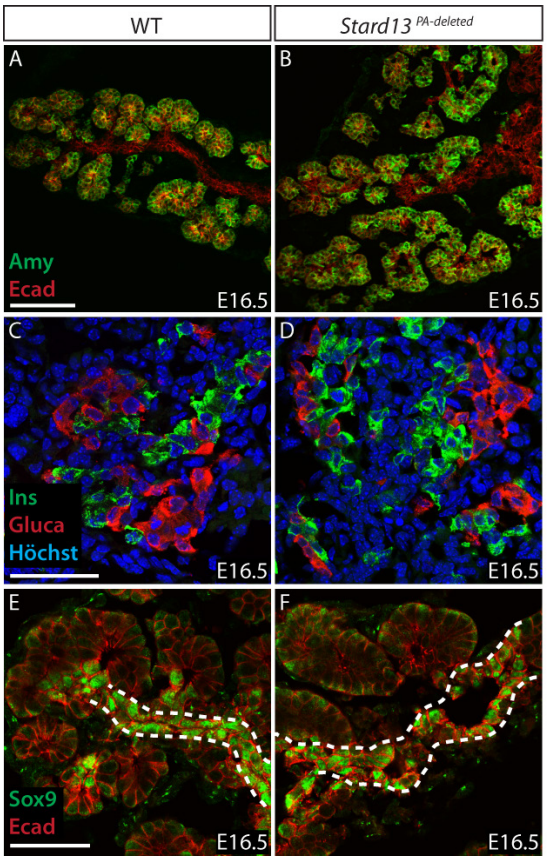

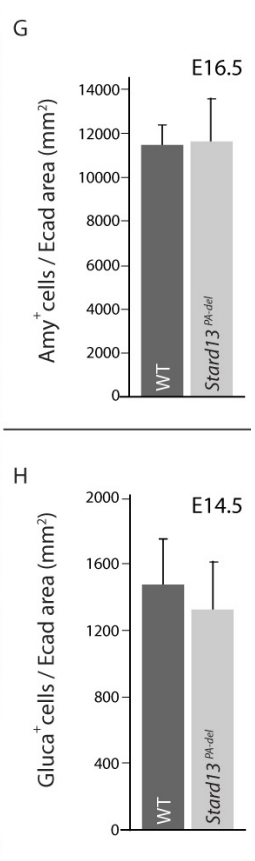

Figure 13: *Stard13* ablation does not influence pancreatic lineage allocation

WT and *Stard13*$^{PA\text{-}deleted}$ pancreas sections were immunostained for the three pancreatic cell lineages. (A-B) Amylase staining marks exocrine acinar cell goups, which were disorganized in the mutant. (C-D) Insulin and Glucagon staining for endocrine cells in WT and mutant pancreas. (E-F) Sox9 staining marks the duct lineage population. White dashed lines highlight the ductal epithelium. (G) Quantification of exocrine cells (Amylase^{+}) versus total E-cadherin area in WT and *Stard13*$^{PA\text{-}deleted}$ pancreas at E16.5. n=3. (H) Quantification of Gluca^{+} endocrine cells versus total Ecad^{+} area at E14.5. n=3. All results are expressed as means ± SEM. Scale bars, 100 µm (A-B), 50 µm (C-F).

Altogether, these results suggest that *Stard13* does not control cell differentiation of any specific pancreatic cell lineage. Moreover, the fact that the different cell types maintain the same relative number in *Stard13*$^{PA\text{-}deleted}$ compared to WT pancreata supports the notion that pancreatic progenitor depletion is the main causes of the hypoplastic phenotype observed in mutants.

2.8 *Stard13* Controls the Remodeling of the Pancreas Epithelium

Branching morphogenesis involves the restructuring of the pancreatic epithelium into a complex and highly organized tubular network. The transition of non-polarized stratified epithelial cells into polarized monolayered epithelial cells was described as the first step of this process, occuring between E11.5 and E12.5 in the mouse embryo (see also Chapter 1.1.2, Figure 2) [**2**] [**20**] [**69**]. To further understand the morphogenetic defects observed in *Stard13* mutants, I investigated cell morphology and epithelial polarity, including cell-cell and cell-ECM adhesions, and cytoskeleton organization in both WT and mutant pancreata (Figure 10).

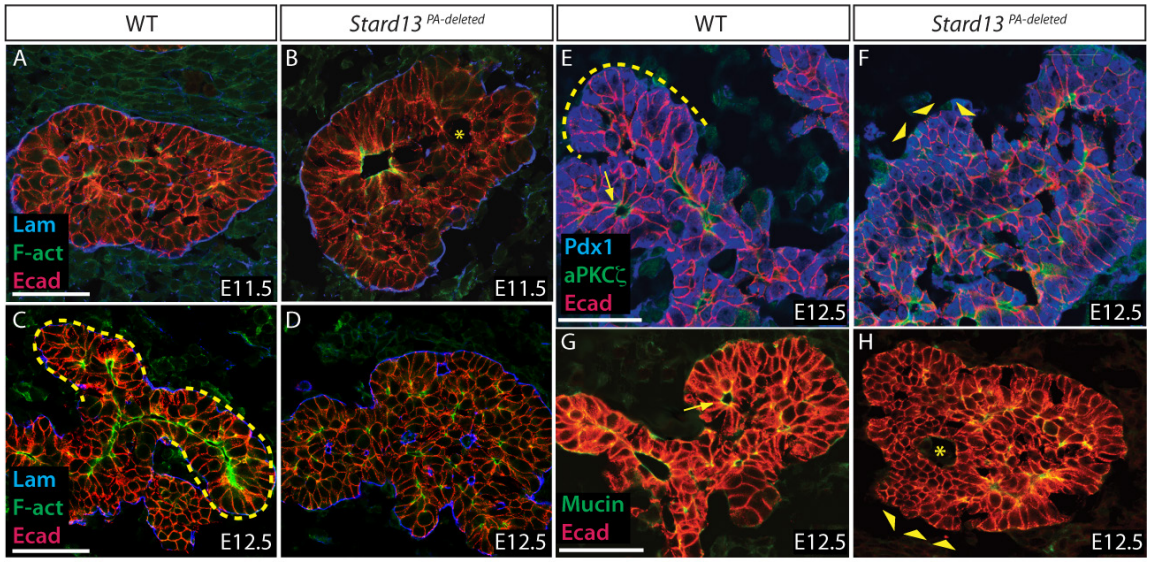

Figure 14: Epithelial remodeling defects in *Stard13*$^{PA\text{-}deleted}$ developing pancreas

(A-H) WT and *Stard13*$^{PA\text{-}deleted}$ pancreatic sections were analyzed for epithelial cell organization by immunofluorescence analysis for Laminin (Lam), F-actin (F-act), E-cadherin (Ecad), Pdx1, aPKCζ and Mucin-1 at E11.5 (A-B) and E12.5 (C-H). Apical markers, F-actin, aPKCζ and Mucin-1 were properly expressed at the cell membranes facing lumina in WT and some microlumina in mutant pancreas. Yellow arrows indicate lumina surrounded by a continuous layer of epithelial cells with typical cylindrical shape in (E) and (G). Asterisks indicate cavity surrounded by non-polarized cells in (B) and (H), that show E-cadherin all around the cell periphery. Yellow dashed lines mark the tip of the branches in (C) and (E). Yellow arrowheads indicate stratified tissue areas in (F) and (H). Scale bars, 50 µm (A-H).

First, I compared cell-polarity patterns between WT and mutant epithelia, from E11.5 onward. In WT tissue between E11.5 and E12.5 epithelial cells started to i.) orient themselves concertedly in the same direction and ii.) acquire columnar polarized shape with the apical pole facing a luminal network and the basal pole contacting the basal lamina, gradually resolving into a monolayer of cells (Figure 14A,C,E). Polarized cells displayed E-cadherin at the basolateral membrane and F-actin, aPKCζ, Mucin1 at the apical surface, whereas Laminin was localized at the basal membrane (Figure 14A,C,E,G). The *Stard13*-ablated

pancreatic tissue did not undergo similar epithelial remodeling, as in the WT (Figure 14C-D). At E12.5, the epithelium stayed stratified (see arrowheads in Figure 14), cells displayed cuboidal shape and were randomly oriented to surround scattered microlumina (Figure 14D,F,H). Apico-basal polarity was overall established, displaying F-actin, Mucin1 and aPKCζ at the apical pole of the cells that surrounded microlumina, Laminin at the basal membrane and E-cadherin at the basolateral membrane (Figure 14B,D,F,H). Occasionally, Laminin was detected inside the epithelium (Figure 14D).

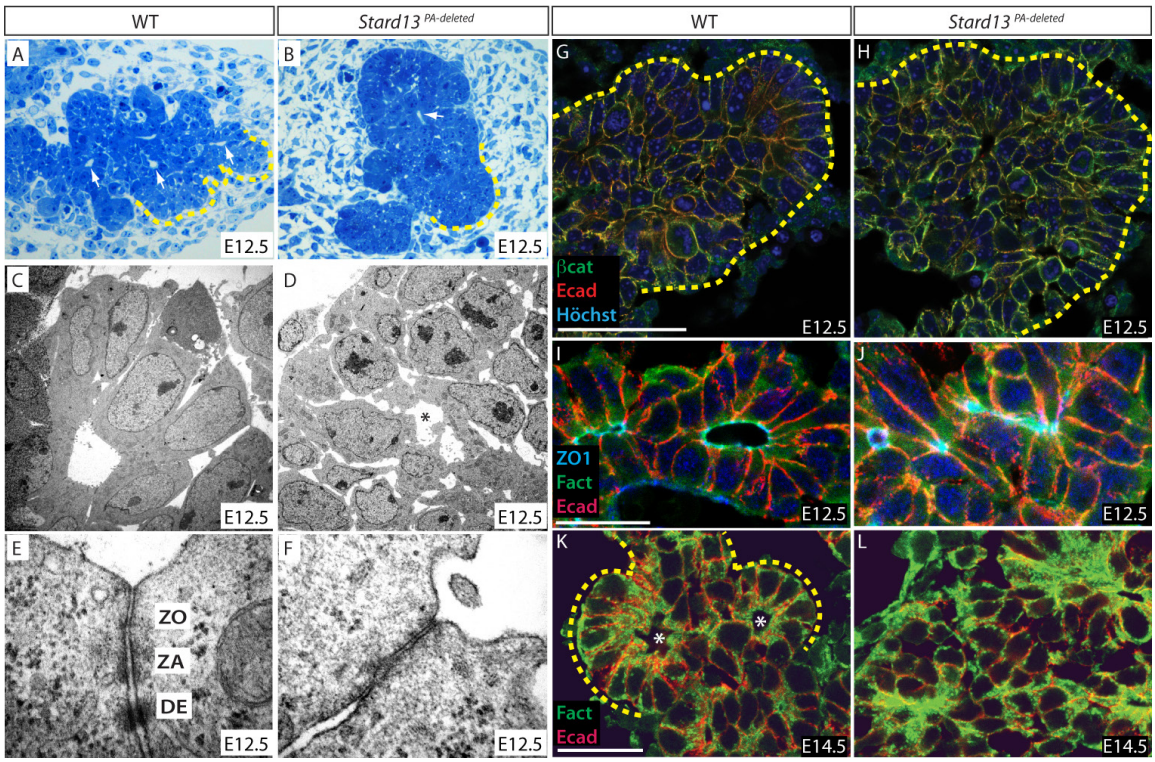

Figure 15: Defects in epithelial cell organization in *Stard13*$^{PA\text{-}deleted}$ pancreata

(A-B) E12.5 WT and *Stard13* mutant pancreatic epithelium with microlumina (white arrows). (C-F) TEM analysis shows WT cells of cylindrical shape surrounding common lumen (C), and mutant cells displayed cuboidal shape and were randomly oriented around microlumen (demarcated by asterisk, D). (E) Typical apical junctional complexes, including tight junction (ZO, "Zonula occludens"), adherens junction (ZA, "Zonula adherens") and desmosomes (DE) were detected in WT pancreatic epithelium (E). In contrast, only immature junctional complexes were found in the mutant epithelium (F). (G-H) Immunofluorescence stainings showed β–catenin distribution to cell basolateral membranes in WT and mutant pancreas at E12.5. (I) Immunostaining for ZO-1 protein at the apical edge of junctional complexes. (J) *Stard13* mutant tissue showed a dispersed localization of ZO-1 and increase in cytoplasmic F-actin staining. (K-L) At E14.5, a higher increase in cytoplasmic F-actin staining is visible in the mutant vs. WT pancreas. Note future duct openings demarcated by white stars in (K). Yellow dashed lines mark tissue peripheries in (A), (B), (G), (H), (K). Magnification, 20x (A-B), 4000x (C-D), 100.000x (E-F). Scale bars, 50µm (G-H), 20 µm (I-L).

Second, I focused on characterizing cell-cell adhesion and cytoskeleton organization in the developing pancreas. Ultrastructural analyses emphasized the differences in cell shape, cell arrangement around lumina and cell-cell junctions between WT and *Stard13* mutant tissue

(Figure 15). In the E12.5 WT pancreas, epithelial cells were of cylindrical shape and surrounded microlumina in an ordered fashion, displaying constriction at the apical lumen-facing side and basal nuclei (Figure 15A,C). Typical apical junctional complexes, such as tight and adherens junctions as well as desmosomes, were present at E12.5 in the WT (Figure 15E). By contrast, at E12.5 mutant cells showed cuboidal shape and surrounded occasional microlumina in a disorganized fashion (Figure 15B,D). Moreover, mutant epithelial cells formed immature junctional complexes, composed of adherens-type junctions and tight junctions, but devoid of typical desmosomal plaque (Figure 15F). Accordingly, discrete distribution of the tight junction-specific protein ZO-1 was seen at the boundary between apical and lateral domains in WT cells facing lumina (Figure 15I,J), while ZO-1 irregularly accumulated in clusters in the *Stard13* mutant.

β–catenin plays a role in cell-cell adhesion through binding to the cytoplasmic domain of type 1 cadherins, e.g. E-cadherin, and linking them through α-catenin to the actin cytoskeleton [**72**]. To address if β–catenin distribution was perturbed at the time when the most obvious branching problems occured in *Stard13*$^{PA\text{-}deleted}$ pancreata, I analyzed the localization of β–catenin at E12.5. In WT pancreas β–catenin localized to the basolateral membrane of the cells overlapping with E-cadherin staining (Figure 15G). Similar distribution of β–catenin was also observed in the mutant at E12.5, ruling out the possibility that perturbed β–catenin signaling underlied the remodeling defects of *Stard13*$^{PA\text{-}deleted}$ pancreata (Figure 15H).

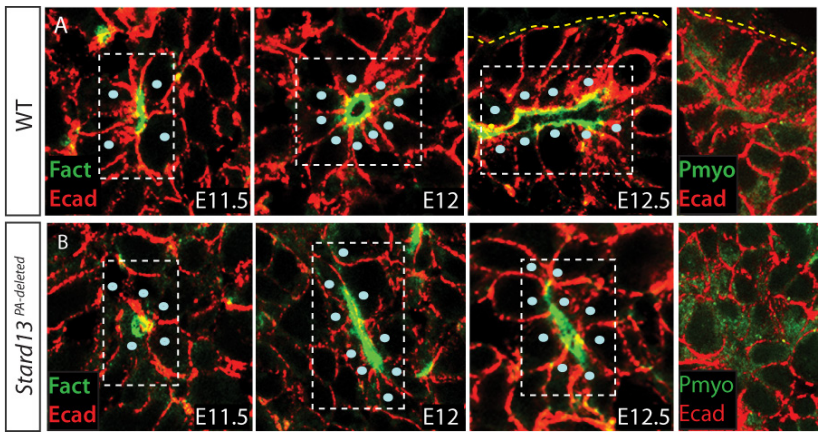

Figure 16: Formation of "rosette-like" structures in the developing pancreas

(A-B) Immunofluorescence analysis of F-actin and P-myosin (Pmyo) showed dynamics of rosette formation between E11.5 and E12.5 in WT and *Stard13*$^{PA\text{-}deleted}$ pancreatic epithelia (circumscribed by white boxed areas). Dots indicate the center of each cell in the "rosette-like" structures. Yellow dotted lines indicate the tissue borders.

Third, we examined the structural components of the cytoskeleton in the developing pancreas, including microfilaments and intermediate filaments. Importantly, I found that the two main cytoskeletal components actin (F-actin) and non-muscle myosin (activated phospho-Myosin II) not only accumulated to high levels but also were irregularly distributed

throughout the cytoplasm of *Stard13* mutant cells (Figure 15J,L & Figure 16B). In WT pancreatic cells F-actin and phospho-Myosin II (Pmyo) staining was polarized at the apical membrane of cells, which lined microlumina (Figure 16A). Polarized distribution of actinomyosin network normally form cable-like structures that span multiple cells and their coordinated apical contraction result into multicellular structures, which are named rosettes in various epithelial tissues undergoing morphogenesis [**70**]. Upon closer analysis of E11.5 and E12.5 WT pancreas epithelium, similar "rosette-like" structures were detected. F-actin and phospho-Myosin II were enriched at the apical pole of WT cells in forming rosettes (E11.5), in high-order vertices (E12) and in resolving rosettes (E12.5), in which cell aggregates constricted their shared interfaces to form continuous lumina (Figure 16A). By contrast, *Stard13*$^{PA\text{-}deleted}$ epithelial cells occasionally clustered together at a common interface, lacking localized actinomyosin distribution and coordinated apical constriction (Figure 16B). Consequently, fewer higher-order rosettes were formed and did not properly resolve (Figure 16B).

Keratins are epithelial-specific intermediate filaments and represent the largest component of the cytoskeleton. Cytokeratin 8 (CK8) has been shown to localize at the apical region of pancreatic acinar cells and to anchor to desmosomes [**108**]. I analyzed whether the distribution of CK8 was perturbed in the *Stard13* mutant pancreatic epithelium during branching stage. In E12.5 WT pancreatic tissue, I detected CK8 close to the apical domain of cells surrounding lumina (Figure 17A'-A''), being localized right below the F-actin cytoskeletal network. Interestingly, delaminating endocrine precursor cells, which were weakly positive for PDX1^{+}, showed strong CK8 expression throughout the cytoplasm (Figure 17A').

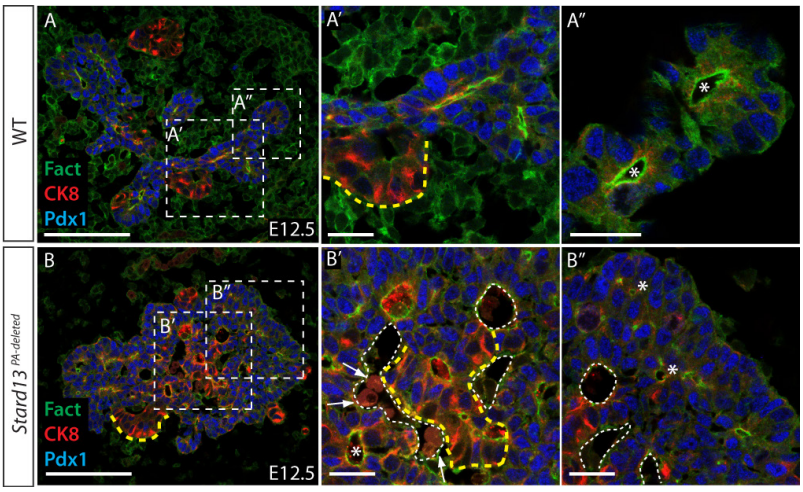

Figure 17: Intermediate filament assembly in *Stard13*$^{PA\text{-}deleted}$ epithelium

(A-B'') Immunofluorescence analysis of E12.5 WT and mutant pancreatic tissue for Cytokeratin8 (CK8) and F-actin (Fact). A', A'' and B', B'' are higher magnifications of the micrographs in A and B, respectively. Yellow and white dotted lines circumscribe delaminating CK8^{+} cells and cystic spaces, respectively. White asterisks indicate microlumina. White arrows point out pyknotic cells. Scale bars, 100 µm (A,B), 20 µm (A'-A'', B'-B'').

Upon *Stard13* ablation in the mutant tissue, the intermediate filament CK8 was irregularly distributed within the cytoplasm of stratified epithelial cells, similarly to the disorganized F-actin cytoskeleton (Figure 17B, B''). Apical localization of CK8 was still detectable to some extent in some of the cells facing the small microlumina (see white asterisks inFigure 17B''). Figure 17B' shows large cystic spaces (demarcated by white lines), which were surrounded by unpolarized cells, devoid of any apical membrane marker, including CK8. These cystic spaces were filled by rounded cells with pyknotic nuclei (Figure 17B'). Moreover, in the mutant epithelium, I detected cells with very bright CK8 staining in the whole cytoplasm, that were reminiscent of delaminating cells in the WT (Figure 17A',B-B', yellow line). However, unlike the WT delaminating endocrine cell population, these mutant cells localized not only at the tissue periphery, but also inside in the epithelium (Figure 17B,B', yellow line).

Collectively, these results suggest defects in the actinomyosin and intermediate filament cytoskeletal organization as the source of defective pancreatic epithelium remodeling, including impairments in cell-shape change, ""rosette-like"" formation, cell arrangement and microlumina connection in *Stard13* mutants. These initial remodeling processes appear to be crucial for the progression of the stratified pancreatic epithelium towards a branched monolayered epithelium with typical tip and trunk tissue architecture.

2.9 Cell-Extracellular Matrix Adhesion Is Established in *Stard13* Mutant Pancreas

Cell adhesion to the ECM is established through FAs, macromolecular assemblies, which include FAK, heterodimeric Integrins, Talin, Vinculin and Paxillin (see also Chapter 1.2.4) [**64**]. During embryogenesis proper FA assembly and dynamics control branching morphogenesis [**74**]. For instance, *α7* and *α7integrin* double knock-out mouse showed pancreatic hypoplasia with decreased branching morphogenesis at E13.5-E16.5 [**73**]. $\alpha 6\beta 1-$Integrin heterodimers are also found in acinar and duct pancreatic cells of adult mice [**75**]. Therefore, I analyzed the establishment of FAs and Integrin distribution in the *Stard13*$^{PA\text{-}deleted}$ pancreata. In particular, I compared the expression of subunits $\alpha 6-, \alpha 3-$ and $\beta 1-$Integrin and FA-components, FAK, Talin and Vinculin, in the WT vs. *Stard13*$^{PA\text{-}deleted}$ pancreas.

In preliminary qRT-PCR assays I found that the expression levels of *α3, α7* and *β1integrin* were unchanged between WT and *Stard13* mutant E14.5 pancreata (Figure 18E). We also quantified $\alpha 6$- and $\beta 1-$Integrin protein levels by Fluorescence activated cell sorting (FACS) analysis and identified the same percentage of $\alpha 6$- and $\beta 1-$Integrin protein

expressing pancreatic cells in WT and mutant E13.5 pancreas tissue (data not shown). In line with this, the levels of FAK and p-FAK (active phospho-Tyr397) were the same in both WT and mutant, as shown by Western blot analysis (Figure 18F).

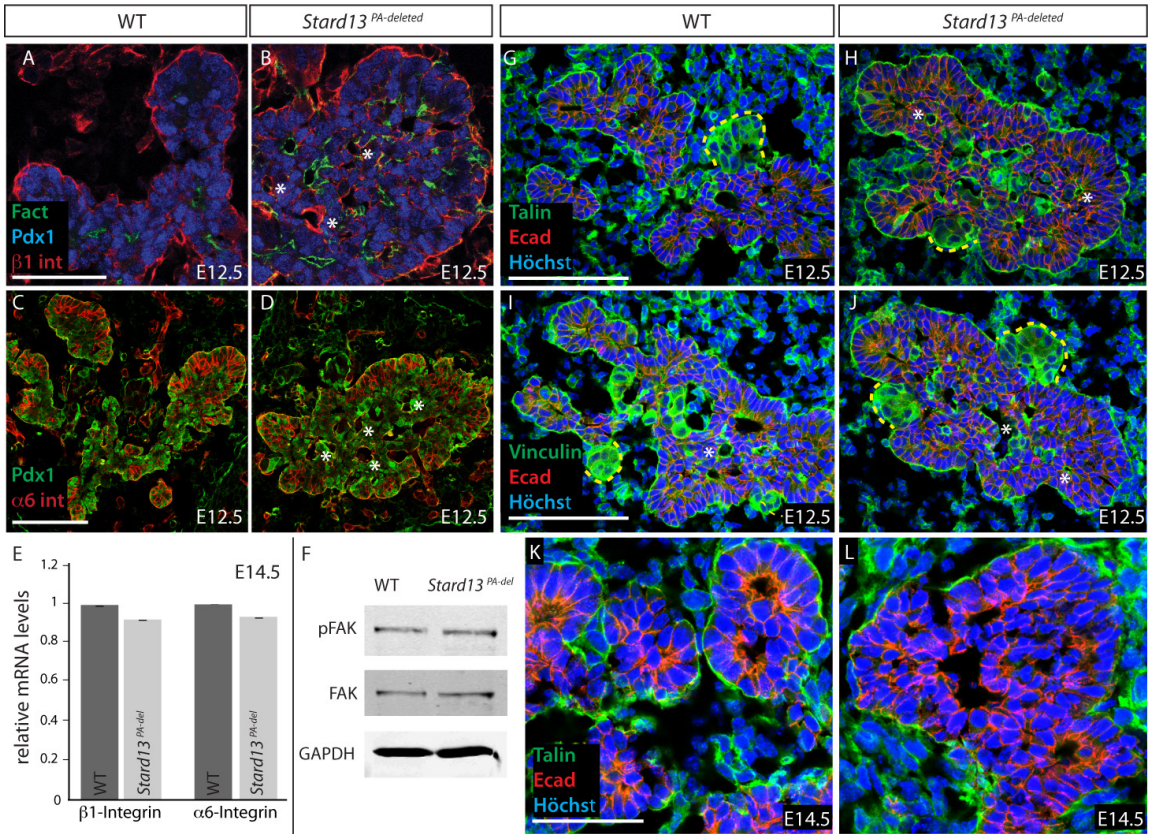

Figure 18: Cell-ECM connection via focal adhesions in the pancreatic epithelium

Immunofluorescence staining on pancreatic E12.5 and E14.5 sections with antibodies against FA molecules. (A-B) At E12.5, β1–integrin localized at basal membranes in WT and mutant. (C-D) α6-integrin localized to the basolateral membrane of tip cells in WT pancreas and cells at the tissue periphery in the mutant. Cells lining cystic spaces in mutant tissue showed diffuse basal staining of α6–Integrin. (E) Quantitative real-time PCR of *β1-Integrin* and *α6-integrin* mRNA levels (normalized to 36B4 and SDHA) in pancreatic tissue of WT and *Stard13*$^{PA\text{-}deleted}$ E14.5 embryos. (F) WB analyses of E14.5 showed no change of pFAK and FAK levels in WT vs. mutant pancreatic lysates. (G-L) Talin and Vinculin are both localized at the basal membrane in WT and *Stard13* mutant pancreas. Delaminating cells at E12.5 showed instense cytoplasmic staining of Talin and Vinculin (see yellow dashed lines). White asterisks indicate cyctic spaces in mutant tissue. Scale bars, 50 µm (A-B, K-L), 100 µm (C-D, G-J).

Next, I analyzed the distribution of FA components α6– and β1–Integrin, Talin and Vinculin. In line with previous reports, β1-Integrin was detected at the basal lamina of E12.5 WT pancreas (Figure 18A). Similarly, α6–Integrin was detected at the basolateral membrane, but exclusively in cells located at the branching tips (Figure 18C). In the E12.5 mutant epithelium, β1-Integrin localized not only to the basal membrane of peripheral pancreas cells, but also lined cystic spaces inside the tissue (Figure 18B). α6–Integrin distribution was maintained at the basolateral membrane of mutant cells, but also in cells lining cystic spaces

(Figure 18D). Talin and Vinculin were detected at the basal lamina in E12.5 and E14.5 pancreas tissue of both WT and mutant embryos (Figure 18G-L, data not shown). Moreover, cells facing cystic spaces in E12.5 mutant tissue were stained for Talin and Vinculin similarly to what observed for β1– and α6–Integrin (Figure 18H,J). Altogether, cell-ECM connection in *Stard13*$^{PA\text{-}deleted}$ mutant pancreas were established, FA complexes were assembled and localized to the cell membrane in a similar fashion as in the WT. Intriguingly, I found α6–Integrin exclusively expressed at the tip of branches, being a possible marker of MPCs or involved in tip morphogenesis. The major difference detected in the mutant was the localization of α6–Integrin staining around the periphery of the tissue and the presence of FA components decorating the cystic spaces inside the tissue. The α6–Integrin mislocalization could be a secondary effect of the lost tip and trunk structure, or alternatively it might be one of the reasons for altered morphogenesis and loss of typical branches in *Stard13* mutant pancreas, suggesting that α6–Integrin might play a role in branching morphogenesis in the pancreas.

2.10 Analysis of Vascularization of *Stard13* Mutant Pancreas Tissue

The vascular endothelium establishes close intercellular connections with the pancreatic epithelium during embryogenesis and controls essential steps of pancreas development, such as growth and differentiation, immediately after organ specification [**109**]. During pancreatic branching, endothelial cells establish tight connection with the trunk epithelium, but are located distantly from tip cells, exerting a negative impact on the growth of the epithelium [**110**] [**109**]. Subsequently, at later stages the endothelium influences endocrine differentiation and, in particular, β-cell maturation, establishing direct contact with the endocrine islets (Figure 1) [**8**] [**111**] [**112**]. Since tissue architecture is perturbed in the *Stard13* mutant pancreas, I asked the question if this might have an impact on endothelial cells and blood vessel formation.

To this aim, I performed immunostaining for the Platelet endothelial cell adhesion molecule (PECAM)-1 on E12.5 and E14.5 pancreas cryosections. In E12.5 WT pancreas, endothelial cells were visible surrounding the epithelial branches and in close association with the delaminating endocrine clusters (Figure 19A). E12.5 mutant pancreas exhibited internal cystic spaces, which contained pyknotic cells and were marked by basal membrane proteins, such as Laminin, Integrins, Talin and Vinculin (see also previous Chapter 2.8, Figure 14D and Chapter 2.9, Figure 18B,D,F,H). Interestingly, the endothelial PECAM-1^{+} cells surrounded the borders of these cystic spaces too. These results suggest that endothelial cells might remain trapped inside the epithelium, which did not properly resolve into a

monolayer, or that they invade the epithelium as a consequence of immature cell-cell adhesion (Figure 19B'). Further analysis is required to better characterize vascular endothelial cells and to distinguish between these two possible defects [**113**]. At E14.5, WT endothelial cells were properly interconnected to form a vascular plexus, which surrounded the pancreatic epithelium, whereas in the *Stard13* mutant endothelial cells appeared disconnected from each other, indicating differences in the degree of vasculogenesis between WT and mutant (Figure 19C,D).

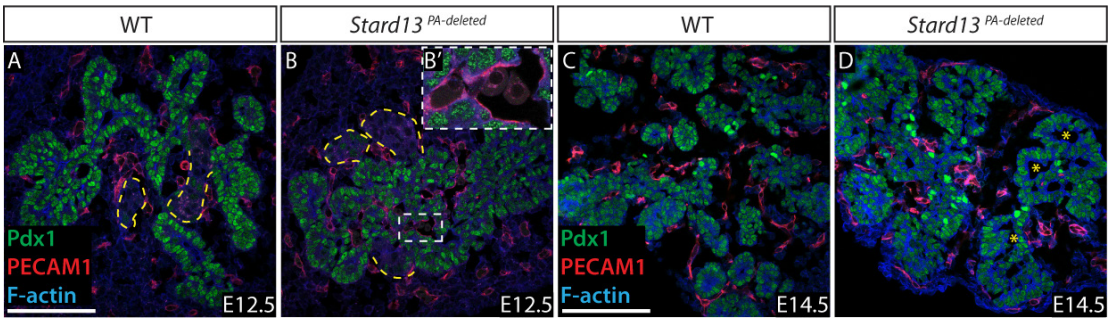

Figure 19: Endothelial cell organization in *Stard13*$^{PA\text{-}deleted}$ embryos

(A-D) Immunofluorescence stainings on pancreatic E12.5 and E14.5 sections showed that endothelial PECAM-1^{+} cells differentiate in WT as well as *Stard13* mutant pancreata. Yellow doted lines indicate delaminating endocrine cells. (B) PECAM-1^{+} staining was observed inside luminal spaces in mutant tissue. B' is a higher magnification micrograph of B, showing pyknotic cells inside one luminal space. (C-D) At E14.5, differences in vasculogenesis were evident between WT and mutant pancreata. Yellow asterisks mark wide open duct structures in mutant pancreatic epithelium. Scale bars, 100 µm (A-D).

2.11 The RhoGAP Protein STARD13 Regulates Rho Signaling in the Pancreas

The protein STARD13 contains a conserved RhoGAP domain, which is well-known for inactivating Rho-GTPases by promoting GTP hydrolysis (see also Chapter 1.2.6, Figure 5). STARD13 has been shown to preferentially regulate the small GTPase RhoA and with less affinity Cdc42 *in vitro*, but its *in vivo* activity has remained unknown [**85**] [**90**].

To elucidate the molecular mechanism of STARD13 function *in vivo*, we first tested whether it negatively regulates Rho activity in the pancreas. We hypothesized that *Stard13* gene ablation leads to elevated levels of active GTP-bound RhoA in the pancreas. Two independent assays were performed: a pull down and an immunolocalization assay (Chapter 4.6.3). Both assays are based on the use of the Rho-binding domain of the Rhotekin Rho effector protein fused to Glutathione-S-transferase (RDB-GST), as substrate [**114**]. These assays are designed to detect RhoA only in its activated GTP-bound stage.

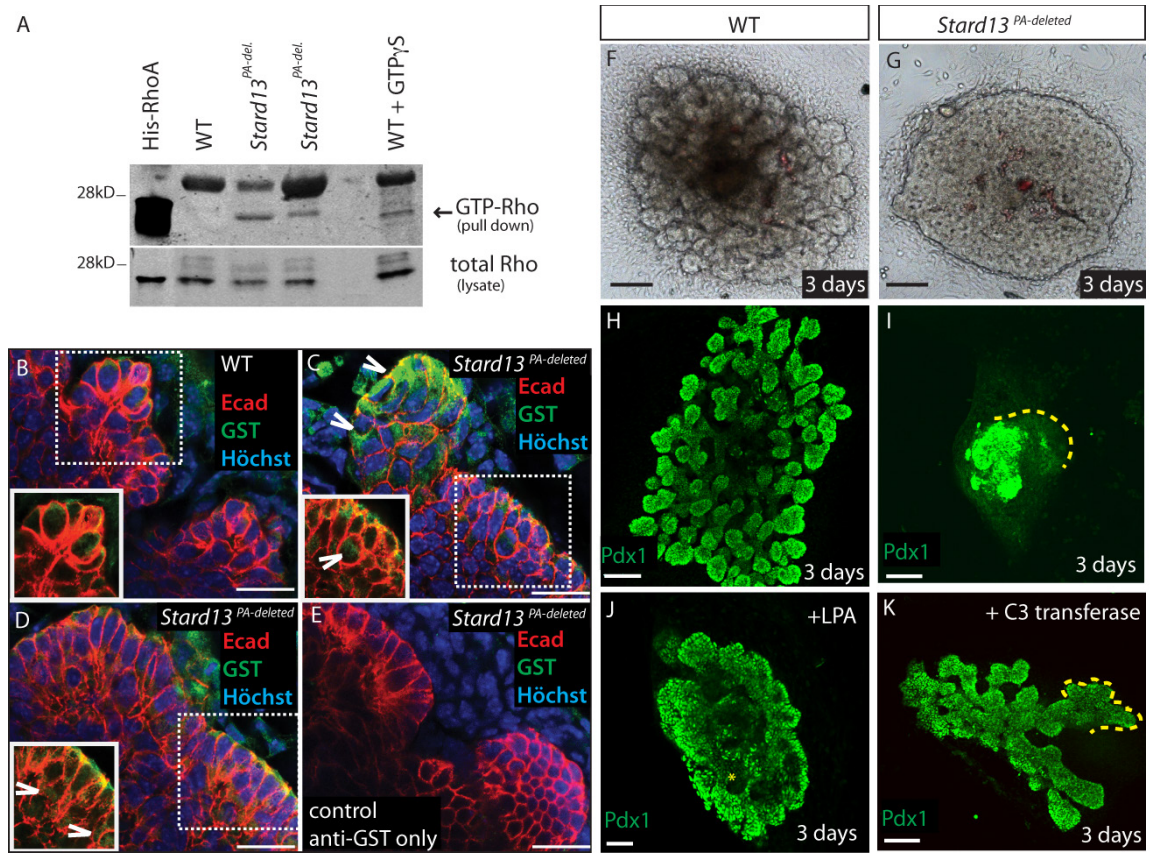

Figure 20: *Stard13* negatively regulates Rho activity in the developing pancreas

(A) Western blot analysis of E17.5 WT and *Stard13*$^{PA\text{-}deleted}$ pancreatic lysates after RDB-GST pull down. Pull-down (see arrow) and total lysates were immunoblotted with anti-RhoA antibody and recombinant protein His-RhoA was used as positive control. The band present above Rho is caused by aspecific binding to the RDB-GST beads. (B-D) Immunolocalization assay with GST-RDB on pancreatic organ cultures. Open arrowheads indicate localization of active Rho-GTP bound (GST; green) in Ecad^{+} pancreatic cells (red) in *Stard13*$^{PA\text{-}deleted}$ explants. Insets show dotted area without nuclear counterstain. (E) Pancreatic explant incubated with anti-GST antibody alone (negative control). (F-G) WT and mutant pancreas organ cultures dissected at E11.5 and cultured for 3 days. (H-K) Pdx1^{+} immunostaining of untreated WT (H) and *Stard13*$^{PA\text{-}deleted}$ (I), WT LPA-treated (J) and *Stard13*$^{PA\text{-}deleted}$ C3 transferase-treated (K) pancreatic explants cultured for 3 days. Red outline marks rescued branches in C3-treated vs. non-treated *Stard13*$^{PA\text{-}deleted}$ explants. Scale bars, 50 µm (B-G), 100µm (H-K).

First, using a RDB-GST pull-down assay we detected elevated levels of activated GTP-bound Rho in E17.5 pancreatic mutant lysates, while no detectable amounts were found in WT pancreas (Figure 20A). Second, to visualize GTP-bound Rho proteins, we performed an immunolocalization assay on pancreatic explant cultures [**113**] [**115**]. *Ex vivo* culturing of E11.5 pancreas provides a simple and valuable model system to analyze branching and tubulogenesis [**24**] [**68**] [**113**]. Pancreas organ culture recapitulates *in vivo* early pancreatic morphogenetic and differentiation events (Figure 20F) [**20**] [**24**] [**69**] [**113**]. The WT pancreatic explants showed tubules, which underwent extensive branching after 3 days (Figure 20F). Strikingly, *ex vivo* mutant pancreatic explants cultured in the same conditions as WT explants displayed smaller size and branching defects, reproducing the *in vivo* phenotype (Figure 10,

Figure 20G). The RDB-GST immunolocalization assay showed clusters of E-cadherin^{+} pancreatic cells exhibiting active Rho in *Stard13*$^{PA\text{-}deleted}$ explants (Figure 20C-D), while no staining was detected in WT cultures (Figure 20B,E). Both pull-down and immunolocalization assays indicate that STARD13 is important to restrain active Rho in the developing pancreas.

The phenotypical defects observed in *Stard13*$^{PA\text{-}deleted}$ pancreata are possibly due to elevated Rho activity. To address this possibility, we first tested if culturing pancreatic WT explants in the presence of the well-known Rho activator, lysophosphatic acid (LPA), mimics the *Stard13* mutant phenotype [**114**]. In line with our hypothesis, WT explants treated with LPA failed to branch and displayed smaller size when compared to untreated WT pancreatic explants (Figure 20H,J). This supports the notion that elevated Rho levels are responsible for the phenotype observed in *Stard13*$^{PA\text{-}deleted}$ pancreata. Second, we performed rescue experiments by exposure of *Stard13*$^{PA\text{-}deleted}$ explants to a membrane-permeable version of the enzyme C3 ribosyltransferase, which is known to inactivate Rho proteins, but not Cdc42 or Rac1. Importantly, upon exposure to C3-transferase mutant pancreatic explants underwent branching initiation and tubule formation and expanded in size, displaying partial rescue of the proliferation rate (Figure 20K, Figure 21G). Taken together, our findings underscored the role of *Stard13* as a tissue-specific negative regulator for the Rho signaling. Furthermore, we found that uncontrolled Rho activity is detrimental to proper pancreas formation.

2.12 Proliferative MAPK Signaling Is Downregulated in *Stard13*-Deficient Pancreas Epithelium

Epithelial–mesenchymal interactions are crucial for the development of the pancreas [**3**]. Continuous crosstalk with the surrounding mesenchyme affects differerentiation and proliferation of pancreatic epithelial cells. For instance, EGF and FGF growth factors are released by the pancreatic mesenchyme and control pancreas organogenesis, being required for epithelial growth and branching [**9**] [**116**].

We hypothesized that positioning MPCs at the tip of the epithelial branches is necessary to expose them to FGF/EGF mesenchymal signals, sustaining their proliferative potential. Since both EGF and FGF primarily act via the MAPK pathway, we analyzed the levels of phosphorylated activated p44/p42 MAPKs [also known as phospho-extracellular signal regulated kinase (pERK1/2)] in the pancreatic epithelium [**117**]. Interestingly, we found higher levels of activated pERK1/2 in the E12.5 WT pancreatic tip cells as well as in *ex vivo* explant

cultures (Figure 21A,C-C'). By contrast, pERK1/2 levels were globally reduced in *Stard13*$^{PA\text{-}deleted}$ tissue and loss of tip morphogenesis was accompanied by loss of pERK1/2 signaling regionalization (Figure 21B). Similarly, Western blots analysis showed that the levels of pERK1/2 proteins were substantially reduced in embryonic pancreas upon *Stard13* ablation, whereas total ERK, PI3K-Akt and FAK pathways were unaffected (Figure 18F, Figure 21F).

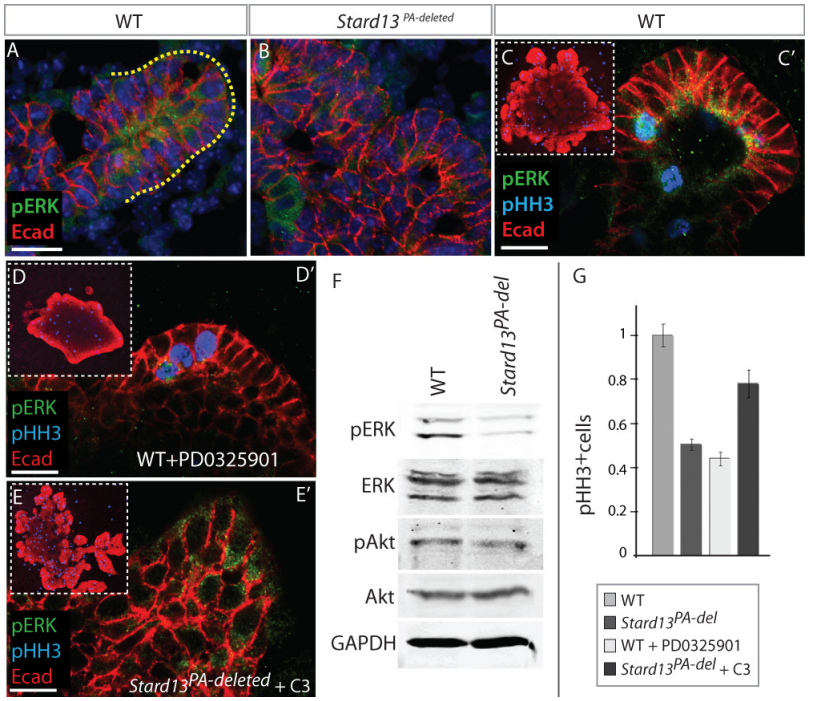

Figure 21: Active pERK signaling accumulates at the tip of pancreatic branches

(A-E') Immunofluorescence staining of pERK1/2 and E-cadherin on pancreatic E12.5 WT (A) and mutant cryo-sections (B), and whole-mount untreated WT (C), PD032590-treated WT (D) and C3-treated *Stard13*$^{PA\text{-}deleted}$ (E) pancreatic explants. Insets are smaller magnification mircographs of (C'), (D'), and (E') confocal optical sections. Yellow outline delineates pancreatic tip. (F) Western blot analysis of WT and *Stard13*$^{PA\text{-}deleted}$ pancreatic lysates. Probed with indicated antibodies. (G) Quantification of pHH3^{+} cells in indicated pancreatic explants. Scale bars, 20 µm (A-C, E-F).

To address whether the differential distribution of pERK1/2 is required for the growth of epithelial branches, we inhibited ERK-kinase activities by using the MEK1/2-selective compound PD0325901, in WT pancreatic explants [**118**]. Strikingly, all samples cultured for two days in the presence of PD0325901 were smaller than untreated WT pancreatic epithelium, displaying smooth surface with no signs of branching and lower pERK1/2 levels (Figure 21D-D'). In addition, we measured cell proliferation in WT, PD0325901-treated WT, *Stard13*$^{PA\text{-}deleted}$ and C3-treated *Stard13*$^{PA\text{-}deleted}$ pancreatic explants. Cell proliferation significantly fell in both PD0325901-treated WT and *Stard13*$^{PA\text{-}deleted}$ pancreatic cultures, exhibiting similar decreased rates (Figure 21G). Importantly, specific inhibition of Rho by C3 rescued pERK1/2 levels as well as cell proliferation in *Stard13*$^{PA\text{-}deleted}$ pancreatic explants at rates similar to WT explants (Figure 21F-G). These results suggest that proliferation of progenitors at the newly formed tips is supported by local activation of the ERK signaling.

Taken together, our results suggest that cells localized to the tips of the WT pancreatic branches during development (e.g. Cpa1^{+} progenitor cells) received signals from the

surrounding mesenchyme and locally activated the downstream ERK signaling, which in turn sustains their proliferative potential. In contrast, epithelial tips in *Stard13* mutant tissue were not well established and, as a consequence, progenitor cells were not properly allocated within the epithelium and unable to receive appropriate signals from the mesenchyme. This might explain the decreased pERK levels and proliferation activity of mutant progenitor cells, which ultimately resulted into a hypoplastic pancreatic phenotype (Figure 9C-D).

2.13 Investigating a Direct Influence of the Cytoskeleton on Cell Proliferation

Rho activation promotes actin polymerization and F-actin filaments accumulation, which in turn can regulate gene expression through the Megakaryoblastic leukemia 1 (MAL)/Serum response factor (SRF) transcriptional activity [**119**] [**120**]. To establish whether cell shape and actin cytoskeleton might directly influence transcription and proliferation in the pancreatic epithelium, we assayed for transcriptional activation of the actin-MAL-dependent genes *Serum response factor (Srf)* and *Vinculin (Vcl)* and the MAL/SRF target genes *Connective tissue growth factor (Ctgf)* and *Mitogen-inducible gene 6* (*Mig6)*, which is a negative regulator of the EGF/MAPK signaling (Figure 22A) [**119**] [**121**]. In the absence of *Stard13*, I observed an induction of Mig6 mRNA levels, being instead expressed at low levels in WT embryonic pancreas (Figure 22B). Accumulation of Mig6 in mutant compared to WT cells was also readily detected by immunofluorescence analysis (Figure 22C-D). I also found a comparable modulation of *Srf, Vcl* and *Ctgf,* confirming transcriptional activation of the actin-MAL /SRF signaling in the mutant (Figure 22B).

Ctgf is a common target for activated MAL/SRF and Hippo/Yes-associated protein (Yap) signalings and Yap has been recently shown to be modulated by high tissue-stiffness and Rho activity [**122**] [**123**]. I therefore examined the status and sub-cellular localization of the two mammalian components of the Hippo organ growth pathway, YAP and phosphorylated YAP (pYAP), in the embryonic pancreas. Importantly, both YAP and p-YAP level and distribution were unchanged in the *Stard13*$^{PA\text{-}deleted}$ tissue as compared to WT (Figure 22E-H). These observations indicate that despite active Rho and F-actin fibers accumulation in the absence of *Stard13*, there is no YAP modulation in the mutant pancreatic epithelium, differently from what reported in mesenchymal cells [**122**]. By contrast, my data suggest that F-actin accumulation converges into the MAPK cascade through MIG6, providing a mechanistic explanation for the reduced pERK levels in *Stard13*$^{PA\text{-}deleted}$ pancreatic epithelium (Figure 21B)**.**

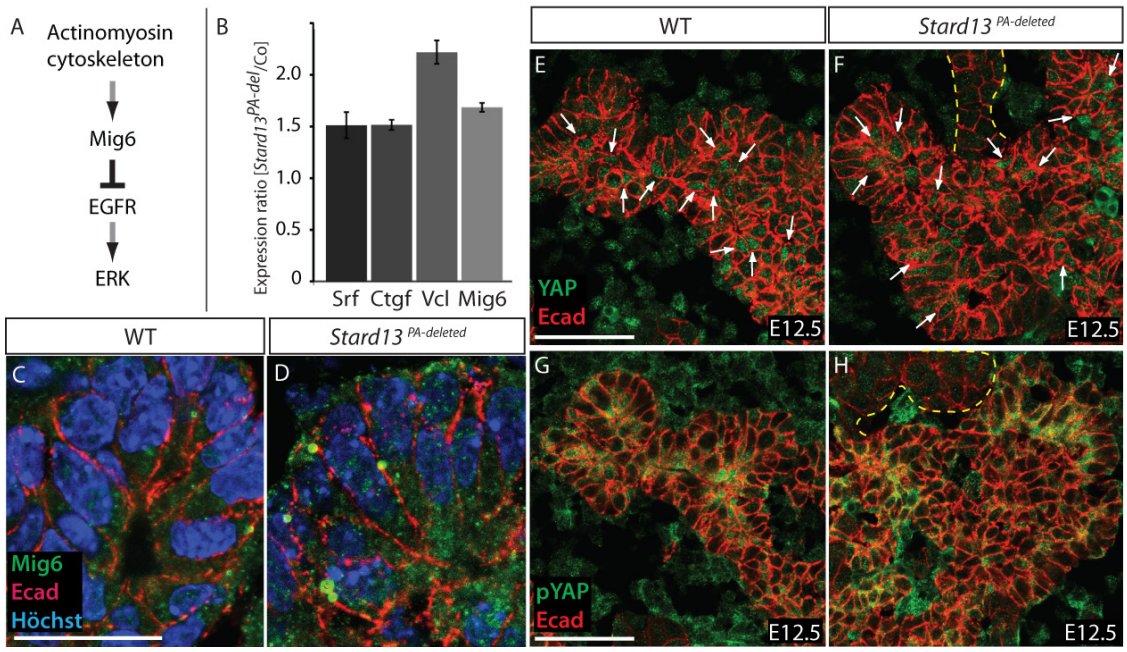

Figure 22: Direct influence of cytoskeleton on SRF/MAL transcriptional response

(A) Model suggesting direct negative regulation of ERK signaling via the cytoskeleton. Adapted from [**119**]. (B) Quantitative real-time RT-PCR showed induction of actin-Srf/Mal transcriptional activity in *Stard13*$^{PA\text{-}deleted}$ versus WT E14.5 pancreata. (C-D) Immunodetection of Mig6 on E12.5 cryosections. (E-F) Immunofluorescence staining for YAP and pYAP HIPPO pathway components in the WT and mutant pancreatic epithelium. White arrows indicate cells displaying nuclear YAP localization, without any clear regional distribution in the tip or trunk domains. (G-H) Cytoplasmic pYAP staining was detected in both WT and mutant epithelia. Note delaminating cells devoid of YAP and pYAP staining (yellow dashed lines). Scale bars, 50 µm (C-H).

3 Discussion

During embryonic development, coordinated growth and morphogenesis are important to ensure proper pancreas formation [**48**] [**49**]. In this study, we show that the new pancreatic factor *Stard13* is crucial for pancreas development, controlling branching morphogenesis through regulation of the Rho signaling (Figure 23A). Furthermore, our findings underscore that the establishment of correct tissue architecture is crucial to properly locate pancreatic progenitors within the tissue, ensuring normal organ growth.

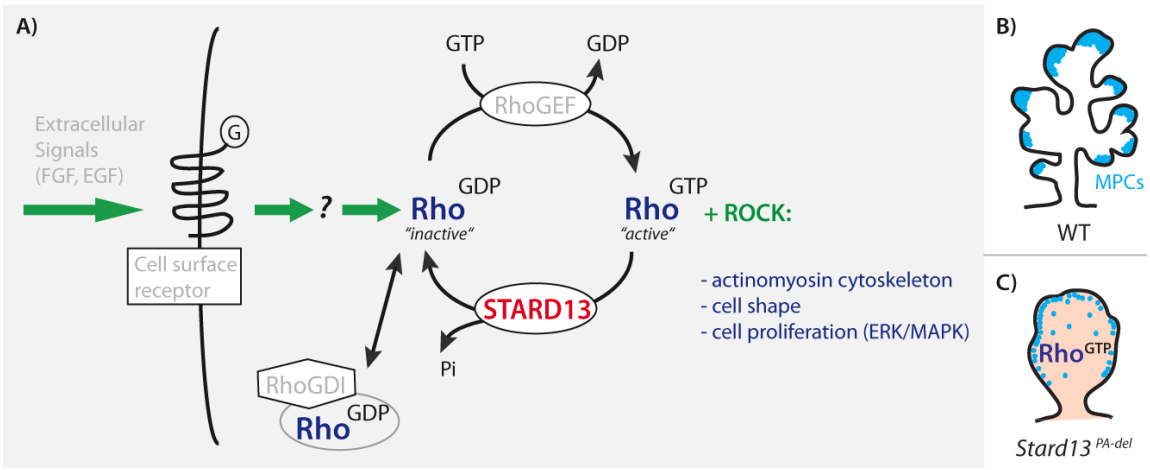

Figure 23: STARD13 regulation of Rho-signaling

(A) Schematic representation of Rho cycling in the pancreas. Through hydrolysis of GTP by the RhoGAP STARD13 downstream effectors are activated and important cell processes are regulated. (B) In WT pancreas MPCs (in blue) are located to the tips of branches. (C) *Stard13* ablation in the embryonic pancreas increases levels of activated GTP-bound Rho and branching of the organ is not initiated. MPCs are mislocalized.

3.1 *Stard13* Controls Proliferation of Pancreas Progenitors and Organ Growth

The *Stard13*$^{PA\text{-}deleted}$ pancreas shows remarkable organ hypoplasia, which starts to be evident at E14.5. In the pancreas, the mechanisms that regulate organ size are still poorly understood. It is known that compensatory growth, which is typical for example of the liver, does not occur. By contrast, pancreas growth relies heavily on the proliferation of progenitor cells, because the number of embryonic progenitor cells is established before E14.5 and defines the final organ size [**25**].

The branching tips during the transition from pancreas primary to secondary transition in embryogenesis harbor fast proliferating MPCs, which express *Cpa1* [**21**]. In *Stard13*$^{PA\text{-}deleted}$ pancreata the overall number of Cpa1^{+} MPCs is reduced. Additionally, proliferative MPCs (double positive for pHH3^{+} and Cpa1^{+}) is reduced by 40%, wheras the proliferation of non-tip

cells is only slightly affected (about 13% reduction). Therefore, defects we observe in MPC proliferation and/or reduction of the pancreatic MPC pool are responsible of pancreatic hypoplasia in the *Stard13*$^{PA\text{-}deleted}$ pancreas. Furthermore, the size of the progenitor pool could be reduced by accelerated differentiation of progenitor cells into exocrine, endocrine or duct cells. However, in the absence of *Stard13* differentiated exocrine, endocrine and duct cells are all specified and their relative numbers are unaffected, ruling out accelerated differentiation as reason for progenitor cell depletion.

Altogether, these data indicate that loss of MPC proliferative potential is responsible for the overall decrease of cell proliferation and the smaller progenitor pool in the mutant, which ultimately results in a hypoplastic phenotype. Our results further support the absence of compensatory growth in the pancreas and the importance of preserving a "reservoir" of progenitor cells in the pancreatic epithelium.

3.2 The RhoGAP STARD13 Regulates Pancreas Epithelial Remodeling through RhoGTPase signaling

Very little is known about branching morphogenesis and tubulogenesis and the mechanisms controlling these events in the developing pancreas. Branching morphogenesis involves remodeling of the pancreatic epithelium, from a non-polarized stratified epithelium into a monolayer of polarized cells lining a complex tubular network [**2**] [**20**] [**69**]. This process initiates between E11.5 and E12.5 in the mouse pancreas.

Small GTPases, such as Cdc42 and Rac1 have been shown to control different aspects in pancreas morphogenesis, including tubulogenesis and islet cell migration (Chapter 1.2.6) [**78**] [**69**]. We characterize here the role of another GTPase, Rho, in pancreas morphogenesis. We show that active Rho protein is detrimental to epithelial morphogenesis in the pancreas and its activity needs to be tightly regulated by the RhoGAP STARD13 during pancreatic development (Figure 23). Indeed, *Stard13* mutant epithelium at E12.5 shows failure of branching and several defects in cell morphology and cytoskeleton organization. Also, activation of Rho signaling by LPA in WT pancreata induces failure of branching.

So far, very few RhoGAPs have been studied *in vivo* in mammals [**124**] [**80**]. STARD13 is the first example of a RhoGAP protein to act in a tissue-specific manner in the developing pancreas [**71**]. RhoGAP proteins can form large molecular complexes and act simultaneously on multiple GTPases [**79**]. For example, DLC2, the human homologue protein of STARD13, has GAP specific activity for RhoA and with less affinity for Cdc42 *in* vitro [**88**]. Moreover,

crosstalk between different RhoGTPases has been described in other contexts [**125**] [**126**] [**127**]. In *Stard13*$^{PA\text{-}deleted}$ pancreata Rho activity is upregulated *in vivo*. In the mutant, inhibition of Rho or its downstream effector ROCK restores the WT pancreatic phenotype, ruling out *Stard13* activity on other small GTPases, like Cdc42, in the developing pancreas [**87**]. Cdc42 acts to establish functional and mature apical polarity surfaces by interacting with the Protease activated receptor (Par) 3/Par6/aPKC polarity complex [**125**] [**128**]. Previous work shows that upon Cdc42 ablation the pancreatic epithelium fails to generate multicellular common apical surfaces. Autocellular lumina are formed and apical markers accumulate inside vacuoles, resulting into a fragmented epithelium without proper tubulogenesis [**69**]. *Stard13*$^{PA\text{-}deleted}$ mutants do not show similar phenotypical features: autocellular lumina are not detected; microlumen formation and apicalbasolateral (eg. PKCζ/mucin/laminin) polarity are properly initiated. In conclusion, Cdc42 and Rho GTPases seem to exert opposite activities in pancreas morphogenesis and STARD13 controls only Rho cycling in the embryonic pancreas. However, this does not exclude a potential crosstalk amongst these two GTPases. For instance, the fact that Cdc42 knockout phenotype is partially rescued in pancreatic organ culture upon addition of a ROCK-inhibitor compound [**69**] might suggest a crosstalk between the downstream Rho-effectors ROCK and Par/PKC.

The *Drosophila melanogaster* orthologue of *Stard13* is called *crossveinless-c (cv-c)* and has been shown to coordinate epithelia morphogenesis and actin reorganization in multiple tissues, including Malpighian tubules, midgut, posterior spiracles and tracheal epithelium by regulating Rho1 cycling *in vivo* [**129**] [**130**]. The common feature among the different morphogenetic processes regulated by *Cv-c* activity is the coordinated reorganization of large groups of cells during tissue remodeling [**129**] [**130**]. This is highly reminiscent of STARD13 activity in the mouse pancreatic epithelium, suggesting an evolutionarily conserved function of this RhoGAP family in epithelial morphogenesis.

A precise spatio-temporal regulation of Rho activity is a prerequisite for proper assembly and tension of the actinomyosin cell cytoskeleton, which undergoes highly dynamic changes during organ morphogenesis [**76**] [**77**]. Uninhibited Rho activity in *Stard13*$^{PA\text{-}deleted}$ embryos has a profound impact on the organization of the actinomyosin network hampering epithelial remodeling events, including cell shape changes and “rosette-like” multicellular structure formation. The formation of multicellular rosettes provides an efficient mechanism for rearrangement of cells into a single epithelial layer [**70**]. For example, in the *Drosophila melanogaster* germ-band epithelium actinomyosin network accumulates at the apical pole of cells, forming cable-like structures that span multiple cells, and their coordinated apical constriction result in multicellular structures, which are called rosettes [**70**]. Rosette

structures are known to resolve through cell intercalations, providing directional elongation [**70**]. Similarly to other elongating epithelia, we have found multicellular "rosette-like" structures in the pancreatic epithelium at the time when epithelial remodeling starts, suggesting that rosette arrangements might contribute to the transition from a stratified to a monolayered epithelium in the pancreas. In line with this, in the absence of *Stard13* very few high-ordered rosettes are formed and the epithelium stays stratified. Moreover, in the *Stard13* mutant cytoskeleton components, such as actin and myosin, accumulate at high levels as stress fibers throughout the cytoplasm of the cells, displaying irregular distribution. These defects hamper concerted apical cell constriction and formation as well as proper resolution of "rosette-like" structures. Finally, it is conceivable that proper arrangement of these multicellular structures is important for coalescence of the microlumina in the developing pancreas in order to form continuous ducts. Monitoring and quantifing rosette formation in the 24h window of time between E11.0 to E12.0 using time-lapse imaging and image analysis software will be used to better understand their contribution to pancreas morphogenesis. In summary, the phenotype observed in *Stard13*$^{PA\text{-}deleted}$ pancreata suggests that in WT pancreas Rho activity has to be tightly regulated in order to ensure coordinated actinomyosin contraction, which drives apical cell constriction, rosette formation and, possibly, microlumina connection/resolution into elongating tubules.

Formation of branches and tubes from non-polarized groups of cells requires proper establishment of cell polarity, as first step. Previous studies have shown that cell-cell adhesion coincides with the development of cell surface polarity in epithelia and represents one of its major triggering mechanisms [**128**] [**131**]. In *Stard13*$^{PA\text{-}deleted}$ pancreata few scattered cells, which surround microlumina, aquire apical polarity features at the membrane, while most of the cells display immature epithelial junctional complexes, as seen by TEM. E-cadherin and β-catenin proteins are both detected at the basolateral epithelial membranes of *Stard13* mutant cells, ruling out major defects in adherens-junction-mediated cell-cell adhesion. On the other hand, cell-cell connections via apical junctions are immature, especially desmosomes are not present. Desmosomes provide strong adhesion to maintain tissue architecture. In the mammary gland, for example, desmosomes play a role in epithelial morphogenesis and are important to position cells, independently of E-cadherin-mediated adhesion [**132**]. Desmosomes are also known as anchor of CK8-positive intermediate filaments, which normally accumulate at the apical membrane of embryonic and adult pancreatic cells [**108**]. CK8 apical localization is in part lost in mutant epithelial cells, being mostly irregularly distributed in the cytoplasm.

The suppression of Rho is a normal part of polarity development in epithelia [**133**] [**127**]. For instance, it is known that dynamic cycling of Rho activity is crucial for maturation of cell-cell adhesion [**131**]. The absence of proper Rho cycling in *Stard13*$^{PA\text{-}deleted}$ pancreas might result into immature cell-cell adhesion, which in turn hamper the spreading of cell-polarity throughout the epithelium. Weakness in cell-cell connections and immature desmosomal structures in *Stard13*$^{PA\text{-}deleted}$ pancreata might be the cause not only of epithelial polarity defects, but also of malformed ducts and wide open lumina in acini at later stages. Moreover, activation of RhoA results in inversion of polarity in MDCK cells, which could be reversed by knockdown of RhoA, ROCK and myosin II [**127**]. In the absence of *Stard13*, we observe large luminal spaces that form inside the pancreatic epithelium and are often filled with pyknotic cells. The cells lining these spaces display a set of basal polarity markers, such as Laminin, Talin and Vinculin, suggesting that uncontrolled Rho activity might be here responsible for inversion of cell polarity inside the pancreatic tissue. Alternatively, cystic spaces might be artefacts of cryosectioning though similar spaces are never found in WT tissue. A final answer about the origin of these cystic spaces and if they are connected to the ECM will come from more detailed 3D analysis of pancreatic explants [**113**].

Rho is known also to control cytoskeleton contraction in migrating cells [**133**] and the immature cell-cell junctions could underlay impaired cell migration within the tissue. Indeed, active cell migration of newly formed cells could be part of localized proliferation/growth of the branches. If solely proliferation of cells within the pancreatic tissue “pushes” cells outward promoting branching or if additionally active cell migration of epithelial cells occurs in the developing pancreas needs to be investigated. Real-time analysis of dynamic processes, such as migration is required [**113**].

In summary, we propose that defects in cytoskeletal organization are primarily responsible of defective epithelial remodeling, including cell-shape changes, cell arrangement and microlumen connection in *Stard13* mutants.

3.3 Positioning of MPCs at the Tip of the Pancreatic Epithelial Branches

During organ development, morphogenesis enables allocation of different cell types to distinct locations in the epithelium [**134**]. For example, at the onset of branching morphogenesis various epithelia, including the lung, kidney, pancreas display their progenitor cells at the distal tips of the branches, which might define a special supporting “niche” for fast proliferating progenitors [**21**] [**135**] [**24**]. Accordingly, at E12.5, we and others have found that pancreatic multipotent Cpa1^{+} progenitor cells are preferentially localized to the tips of the branches, where they are more exposed to the surrounding mesenchyme than the cells

inside the tissue, like the endocrine *Ngn3*$^{+}$ progenitors [**21**]. The preferred tip localization is suggestive of the existence of a presumptive "niche" defined by signals that are released from the mesenchyme and/or by epithelium-mesenchyme cell interactions. During pancreas secondary transition *Stard13* expression becomes localized to branching tips, potentially regulating important signaling in this special area of the tissue. In line with this hypothesis, typical tip and trunk domain organization is lost in the absence of *Stard13* in the developing pancreas and Cpa1^{+} MPCs are mislocalized. We therefore propose a model in which *Stard13* control on morphogenesis is necessary to localize MPCs to distal tips in order to sustain MPCs proliferative activity and ensure final pancreas organ growth [**25**].

Soluble factors secreted by the pancreatic mesenchyme have been shown to regulate different aspects of pancreas organogenesis, including budding, epithelial proliferation and organ growth [**3**] [**4**] [**7**] [**9**] [**136**]. The proliferative FGF/EGF signals are released from the mesenchyme and control pancreas organ growth [**9**] [**116**]. Interestingly, we find higher levels of the downstream MAPK effector pERK1/2 in the tips of epithelial branches than in the trunk, suggesting that these soluble factors might act as "niche-defining factors" in pancreas development. In line with this, pharmacological inhibition of ERK signaling in WT pancreas explants perturbs branching and cell proliferation, resulting in a phenotype reminiscent of the *Stard13*$^{PA\text{-}deleted}$ pancreata. Moreover, we show that downregulation of Rho in *Stard13*$^{PA\text{-}deleted}$ pancreata rescued pERK signaling, proliferation and branching. This finding suggests that FGF/EGF signaling from the mesenchyme is important for sustaining progenitor proliferation at the tip of the branches and exposure to these proliferative signals is impaired when these tips are lost in the *Stard13*$^{PA\text{-}deleted}$ pancreata.

Interaction with ECM and cell-cell adhesion are important parameters for stem cell retention in a niche [**134**]. Adhesion to the ECM and to neighboring cells may be important for pancreas progenitor cell retention too. One interesting observation we make in our study is the exclusive localization of $\alpha 6$–Integrin to the branching tips in the pancreas epithelium. It is conceivable that $\alpha 6$–Integrin is an important Integrin to localize progenitor cells in the pancreas and exclude them from branching trunks. In *Stard13*$^{PA\text{-}deleted}$ pancreata, $\alpha 6$–Integrin displays an expanded and continuous expression pattern at the periphery of the epithelium. Rho and ROCK activities are required for the assembly of Integrins into focal adhesions and thus elevated Rho levels could be responsible for the mislocalization of $\alpha 6$-Integrin [**133**]. The continuous $\alpha 6$–Integrin distribution might hamper proper allocation of progenitors at the tips, being instead distributed throughout the mutant tissue. Furthermore, it might also prevent branch elongation, being all cells tightly adhered to the ECM.

Altogether, this represents an unprecedented example of how establishment of 3D tissue architecture influences progenitor cell positioning in an environment favorable to sustain their proliferation and organ growth.

3.4 Integration of Cell Proliferation and Epithelial Morphogenesis During Pancreas Development

Branching and growth occur concomitantly during pancreas development, but how the two events are integrated is yet unknown. The *Stard13*$^{PA\text{-}deleted}$ pancreas provides a valuable model to investigate this open question, showing both proliferation and epithelial remodeling defects. Activation of Rho promotes actin polymerization and F-actin accumulation in the form of stress fibers, which can directly regulate MAL/SRF transcriptional activity [**119**] [**120**]. In line with this, we find induction of actin-MAL-dependent and MAL/SRF target gene expression in mutant *Stard13* pancreata. In particular, we find among the MAL/SRF targets, induction of *Mig6*, which is a negative regulator of the EGFR/ERK/MAPK signaling cascade [**137**][**119**]. We propose therefore a model in which stress-fiber accumulation in the *Stard13* mutant induce antiproliferative signals via the MAL/SRF transcriptional activity, resulting in reduced pancreas growth. Ongoing investigation aims at understanding how MIG6 controls the EGF pathway either controlling phosphorylation at the receptor status of or the total protein levels.

In addition to the actin-MAL/SRF transcriptional cascade, we have considered other potential crosstalks between epithelial defects and ERK/MAPK pathway. For example, the integrin-FAK signaling axis is known to regulate proliferation through the control of the ERK/MAPK pathway [**138**]. However, no major changes are found in Integrin levels and downstream activation of FAK signaling pathway in the *Stard13* mutant.

Rho proteins are also known to promote cell cycle progression through affecting cyclin-dependent kinases (CDKs) and promoting cleavage furrow formation [**77**] [**139**] [**140**]. For example, Rho proteins affect CDK activity by regulating levels of Cyclin D1, a crucial protein for cell cycle progression [**133**]. Finally, the assembly of a contractile ring rich in actin and myosin is important for cleavage furrow formation and cytokinesis and RhoGTPases are known for regulating this process [**139**]. Thus, constant RhoA activation in *Stard13*$^{PA\text{-}deleted}$ mutant pancreas tissue might also disturb cleavage furrow formation and directly hamper cell cycle progression and/or cytokinesis. Further investigations are required to test this hypothesis. However, defects in cytokinesis caused by failure of cleavage furrow formation would result in double-nucleated cells, and this is not observed in *Stard13*$^{PA\text{-}deleted}$ mutant pancreas tissue.

3.5 Conclusions and Future Directions

In this study, I investigate the biological activity of *Stard13*, a novel regulator of branching morphogenesis in the developing pancreas. Conditional ablation of *Stard13* gene expression in the mouse pancreas leads to a hypoplastic pancreas with branching defects. MPCs are mislocalized and their proliferation rate decreases, resulting in a reduction of the MPC pool size and a smaller organ at birth. I show that STARD13 protein functions in regulating Rho signaling via its RhoGAP domain. Rho GTPase exerts an important control on actin cytoskeletal dynamics during pancreas morphogenesis. Finally, I define a reciprocal interaction between the actin-MAL-SRF and the MAPK signaling to regulate MPC proliferation in the pancreas.

One interesting question to be solved is whether progenitor proliferation is tightly connected with branching, or whether they are two independent events both affected in the absence of *Stard13*. To start adressing this open question, we are using a genetic *in vivo* model, the mouse transgenic strain *R26Stop^{FL}MEK$_1$DD$^{+/+}$* [C57BL/6-Gt*(ROSA)26Sor$^{tm8(Map2k1*,EGFP)Rsky}$*/J] [**141**]. Intercross of a *R26Stop^{FL}MEK$_1$DD$^{+/+}$* mouse with a *Cre* transgenic mouse strain results in constitutive activation of MAPK signal transduction pathways, including Mitogen-activated protein kinase kinase (MEK) and ERK signaling. The offspring of crosses between *R26Stop^{FL}MEK$_1$DD$^{+/+}$;Stard13$^{lox/lox}$* compound mouse strain and the *Stard13$^{\Delta/+}$;Pdx1-Cre* mouse, show constitutive activation of MAPK signaling in the *Stard13* ablated pancreas. Using this approach, we will test if upregulating ERK signaling rescues only proliferation defects or also branching in the *Stard13* mutant.

Furthermore, we are interested in elucidating possibly distinct temporal activities of *Stard13* during branching morphogenesis. To have a temporal control over *Stard13* genetic ablation, we will use a ROSA Tamoxifen-inducible *Cre*-line *(ROSA-Cre^{ERT})* as model. Intra-peritoneal Tamoxifen injection in *Stard13$^{lox/lox}$* pregnant females, which have been bred with *Stard13$^{lox/lox}$;ROSA-Cre^{ERT}* male mice, will drive *Cre*-recombination and *Stard13* ablation at specific developmental time points, for instance before or after initiation of branching morphogenesis in the embryonic pancreas. If branching defects do not occur upon *Stard13* ablation at late time points (after E12.5), we can conclude that STARD13 is critical for the initial steps of pancreas branching morphogenesis.

To start to shed light on the downstream signaling of STARD13, we have analyzed global expression changes in pancreatic *Stard13* ablated cells. We have performed microarray analysis to compare the gene expression profile in WT and mutant E14.5 pancreata. Interestingly, we have found altered expression levels of Polo-like kinase1 (Plk1), which

plays a role in cell division [**139**], and of Secreted frizzled-related protein 1 (sFRP1), a typical Wnt regulator. Convergent extension movements and oriented cell division, which are controlled by planar cell polarity (PCP), are known to elongate tissues during development, as described in zebrafish gastrulation and vertebrate kidney development [**58**] [**142**] [**143**]. If these molecular mechanisms contribute to "rosette-like" formation and pancreas branch outgrowth is unknown and planar cell polarity has not been shown to contribute to pancreas development. Interestingly, I detect the expression of all main components of the PCP/non-canonical Wnt pathway (e.g. *Vangl, Celsr, Dishevelled1 (Dvl1)* and *Wnt11*) by qRT-PCR analysis of WT E14.5 pancreata. Further immunolocalization analyses of these molecules by immunofluorescence stainings on WT sections are ongoing.

To further understand the biochemical mechanism of action of STARD13, I plan to identify binding partners of STARD13 protein by immunoprecipitation of endogenous STARD13 using the STARD13 antibody that I generated. Mass spectrometry will help in the analysis of the interacting partners and will give information about the mechanism of action of STARD13.

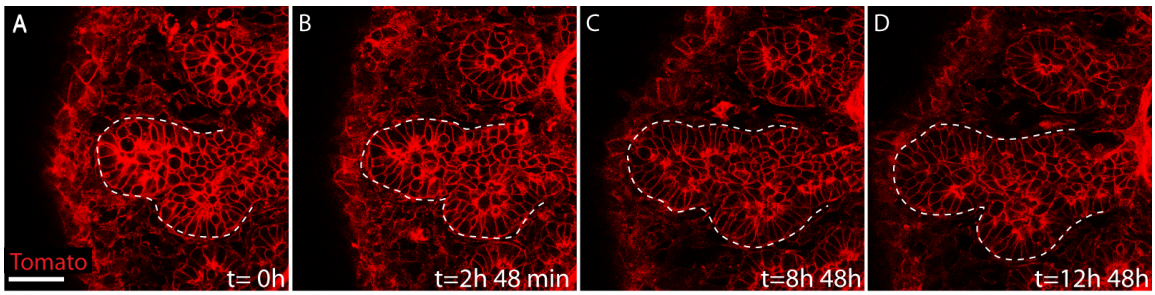

Figure 24: Live-cell imaging of WT pancreatic explant cultures

(A-D) Representative still frames taken every 12 minutes for a total of 15 hours from a time-lapse movie of a membrane-Tomato/membrane-Green (mTmG) pancreatic explant grown in culture. Dashed lines indicate the tip of the branches and the border between the epithelium and mesenchyme. Scale bar, 50 µm.

Steady-state analysis of morphogenetic events on fixed specimens is in general poorly informative. To understand branching and its underlying complex dynamic processes during development, it is necessary to monitor and track the events in real-time using time-lapse imaging techniques. We have started to use live-imaging techniques to investigate the formation of the branched monolayered epithelium in the developing pancreas. To this aim, we have established pancreas explant cultures and have compared *ex vivo* cultures from WT as well as membrane-Tomato/membrane-Green (mT/mG) reporter mouse embryos. Indeed, the use of a fluorescent reporter strain is indispensable for real-time imaging, enabling the visualization of cellular and subcellular structures and the study of their dynamics in a 3D

environment [**113**] [**144**]. For instance, the localization of the mT fluorescent protein to membrane structures enables us to precisely visualize cell morphology and track cell remodeling and migration over time in the pancreatic explants (Figure 24A-D). Future studies in the Spagnoli laboratory will focus on dynamic morphogenetic processes in WT as well as *Stard13* mutant pancreatic explants and take advantage of the real-time imaging conditions that I have set up. This future analysis will shed light not only into the early events driving pancreatic morphogenesis in WT mouse embryo but also their disruption upon *Stard13* gene ablation and activation of the Rho signaling.

4 Materials and Methods

4.1 Chemicals and Reagents

Unless otherwise stated chemicals, enzymes, markers, and oligonucleotides were purchased from Ambion, Applied Biosystems, Biorad, Biozym, Calbiochem, Cytoskeleton, Inc., Fermentas, Fisher, Invitrogen, New England Biolabs, PAA, Perkin Elmer, Qiagen, Promega, Roche, Roth, R&D Systems, Sigma-Aldrich, Stratagene, Tebu-Bio and VWR.

Oligonucleotides for genotyping and qRT-PCR were purchased from Eurofins (Hamburg) or Biotez (Berlin).

4.1.1 Buffers and Solutions

All buffers and solutions were set up in MiliQ water, which was previously purified to the grade “aqua bidest”, unless otherwise stated. Buffers and solutions listed in this table are highlighted in bold in the next Chapters.

Name	Composition
Antibody incubation buffer	3 % horse serum; 0.3 % BSA buffer
Cell blocking buffer	3% donkey serum, 1xPBS, 0.1 % Triton
Cell lysis buffer	1M NaCl, 1xPBS pH 7.5, 1mM PMSF, 1xDNase I, 2mM DTT, 1x Complete mini tablet/10ml (Roche)
Cell washing buffer	PBST: 1xPBS; 0,1 % Tween
Coomassie brilliant blue	Stock: 80mg Coomassie brilliant blue G250, Sigma in 1l water, mix 3hr at RT and add HCl to 35mM (3ml conc.37%) protect from light, store at RT
Digestion solution	1x Trypsin/EDTA (Gibco), 100µl EDTA/100ml, 10µg/ml DNase I
HybeMix	40% formamide, 5x saline sodium citrate (SSC), 10x Denhardt’s, 100µg/ml salmon sperm-DNA, 100µg/ml Turola tRNA
***In situ* blocking solution**	1% blocking reagent (Boehringer) in 100mM maleic acid, 150mM NaCl in DEPC-H_2O, pH7.5
MEF culture medium	DMEM with high glucose (Invitrogen), 10% FCS Gold (PAA), 1% Pen/Strep (Gibco), 1x NEAA (Invitrogen), 100µM β–mercaptoethanol (Invitrogen)
NTE buffer	0.5M NaCl, 10mM Tris pH7.0, 5mM EDTA in DEPC-H_2O
Phosphatase inhibitor cocktail	2.5mM sodium pyrophosphate, 1mM sodium vanadate, 1mM β-glycerophosphate, 1x Complete mini tablet/10ml (Roche)

Protein lysis buffer	150mM NaCl, 20mM Tris-HCl pH=7.5, 1mM EDTA, 1mM EGTA, 1% Triton X-100
Rinsing solution	0.1M phosphate buffer pH:7.3, 2mM $MgCl_2$, 0.01% sodium deoxycholate, 0.02% NP-40 in H_2O_{dest}
Running buffer	25mM Tris-base; 192mM glycine, 0.1% SDS
Separating gel (10%)	2.7ml 30% acrylamide/bis-acrylamide, 2.1ml 1.5M pH 8.8 Tris-HCl; 0.2 ml 10% SDS; 30µl 10% APS; 30µl TEMED
Stacking gel	350µl 30% acrylamid/bis-acrylamide; 625µl 0.5M pH 6.8 Tris-HCl; 25µl 10% SDS; 9µl 10% APS; 9µl TEMED
Staining solution	BM-purple with 10µl/ml 100x Tween-20/levamisole
Synthesis reagent	2µl 10x transcription buffer (Roche), 2µl RNA labelling Mix (Roche), 2µl 0.1M DTT, 0.5 µl RNase inhibitor (Promega), 1µl RNA polymerase (T3, T7 or SP6), 12 ml DEPC-H_2O
Tail lysis buffer	100mM Tris pH:8, 50mM KCl, 2mM $MgCl_2$, 0.1 mg/ml gelatin, 0.45% NP40, 0.45%Tween
TBST	10mM Tris-HCl pH 8; 150mM NaCl; 0.1% Tween20
TEA-HCl solution	3.71 g triethanolamine-HCl, 900 µl 10M NaOH ad 200ml with DEPC-H_2O, pH8
Transfer buffer I (5x)	29g Tris-base, 145g glycine, 2.5 ml 20% SDS ad 1l dH_2O, adjust pH 8.3, dilute to 1x and add 20% methanol
Transfer buffer II (10x)	30.3g Tris-base, 144.1g glycine, ad 1l dH_2O, adjust pH 8.3 and add 20% methanol
Tris/Glycine buffer	24.2g Tris-base, 15g glycine, ad 2l with DEPC-H_2O
TSA blocking buffer	10% horse serum, 1xPBS, 0.5mg/ml TSA blocking powder (Perkin Elmer)
Washing buffer	PBST: 1xPBS; 0,1 % Triton

4.1.2 Genotyping Primers

Gene	Primer	Sequence (5'-3')	Size (bp)
WT Stard13	F	cag ttc cat gtt ggg tct tcg t	259
	R	cct tcc agc tgg ggg gta gg	
Floxed Stard13	F	cag ttc cat gtt ggg tct tcg t	330
	R	cca gct ggc tag ctg gca aac	
Post-recombination product	F	cag ttc cat gtt ggg tct tcg t	710
	R	aac ata cct tag atc tat tg	
Pdx1 WT	F	cta ggc cac aga att gaa aga tct	324
	R	gta ggt gga aat tct agc atc atc c	
Pdx1 Cre	F	gcg gtc tgg cag taa aaa cta tc	100
	R	gtg aaa cag cat tgc tgt cac t	

4.1.3 qRT-PCR Primers

Gene	Accession No.	Primer	Sequence (5' □3')	Size (bp)
36B4	NM_007475.5	F	GGCCCTGCACTCTCGCTTTC	124
		R	TGCCAGGACGCGCTTGT	
Srf	NM_020493.2	F	GGCCGCGTGAAGATCAAGAT	159
		R	CACATGGCCTGTCTCACTGG	
Ctgf	NM_010217.2	F	CCCTAGCTGCCTACCGACT	113
		R	CATTCCACAGGTCTTAGAACAGG	
Vcl	NM_009502.4	F	GCAACCTCGTCCGGGTTGGAA	163
		R	TCCCGCGCAGGAACCGAGTA	
Mig6	NM_133753.1	F	TGGCCTACAATCTGAACTCCC	102
		R	GACCACACTCTGCAAAGAAGT	

4.1.4 Antibodies

Antibody	Specificity	Raised in	Dilution	Source
Amylase	Digestive enzyme, product of the exocrine pancreatic tissue	Rabbit	1:500	Sigma
pAkt	Activated protein kinase B	Rabbit	1:1000	Cell Signaling
Akt	Protein kinase B	Rabbit	1:1000	Cell Signaling
β-catenin	Basolateral membrane marker	Rabbit	1:500	Santa Cruz
Carboxypeptidase	Multipotent pancreatic progenitor marker	Rabbit	1:500	AbD Serotec
Cytokeratin 8	Intermediate filaments	Rat	1:50	Hybridoma Bank
E-cadherin	Basolateral membrane marker	Rat	1:500-1:1000	Invitrogen
pERK1/2	Activated MAPK marker	Rabbit	1:250-1:1000	Cell Signalling
ERK	MAPK marker	Rabbit	1:1000	Cell Signalling
F-actin-FITC coupled	Apical membrane marker	-	1:500-1:750	Molecular Probes
pFAK (Tyr397)	Activated focal adhesion kinase	Rabbit	1:1000	Cell Signaling
FAK	Focal adhesion kinase	Rabbit	1:1000	Cell Signaling
GAPDH	Glyceraldhyde-3-phophate dehydrogenase	Rabbit	1:1000	Cell Signalling
Glucagon	Hormone of the α-cells	Rabbit	1:500	Immunostar
GST	Glutathion-S-Transferase	Mouse	1:1000	Cell Signalling
Hes1	Hairy-and-Enhancer-of-split 1	Guinea pig	1:500	Gift of C. Birchmeier-Kohler lab, MDC
α6-Integrin	FA component	Rat	1:400	Serotec
β1-Integrin	FA component	Rat	1:100	Millipore
Phospho-Histone H3 (Er10)	General proliferation marker	Rabbit	1:200	Millipore
Insulin	Hormone of the β-cells	Guinea Pig	1:250	Millipore
Laminin	Basal membrane marker	Rabbit	1:1000	Sigma
Mig6	Mitogen-inucible gene 6 protein marker	Goat	1:50	Santa Cruz
Mucin	Apical membrane marker	Armenian Hamster	1:1000	Thermo Scientific
Ngn3	Progenitor marker	Guinea Pig	1:2000	Gift of M. Sander lab, USCD
ΔNp63	Potential progenitor marker	Goat	1:150	Santa Cruz

p120-catenin	Basolateral membrane marker	Mouse	1:250	Zymed
Pdx1	Pancreas progenitor marker	Rabbit	1:2000	Abcam
Pdx1	Pancreas progenitor marker	Mouse	1:100	Hybridoma Bank
PECAM-1				
Pmyo	Phospho-Myosin II	Rabbit	1:200	Cell Signalling
aPKCζ	Protein kinase C ζ	Rabbit	1:100	Santa Cruz
RhoA	RhoA GTPase marker	Mouse	1:500	Cytoskeleton Inc.
Sox-9	Progenitor and duct marker	Rabbit	1:2000	Gift of M. Wegner lab, Uni Nürnberg
Stard13 (rb)	Stard13 marker	Rabbit	1:50-1:1000	Sigma
Stard13 (goat)	Stard13 marker	Goat	1:50-1:1000	Santa Cruz
STARD13-Nterm (rb)	Stard13 marker	Rabbit	1:50-1:1000	F.M. Spagnoli lab
STARD13-Nterm (ch)	Stard13 marker	Chicken	1:50-1:1000	F.M. Spagnoli lab
Talin	FA component	Mouse	1:100	Sigma
Tubulin	Mikrotubuli marker (House keeping gene)	Mouse	1:1000	Sigma
Vinculin	FA component	Mouse	1:150	Sigma
pYAP	Activated Yes-associated protein	Rabbit	1:100	Cell Signalling
YAP	Yes-associated protein	Rabbit	1:100	Cell Signalling
Zo-1	Tight junction marker	Rabbit	1:100	Invitrogen

For IF Alexa-conjugated secondary antibodies were used at a dilution of 1:750 (Molecular Probes) or 1:500 (Jackson ImmunoResearch) and for WB fluorophore-coupled IRDye® secondary antibodies were used at a dilution of 1:10 000 (LI-COR).

4.2 Mouse Experiments

4.2.1 Mouse Strains

A conditional knock-out mouse for *Stard13 (Stard13 $^{lox/lox}$)* was generated by Dr. Francesca M. Spagnoli by flanking exon5 with *LoxP* sites. Deletion of exon 5 in *Stard13 $^{lox/lox}$* mice results in absence of the functional STARD13 protein (Figure 9A).

Details of *Stard13 $^{lox/lox}$* mouse generation can be found in Petzold et al. (submitted) [**71**]. Briefly, gene targeting vector for creating a floxed allele of mouse *Stard13* gene was generated using bacterial homologous recombination. The BAC clone RP23-11K10 containing the entire *Stard13* gene locus was converted into loxP-Stard13-loxP-frt-hygro-frt targeting vector using BAC recombineering [**145**]. The targeted BAC was subcloned into a modified pMCDT-A (A1T/pau TK-DTA) vector, which lacks the Neomycin resistance gene, using HindIII restriction enzyme. The final construct was electroporated into CY2.4 albino C57BL/6J-Tyrc-2J-derived ESCs and targeted ES clones were selected in the presence of

Hygromicin. Correctly targeted ES clones were injected into recipient blastocysts. The resulting male chimeric animals were crossed to C57BL/6J-Tyrc-2J mice to allow for coat-color screening of germline transmission. Chimeras that were complete transmitters of ES-derived sperm were bred to C57BL/6 females to generate F1 heterozygous mice. The Hygro selection cassette was removed by breeding to Flp-deleter mouse strain [**146**] and the recombination was passed to germline. The resulting F2 mice were crossed to C57BL/6J mice and bred to homozygosity. Homozygous *Stard13* $^{lox/lox}$ appeared healthy and phenotypically indistinguishable from their wild-type littermates.

The *Stard13* $^{\Delta/+}$*; Pdx1-Cre* mice were generated by crossing a *Stard13* $^{lox/lox}$ mouse with a germline deleting Cre mouse [(Tg(CMV-cre)1Cgn/J] obtained from Jackson Laboratory) [**97**]. The progeny resulted in *Stard13* $^{\Delta/lox}$*; CMV-Cre* mice. The *CMV-Cre* was outbred by mating with WT mice in order to obtain *Stard13* $^{\Delta/+}$ mice, with one allele of germline deleted *Stard13*. *Stard13* $^{\Delta/+}$ mice were either intercrossed for obtaining *Stard13*$^{\Delta/\Delta}$ mice or crossed to *Pdx1-Cre* mice to yield *Stard13* $^{\Delta/+}$*; Pdx1-Cre*.

All *Pdx1-Cre* deleter mice were tested for recombination efficiency using the R26R *lacZ* reporter line obtained from the Jackson Laboratory [Gt(ROSA)26Sortm1Sor] [**80**] and staining for β-galactosidase [**147**] (Chapter 4.2.4).

Mice were housed with ad libitum access to food and water in room air conditioned at 22-23 ^{0}C with a standard 12 h light/dark cycle. All procedures were in accordance with ethical guidelines laid down by the local governing body.

4.2.2 Isolation of Genomic DNA from Mouse Tails

The genotype of mouse embryos was determined by PCR reaction on DNA extracted from tail or pancreas biopsies. The tissue was lysed in 100µl (tail) or 75 µl (pancreas pieces) **Tail lysis buffer** containing Proteinase K (0.5 mg/ml) at 55°C overnight. 1-2 µl of this sample were used in a PCR reaction.

4.2.3 Genotyping by Analytical Polymerase Chain Reaction (PCR)

For analytical PCRs genomic DNA was extracted from mouse tails or pancreas pieces as described in Chapter 4.2.2. The PCR reaction contained 1-2 µl of heat-inactivated lysate, 10 µl 2x DreamTaq™ Green PCR MasterMix (Fermentas) (contains TaqPolymerase and PCR buffer, 4mM $MgCl_2$, 40mM dNTPs, loading dye) 1 µl F-primer (10 µM) and 1 µl R-primer (10 µM) in a volume of 20 µl. For detection of the WT *Stard13*, the floxed *Stard13*, the post-recombination product and the *Pdx1-Cre* primers were used as described in Chapter 4.1.2.

All PCRs were carried out in the PCR cycler PTC-200 (MJ Research). The cycler program was chosen as followed: 2 min at 94 ^{0}C, 35 cycles of 45 sec at 94 ^{0}C, 30 sec at 50–60 ^{0}C, 45 sec at 72 ^{0}C followed by a final elongation time of 10 min at 72 ^{0}C. PCR products were analyzed on an agarose gel.

4.2.4 β-Galactosidase Staining of the Pancreas

Stomach, duodenum, spleen and pancreas tissue altogether was dissected from the embryo. The tissue was briefly fixed in 0.2% Glutaraldehyde/H_2O_{dest} for 30min at room temperature (RT) and washed 3x 10-30min at RT in **Rinsing solution.** Staining was carried out in 1mg/ml X-gal, 5mM potassium ferrocyanide, and 5mM potassium ferriccyanide in **Rinsing solution** at 37°C for 1-2 h in the dark. X-gal staining was stopped by washing 3x with 1xPBS and followed by imaging analysis.

4.2.5 Isolation of Embryonic Fibroblasts from WT and *Stard13* $^{\Delta/\Delta}$ Mice

WT MEFs and *Stard13* $^{\Delta/\Delta}$ MEFs were derived from E14.5 embryos. Carcasses were separated from head and viscera, then washed several times in 1xPBS, minced and digested in 2ml **Digestion solution**/embryo for 15min at 37°C with shaking. After up and down pipetting the tissue was further dissociated by addition of 10ml **Digestion solution**/embryo and incubation for 15min at 37°C with shaking. Cells were sedimented, resuspended in **MEF culture medium** and passed onto gelatin-coated (0.1%, Sigma) 15 cm culture dishes. MEFs were grown to near confluency and split to maintain the culture.

4.3 Cell Culture Methods

Mammalian cells were handled in a hood under sterile conditions. 70 % ethanol, autoclaving and ultrafiltration were used for sterilization. The cells were grown at 37 ^{o}C in a tissue culture incubator with a humidified atmosphere containing 5 % CO_2.

4.3.1 HEK Cell Transfection

Transfection of HEK-293 T cells was done using Polyethylenimine (PEI) (Polysciences), a cationic polymer, which condenses plasmid DNA into positively charged particles and enables its uptake into the cells via endocytosis. 0.5-2 µg of plasmid DNA was mixed with the appropriate amount of PEI. EGFP was used as a control to enable the determination of transfection efficiency. DMEM supplemented with Glutamine (Gibco) and 10% fetal calf serum (FCS) (PAA) and 1x Penicillin/Streptomycin (Pen/Strep) (PAA) was used as a media. Transfections were performed according to the manual.

4.3.2 *Ex Vivo* Culturing of Pancreatic Explants

Pancreatic explants cultures were obtained as described [**113**]. Dorsal pancreatic buds were microdissected from mouse embryos at E11.5 and cultured on glass bottom dishes (Matek) pre-coated with 50 µg/ml sterile bovine fibronectin (Invitrogen) in BME medium supplemented with 10% fetal bovine serum, which was renewed every two days. Cultures were maintained for up to 6 days at 37°C in 5% CO_2. The day of plating is referred to as day 0. In Rho activation assay, LPA (Sigma) was added at the final concentration of 10 µg/ml to the culture medium on day 1 and replaced every 24 hours. In Rho inhibition assay, membrane-permeable C3 transferase (Cytoskeleton, Inc.) and Y27632 (Sigma) were added at the final concentration of 2.5 µg/ml and 15 µM, respectively, to the culture medium on day 1 and replaced every 24 hours. In ERK inhibition assay, PD0325901 (Selleck) was added at the final concentration of 2 µM to the culture medium. Explants were fixed in 4% PFA, stained as whole-mounts and analyzed by Zeiss LSM 700 confocal laser scanning microscope.

4.4 Histological Analysis

4.4.1 Sample Embedding and Cryosectioning

Mouse embryos and pancreata were fixed in 4% paraformaldehyde at 4°C from 2 hr to overnight depending on embryonic stage. Subsequently, samples were immmersed in 20 % sucrose/1x PBS solution overnight and embedded in OCT compound (Sakura). Cryosections were cut with 10 µm thickness.

4.4.2 *In Situ* Hybridization

In situ hybridization experiments were performed to analyze mRNA expression in WT animals. Therefore RNA-probes were digoxigenin (DIG)-labelled. Binding of these probes to their target RNA on cryosections was verified by color reaction.

For DIG-labelling of RNA-probes 2µl linearized plasmid DNA was purified by phenol/chloroform extraction and incubated 2h at 37°C in **Synthesis reagent**. DIG-labeled RNA transcripts were precipitated with 0.1V 4M LiCl/ 2.5V 100%EtOH. After elution in 50 µl of RNase-free water the probe was analyzed on an agarose gel and stored at -20 ^{0}C until use.

Cryo-embedded sections were first dried at RT, and then postfixed in 4% PFA/DEPC-PBS for 10min. Slides were 2x washed in DEPC-PBS for 5min each. To improve accessibility of the *in situ* probes to the target sequence sections were pre-digested with 5µg/ml Proteinase

K/DEPC-PBS for 2min and afterwards washed 5min in DEPC-PBS, before another fixation step in 4% PFA/DEPC-PBS for 5min. Following a washing step for 5min in DEPC-PBS cryosections were acetylated in 0.1M **TEA-HCl solution** supplemented with freshly added acetic anhydride (125 µl/50ml **TEA-HCl solution**) for 10min. Cryosections were washed for 5min in DEPC-PBS and dehydrated in 70% EtOH (Molecular biology grade) for 5min and 95% EtOH for 2min, then air dried and washed in **Tris/Glycine buffer** for at least 30min. To detect the target-RNA cryosection were incubated with the 1µg/ml of digoxigenin (DIG)-labeled *in situ* probes diluted in **HybeMix** o.n. at 65°C. Two different *Stard13 in situ* probes were used: one spanning the 3'UTR and one including the sequence spanning exon 5. Next day, sections were washed in a series of SSC and **NTE buffers**, blocked with ***In situ* blocking solution** and labeled with anti-DIG antibody [1:5000 diluted in 1%blocking reagent (Boehringer)] o.n. at 4°C. Third day, samples were washed several times in TBS buffer 10min each and 1x in Tween-20/levamisole (in DEPC-H_2O), before incubation in **Staining solution** for at least 30min at RT protected from light until the staining showed the desired intensity. The sections were finally washed in PBS/1mM EDTA for three times and mounted with Dako Mounting medium (Dako).

4.4.3 Immunofluorescence Staining

Different protocols for IF stainings for cells or cryosections were used.

The cells were grown on a coverslip and fixed in 4% PFA for 20 min at RT, washed twice with 1xPBS and blocked in **Cell blocking buffer** for 30 min at RT. Subsequently, cells were incubated with primary antibodies diluted in **Cell blocking buffer** o.n. at 4°C. After 3x30min washes with **Cell washing buffer** Alexa-conjugated secondary antibodies (Molecular Probes) were used for incubation at a dilution of 1:750 or 1:500 (Jackson ImmunoResearch) in **Cell blocking buffer** for 30 min at RT. Immunostainings were analyzed with the Zeiss AxioObserver, the Zeiss LSM 700 or the LeicaSPE confocal laser scanning microscope.

Cryosections of 10 µm thickness were blocked with **TSA blocking buffer** 1hr at RT and afterwards incubated with primary antibodies (dilutions: see methods section: 4.1.4) in **Antibody incubation buffer** o.n. at 4°C. After 3x5min washes with **Washing buffer** Alexa-conjugated secondary antibodies were used at a dilution of 1:750 (Molecular Probes) or 1:500 (Jackson ImmunoResearch) in **Antibody incubation buffer**. Following 3x5min washes with **Washing buffer** and 1x with 1xPBS slides were dried and mounted in Dako Fluorescent Mounting media (Dako). Immunostainings were analyzed with Zeiss AxioObserver, Zeiss LSM 700 or LeicaSPE confocal laser scanning microscope. For counting, pancreatic tissue of at least three WT and three *Stard13*$^{PA\text{-}deleted}$ embryos were cut

into serial sections and stained cells were counted every three sections. E-cadherin^{+} pancreatic epithelium area was measured using AxioVision software (Zeiss, Germany) or ImageJA (Fiji). Immunohistochemical markers were quantified only in dorsal pancreas.

4.4.4 Proliferation and Apoptosis Characterization

Proliferation was evaluated by immunofluorescence staining against phospho-histone H3 or *in vivo* BrdU labeling. For the later, pregnant females were injected intraperitoneal (i.p.) with 75 µg of BrdU (Sigma) per gram of body weight and embryos harvested 30 min after injection. For the apoptosis analysis the TdT-mediated dUTP-biotin nick end labeling (TUNEL) assay was done with the ApopTag Fluorescein *In Situ* Apoptosis Detection Kit (Chemicon).

4.4.5 Cell Counting

Slides were counterstained with an antibody against E-cadherin. Apoptotic, proliferating or differentiated cells were counted from in several 40x microsope fields using the counting tool macro in Adobe Photoshop CS3. The E-cadherin positive pancreatic area was measured with the software Zeiss AxioVision or ImageJA (Fiji). The ratio between the number of counted cells and the pancreatic area was used for evaluation.

4.4.6 Morphometric Analysis

E18.5 pancreata were fixed in 4% paraformaldehyde and paraffin embedded. The analysis was done in collaboration with the Dept. of Pathology, University of Rome “Tor Vergata”. They sectioned each pancreas at three different levels and collected for each level 3 sections (4 µm) on a slide. Total pancreatic area identified by hematoxylin-eosin staining was quantified using a Scan scoope microscope, analyzed by Image Scope viewer (Aperio, Technologies Inc, USA) and expressed in μm^2. The average cell surface was determined on at least five pancreata for each genotype. All results are expressed as mean ± SEM with the number of observations.

4.4.7 Transmission Electron Microscopy

E12.5 pancreata were fixed in phosphate-buffered 2% PFA/ 2.5% glutaraldehyde solution for 4 hours at 4°C and postfixed in 1% OsO4. The analysis was done in collaboration with the Dept. of Pathology, University of Rome “Tor Vergata”. They dehydrated the samples and embedded them in epoxy resin. Semi-thin sections (1.2 µm) were counterstained with Toluidine blue. Thin sections were counterstained with uranil acetate and lead citrate and examined with a HITACHI H- 7100FA microscope.

4.5 RNA Isolation, cDNA Synthesis and Quantitative PCR (qRT-PCR)

Total RNA was isolated from E14.5 pancreas with RNAzol (Biozol) or TRIzol (Invitrogen) according to manufacturer's instructions. For reverse transcription of mRNA into cDNA, random hexamers and Oligo dT from the SuperScript III First-Strand Synthesis System (Invitrogen) were used with 3µg of RNA following the manufacturer's protocol. For the qRT-PCR, 5 µl cDNA, 0.5µl of 10µM primers mix, 2µl dH_2O and 7.5µl 2x SYBR-Green (Roche) were analyzed in triplicates on a 96 well-plate in StepONE Plus™ cycler (Applied Biosystems). The primers were designed as to have an annealing temperature of 62°C and an amplicon length of 100-200bp in the following program (95°C 10min; 95°C 15sec, 62°C 1min; 40 cycles). The qRT-PCR analyses were carried out with three different cDNAs and ribosomal protein 36B4 was used as reference gene. See Table 3 for primer sequences.

4.6 Protein Analysis

4.6.1 Total Protein Extraction

Protein was extracted from transfected HEK cells, MEFs or pancreatic tissue. After washing away the medium with 1x PBS, HEK or MEF cells were harvested with a cell scraper and pelleted at 4 min at 4°C and 1000rpm. Due to the required minimum amount of pancreas protein for loading a Western Blot-SDS-gel, the minimum age of embryos for protein extraction from pancreatic tissue had to be E14.5. Several E14.5 pancreata or one E17.5 pancreas were homogenized with a Xenox MHX-E Homogeniser (Xenox).

Proteins from cells or pancreatic tissue were lyzed in **Protein lysis buffer** provided with fresh protease and **Phosphatase inhibitor cocktail** for 1min at 4°C. The lysed tissue was centrifuged for 10min at 4°C at max. speed and the supernatant was aliquoted, snap-frozen, and stored at -80°C. The protein concentrations were determined by Bradford-method (Bio-Rad) at 595nm.

4.6.2 SDS-PAGE, Coomassie Staining, Western Blotting, Ponceau Staining

Equal quantities of protein were diluted 3:1 in 4x SDS-sample buffer (Roth), heated at 95°C for 5min, loaded next to prestained protein markers (Fermentas) and separated using Sodium dodecyl sulfate polyacrylamide gel electrophoresis (SDS-PAGE) (e.g. 10% **Separating gel** and **Stacking gel**, Chapter 4.1.1) at 120V for 2-3h in **Running buffer**.

To evaluate protein expression after GST-pulldown of GST-STARD13-FL or the GST-STARD13-Nterm constructs (Chapter 4.7.2) Coomassie staining was performed after SDS-

PAGE: the gel was 2x heated up in dH_2O for 15-30 sec and quickly rinsed, dH_2O was replaced by **Commassie brilliant blue**, heated up for 15-30 sec and shaked for 5-10 min until staining was visible. Then the gel was destained in dH_2O as above.

By WB proteins were transferred from the gel onto a nitrocellulose membrane (Hybond ECL, 45µm, GE Healthcare) by the wet-transfer method in **Transfer buffer I** (for proteins >80 kDa) or **Transfer buffer II** (for proteins <80 kDa) for 1-2h at 0.2A/gel. Successful transfer onto the membrane was verified by staining with Ponceau S solution (Sigma, P7170) with subsquent washes in DEPC-H_2O to remove Ponceau S.

After membrane blocking in 5% milk/1x**TBST** for 1h at RT with constant shaking, primary antibodies were incubated in 1x**TBST** o.n. with constant shaking at 4°C. Following 3x washing in 1x**TBST**, fluorophore-coupled IRDye® secondary antibody (LI-COR) incubation in 1x**TBST** was performed for 1h at RT in the dark with constant shaking and subsequent washing in 1x**TBST**. Protein bands were visualized by infrared light with an Odyssee®Imager (LI-COR).

4.6.3 Rho-GTP Pull-Down and Immunolocalization Assays

For Rho-GTP pull down assay, dissected E17.5 pancreata were snap frozen in liquid nitrogen. After genotyping, pancreata were lysed in **Protein lysis buffer** and about 300 µg total protein extract incubated with 25 µg Rhotekin-RDB beads for pull-down from the RhoA activation assay kit (Cytoskeleton, Inc.), according to manufactor's instructions. $1/10^{th}$ of total lysate (approximately 25-30 µg) was used for total RhoA detection on Western blot with anti-RhoA antibody (see methods section: 4.1.4). WT lysate pre-loaded with non-hydrolysable GTP analog, GTPγS, (WT+GTPγS) and Histidin (His)-tagged RhoA fusion protein were used as positive controls in the assay.

Rho-GTP immunolocalization assay was performed as in Cascone et al. [**115**]. Briefly, explants were fixed in 4% PFA on ice, incubated with Rhotekin-RDB-GST purified protein (Cytoskeleton, Inc.) overnight at 4°C, and as whole-mounts processed for immunofluorescence with anti-GST and anti-Pdx1 antibodies (see methods section: 4.1.4). As negative controls pancreatic explants were incubated with anti-GST antibody alone. Zen3D (Zeiss) software was used to analyze confocal images and create 3D reconstructions.

4.7 Generation of the STARD13 Antibody

4.7.1 Molecular Cloning

The following standard molecular biological techniques were carried out as described in Sambrook & Russell (2001) unless otherwise stated:

- Molecular cloning
- Restriction digest
- Vector dephosphorylation
- Ligation
- Transformation via heat shock
- Plasmid DNA extraction (Plasmid Miniprep/Maxiprep kit)
- DNA extraction from agarose gels (Gel purification kit)
- Determination of nucleic acid concentration
- Sequencing (carried out by InViTek, Berlin Buch)
- TOPO cloning (TOPO cloning kit)
- Phenol/Chlorofoem extraction
- Precipitation of nucleic acids

To generate custom-made antibodies against the full-length STARD13 protein (NCBI: NP_666370.3) and an N-terminal STARD13 protein fragment (NCBI: NP_666370.3: from aa 208 to 449) with a GST-tag, the full length *Stard13* cDNA (NM_146258.2; referred to as STARD13-FL**,** see Figure 6) and a 737-bp cDNA fragment of *Stard13* (corresponding to nucleotides 721 to 1458; referred to as STARD13-Nterm**,** see Figure 6) were cloned into the pGEX-4T-1 bacterial expression vector in the following procedure:

First the full-length and a 753 bp fragment of Exon 5 of *Stard13* were amplified from a *Stard13* cDNA (NCBI: NM_146258) containing pCMV-SPORT6 Vector (Forward primer: GGA ATT CCG GAG CCG CAG CCA AATC AGG G, Reverse Primer: CCG CTC GAG CGG TTA GGC CCT GTG GCA GGA). This fragment was cut and ligated into a GST-containing pGEX-4T-1 expression vector (Amp^R) using EcoRI/XhoI restriction sites.

Second, this vector was transfected with heat-shock into BL21-E.coli (#230134, Stratagene) cells. Resistant colonies grew at 37°C in LB-medium supplemented with 50µg/ml Ampicillin until OD 600 nm reached 0.4 to 0.6. At this point expression of the Glutathione-S-Transferase (GST)-tagged proteins (referred to as GST-STARD13-FL and GST-STARD13-Nterm) was accelerated by induction with 1 mM Isopropyl β-D-1-thiogalactopyranoside

(IPTG). After an optimal expression time of 5h the cells were harvested by spinning at 4°C for 10min and storing them at -80°C.

4.7.2 GST-Purifications of Antigens

Through resuspension of the cell pellet in **Cell lysis buffer** and iterative freeze and thaw cycles in liquid nitrogen BL21-E.coli containing the GST-STARD13-FL or the GST-STARD13-Nterm construct were lysed. By immunoprecipitation with Glutathione Sepharose 4 Fast Flow beads (GE Healthcare) the 138kDa GST-STARD13-FL and the 54kDa GST-STARD13-Nterm constructs were pulled down according to manufacture's instructions. After verification of the fusion protein on a commassie-stained SDS-gel and due to low yield concentration of the GST-STARD13-FL construct only the GST-STARD13-Nterm construct was sent to a company (Davids Biotechnology GmbH, Regensburg) for antibody production in rabbit and chicken. GST was depleted and the sera purified by the company. The antibody was called STARD13-Nterm.

4.7.3 Validation Tests of the Antibodies

The three commercial antibodies against STARD13 (anti-Stard13 from Sigma: S9573 and S9698; anti-Stard13 fom Santa Cruz: sc-67843) and STARD13-Nterm antibody were tested by WB and IF and their specificity was evaluated by comparing to negative controls.

For WB analysis protein lysates of GST-STARD13-FL and GST-STARD13-Nterm eluates after GST-immunoprecipitation (Chapter 4.7.2) and cell lysates from pCS2^{++}-*mStard13*-transfected (FM Spagnoli, unpublished) and non-tranfected (control) HEK cells (Chapter 4.3.1) and/or from MEFs isolated from WT or *Stard13*$^{\Delta/\Delta}$ embryos were used for SDS-PAGE and blotting (Chapter 4.6.1 & 4.6.2).

For IF analysis, either, cyrosections of E12.5, E14.5, E17.5 embryonic pancreata and/or newborn pancreata (Chapter 4.4.1) or *Stard13*-transfected HEK cells (Chapter 4.3.1) were stained with the commercial antibodies or STARD13-Nterm as primary antibody (Chapter 4.4.3).

Abbreviations

%	percent
µ	micro
°C	Celsius degree
36B4	Large subunit ribosomal protein LP0 (RPLP0)
aa	Amino acid
Amp	Ampicillin
Amy	Amylase
AKT	Protein kinase B
a-p	Anterior-posterior
aPKC	Atypical protein kinase C
βcat	β–catenin
BMP	Bone morphogenetic protein
bp	base pair(s)
BrdU	5-bromo-2'deoxyuridine
C3	Ribosyltransferase, Rho protein inactivator
Cdc42	Cell division control protein 42
CDK	Cyclin-dependent kinases
cDNA	Complementary desoxyribonucleic acid
CK8	Cytokeratin 8
CMV	Cytomegalovirus
Cpa1	*Carboxypeptidase A1*
Ctgf	*Connective tissue growth factor*
3D	Three-dimensional
DE	Desmosomes
DEPC	Diethylpyrocarbonate
DIG	Digoxygenin
DLC2	*Deleted in Liver Cancer 2*
DNA	Desoxyribonucleic acid
dNTP	Deoxynucleotide triphosphate
dp	Dorsal pancreas
DRG	Dorsal root ganglion
DTT	Dithiothreitol
duo	Duodenum
Dvl1	*Dishevelled1*
E	Embryonic day
Ecad	Epithelial-cadherin
ECM	Extracellular matrix
ESC	Embryonic stem cells
EDTA	Ethylenediamine tetraacetic acid
e.g.	example given
EGF	Epidermal growth factor
EGFR	Epidermal growth factor receptor
EGTA	Ethylene glycol tetraacetic acid
ERK	Extracellular-signal regulated kinase
F	Forward
FA	Focal adhesion
Fact	F-actin
FACS	Fluorescence activated cell sorting
FAK	Focal adhesion kinase
FCS	Fetal calf serum
FGF	Fibroblast growth factor
FL	Full-length
FN	Fibronectin
GAP	GTPase-activating protein
GAPDH	Glycerinaldehyd-3-phosphat-dehydrogenase

GDI	GDP-dissociation inhibitors
GDP	Guanosine diphosphate
GEF	Guanine-nucleotide exchange factors
Glu or Gluca	Glucagon
GST	Glutathione-S-transferase
GST-STARD13-FL	GST-tagged STARD13-FL
GST-STARD13-Nterm	GST-tagged STARD13-Nterm
GTP	Guanosine triphosphate
h	hour
Hes1	*Hairy-and-Enhancer-of-split 1*
HEK	Human embryonic kidney
His	Histidin
Hnf1 β	*Hepatocyte nuclear factor 1 β*
IF	Immunofluorescence
IPF1	*Insulin-promoter factor 1*
IPTG	Isopropyl β-D-1-thiogalactopyranoside
Ins	Insulin
Int	Integrin
lacZ	Gene coding for β-galactosidase enzyme
Lam	Laminin
LB	Lysogeny broth
LoxP	*Lox* site from bacteriophage P1
LPA	lysophosphatic acid
m	milli
M	Molar
MAL	Megakaryoblastic leukemia 1
MAPK	Mitogen-activated-protein-kinase
max	Maximum
MDCK	Madin-Darby canine kidney
MEFs	Mouse embryonic fibroblasts
MEK	Mitogen-activated protein kinase kinase
Mig6	*Mitogen-inducible gene 6*
min	Minute
MMP2	Matrix metalloproteinase-2
MODY	Maturity-onset diabetes of the young
MPCs	Multipotent progenitor cells
mRNA	Messenger RNA
mTmG	membrane-Tomato/membrane-Green
nc	Neural crest
NEAA	Non-essential amino acids solution
Ngn3	*Neurogenin 3*
Nkx6.1	*NK6 homeobox 1*
ΔNp63	*one isoform of p63*
nt	Nucleotide
Nterm	N-terminus
p120	p120-catenin
Pa.	Pancreatic
pAKT	Phospho-protein kinase B
Par3 (or 6)	*Protease activated receptor 3 (or 6)*
Pax4 (or 6)	*Paired box gene 4 (or 6)*
PCL	Primary central lumen
PCP	Planar cell polarity
PCR	Polymerase chain reaction
PD0325901	ERK-kinase inhibitor, anti-cancer agent
Pdx1	Pancreas duodenal homeobox factor 1
PECAM	Platelet endothelial cell adhesion molecule
PEI	Polyethylenimine
Pen/Strep	Penicillin/Streptomycin

pERK1/2	Phospho-extracellular signal regulated kinase 1/2
pH	Potentium hydogenii
PFA	Paraformaldehyde
pFAK	Phospho-focal adhesion kinase
pHH3	Phospho-histone H3
PBS	Phosphate-buffered saline
Plk1	*Polo-like kinase1*
PMSF	Phenylmethylsulfonylfluorid
Pmyo	Phospho-Myosin II
pYAP	Phospho-yes-associated protein
Ptf1a	*Pancreatic transcription factor 1*
qRT-PCR	quantitative reverse transcription PCR
R	Reverse
RA	Retinoic acid
Rac1	Ras-related C3 botulinum toxin substrate 1
RBPJ	Recombination signal binding protein for immunoglobulin kappa J
RDB-GST	Rho-binding domain of the Rhotekin fused to GST
RhoA	Ras homolog gene family member A
RhoGAP	RhoGTPase-activating protein
RNA	Ribonucleic acid
ROCK	Rho kinase
rpm	Rotations per minute
RT	Room temperature
SAM	Sterile alpha motif
SDHA	Succinate dehydrogenase complex, subunit A
SDS	Sodium dodecyl sulphate
SDS-PAGE	Sodium dodecyl sulfate polyacrylamide gel electrophoresis
sec	seconds
SEM	Standard error of the mean
sFRP1	Secreted frizzled-related protein 1
Shh	*Sonic hedgehog*
SM	Self-made
SMG	Submandibular salivary gland
Sox9	*SRY (sex determining region Y)-box 9*
Srf	*Serum response factor*
SSC	Saline sodium citrate
Stard13	*Steroidogenic acute regulatory protein-related lipid transfer (START) domain containing protein 13*
$Stard13^{\Delta/\Delta}$	Mice with ubiquitous homozygous ablation of *Stard13*
$Stard13^{lox/lox}$	Floxed *Stard13* homozygous mice
$Stard13^{PA\text{-}deleted}$	Mice with homozygous ablation of *Stard13* only in the pancreas
STARD13-FL	Full length STARD13
STARD13-Nterm	N-terminal fragment of STARD13
START	StAR-related lipid transfer
Tcf2	*Transcription factor 2*
TBS	Tris-buffered saline
TEM	Transmission electron microscopy
TEMED	N, N, N', N'-Tetra-methylethylenediamine
TGFβ	*Transforming growth factor β*
Tris	Tris-(hydroxymethyl) aminoethane
tRNA	transfer RNA
TUNEL	TdT-mediated dUTP-biotin nick end labeling
Vcl	*Vinculin*
VEGF-A	Vascular endothelial growth factor A
Vg1RBP	Vg1-RNA binding protein
vp	Ventral pancreas
vs.	Versus
WB	Western blot

Wnt	Wingless/Integration
WT	Wildtype
X-Gal	5-bromo-4-chloro-indolyl-β-D-galactopyranoside
YAP	Yes-associated protein
ZA	Zonula adherens
ZO	Zonula occludens

Bibliography

1 Slack JM. Developmental biology of the pancreas. Development (Cambridge, England). 1995 Jun 1;121(6):1569-80.

2 Villasenor A, Chong DC, Henkemeyer M, Cleaver O. Epithelial dynamics of pancreatic branching morphogenesis. Development (Cambridge, England). 2010 Dec 1;137(24):4295-305.

3 Gittes GK. Developmental biology of the pancreas: a comprehensive review. 2009 Feb 1:4-35.

4 Spagnoli FM. From endoderm to pancreas: a multistep journey. Cellular and molecular life sciences : CMLS. 2007 Sep 1;64(18):2378-90.

5 Pictet RL, Clark WR, Williams RH, Rutter WJ. An ultrastructural analysis of the developing embryonic pancreas. 1972 Dec 1:436-67.

6 Puri S, Hebrok M. Cellular plasticity within the pancreas--lessons learned from development. Developmental Cell. 2010 Mar 16:342-56.

7 Pan FC, Wright C. Pancreas organogenesis: from bud to plexus to gland. 2011 Mar 1:530-65.

8 Lammert E, Cleaver O, Melton D. Induction of pancreatic differentiation by signals from blood vessels. Science (New York, NY). 2001 Oct 19;294(5542):564-7.

9 Edlund H. Pancreatic organogenesis--developmental mechanisms and implications for therapy. 2002 Jul 1:524-32.

10 Jiang G, Zhang BB. Glucagon and regulation of glucose metabolism. American journal of physiology Endocrinology and metabolism. 2003 Apr 1;284(4):E671-8.

11 Roach PJ, Depaoli-Roach AA, Hurley TD, Tagliabracci VS. Glycogen and its metabolism: some new developments and old themes. The Biochemical journal. 2012 Feb 1;441(3):763-87.

12 Promeet D, Rogers K. Encyclopædia Britannica Online. [Internet]. 2007 [cited 2012 June 21]. Available from: http://www.britannica.com/EBchecked/media/101913/The-islets-of-Langerhans-are-responsible-for-the-endocrine-function.

13 Bell GI, Polonsky KS. Diabetes mellitus and genetically programmed defects in beta-cell function. Nature. 2001 Dec 13;414(6865):788-91.

14 Fajans SS, Bell GI, Polonsky KS. Molecular mechanisms and clinical pathophysiology of maturity-onset diabetes of the young. The New England journal of medicine. 2001 Sep 27;345(13):971-80.

15 Efrat S. Cell replacement therapy for type 1 diabetes. Trends in molecular medicine. 2002 Jul 1;8(7):334-39.

16 Gu G, Dubauskaite J, Melton DA. Direct evidence for the pancreatic lineage: NGN3+ cells are islet progenitors and are distinct from duct progenitors. 2002 May 1:2447-57.

17 Kawaguchi Y, Cooper B, Gannon M, Ray M, MacDonald RJ, Wright CVE. The role of the

transcriptional regulator Ptf1a in converting intestinal to pancreatic progenitors. Nature genetics. 2002 Sep 1;32(1):128-34.

18 Akiyama H, Kim JE, Nakashima K, Balmes G, Iwai N, Deng JM, Zhang Z, Martin JF, Behringer RR, Nakamura T, et al. Osteo-chondroprogenitor cells are derived from Sox9 expressing precursors. Proceedings of the National Academy of Sciences of the United States of America. 2005 Oct 11;102(41):14665-70.

19 Solar M, Cardalda C, Houbracken I, Martin M, Maestro MA, Medts ND, Xu X, Grau V, Heimberg H, Bouwens L, et al. Pancreatic Exocrine Duct Cells Give Rise to Insulin-Producing β Cells during Embryogenesis but Not after Birth. Developmental cell. 2009 Jan 12;17(6):849-860.

20 Hick AC, van Eyll JM, Cordi S, Forez C, Passante L, Kohara H, Nagasawa T, Vanderhaeghen P, Courtoy PJ, Rousseau GG, et al. Mechanism of primitive duct formation in the pancreas and submandibular glands: a role for SDF-1. 2009 Jan 1:66.

21 Zhou Q, Law AC, Rajagopal J, Anderson WJ, Gray PA, Melton DA. A multipotent progenitor domain guides pancreatic organogenesis. Developmental cell. 2007 Jan 1;13(1):103-114.

22 Gradwohl G, Dierich A, LeMeur M, Guillemot F. neurogenin3 is required for the development of the four endocrine cell lineages of the pancreas. Proceedings of the National Academy of Sciences of the United States of America. 2000 Feb 15;97(4):1607-11.

23 Schwitzgebel VM, Scheel DW, Conners JR, Kalamaras J, Lee JE, Anderson DJ, Sussel L, Johnson JD, German MS. Expression of neurogenin3 reveals an islet cell precursor population in the pancreas. Development (Cambridge, England). 2000 Aug 1;127(16):3533-42.

24 Horb LD, Slack JM. Role of cell division in branching morphogenesis and differentiation of the embryonic pancreas. 2000 Oct 1:791-6.

25 Stanger BZ, Tanaka AJ, Melton DA. Organ size is limited by the number of embryonic progenitor cells in the pancreas but not the liver. Nature. 2007 Feb 22;445(7130):886-91.

26 Jørgensen MC, Ahnfelt-Rønne J, Hald J, Madsen OD, Serup P, Hecksher-Sørensen J. An illustrated review of early pancreas development in the mouse. Endocrine reviews. 2007 Oct 1;28(6):685-705.

27 Rukstalis JM, Habener JF. Snail2, a mediator of epithelial-mesenchymal transitions, expressed in progenitor cells of the developing endocrine pancreas. Gene expression patterns : GEP. 2007 Feb 1;7(4):471-9.

28 Gouzi M, Kim YH, Katsumoto K, Johansson K, Grapin-Botton A. Neurogenin3 initiates stepwise delamination of differentiating endocrine cells during pancreas development. Developmental dynamics : an official publication of the American Association of Anatomists. 2011 Mar 1;240(3):589-604.

29 Kumar M, Melton D. Pancreas specification: a budding question. Current opinion in genetics & development. 2003 Aug 1;13(4):401-7.

30 Oström M, Loffler KA, Edfalk S, Selander L, Dahl U, Ricordi C, Jeon J, Correa-Medina M, Diez J, Edlund H. Retinoic acid promotes the generation of pancreatic

endocrine progenitor cells and their further differentiation into beta-cells. PloS one. 2008 Jan 1;3(7):e2841.

31 Hebrok M, Kim SK, Melton DA. Notochord repression of endodermal Sonic hedgehog permits pancreas development. Genes & development. 1998 Jun 1;12(11):1705-13.

32 Murtaugh LC, Stanger BZ, Kwan KM, Melton DA. Notch signaling controls multiple steps of pancreatic differentiation. Proceedings of the National Academy of Sciences of the United States of America. 2003 Dec 9;100(25):14920-5.

33 Deutsch G, Jung J, Zheng M, Lóra J, Zaret KS. A bipotential precursor population for pancreas and liver within the embryonic endoderm. Development (Cambridge, England). 2001 Mar 1;128(6):871-81.

34 Rossi JM, Dunn NR, Hogan BL, Zaret KS. Distinct mesodermal signals, including BMPs from the septum transversum mesenchyme, are required in combination for hepatogenesis from the endoderm. Genes & development. 2001 Aug 1;15(15):1998-2009.

35 Spagnoli FM, Brivanlou AH. The Gata5 target, TGIF2, defines the pancreatic region by modulating BMP signals within the endoderm. Development (Cambridge, England). 2008 Feb 1;135(3):451-61.

36 Apelqvist A, Li H, Sommer L, Beatus P, Anderson DJ, Honjo T, Hrabe de Angelis M, Lendahl U, Edlund H. Notch signalling controls pancreatic cell differentiation. Nature. 1999 Aug 26;400(6747):877-81.

37 Fujikura J, Hosoda K, Iwakura H, Tomita T, Noguchi M, Masuzaki H, Tanigaki K, Yabe D, Honjo T, Nakao K. Notch/Rbp-j signaling prevents premature endocrine and ductal cell differentiation in the pancreas. Cell metabolism. 2006 Jan 1;3(1):59-65.

38 Jensen J, Pedersen EE, Galante P, Hald J, Heller RS, Ishibashi M, Kageyama R, Guillemot F, Serup P, Madsen OD. Control of endodermal endocrine development by Hes-1. Nature genetics. 2000 Jan 1;24(1):36-44.

39 Jonsson J, Carlsson L, Edlund T, Edlund H. Insulin-promoter-factor 1 is required for pancreas development in mice. Nature. 1994 Oct 13;371(6498):606-9.

40 Stoffers DA, Zinkin NT, Stanojevic V, Clarke WL, Habener JF. Pancreatic agenesis attributable to a single nucleotide deletion in the human IPF1 gene coding sequence. Nature genetics. 1997 Jan 1;15(1):106-10.

41 Offield MF, Jetton TL, Labosky PA, Ray M, Stein RW, Magnuson MA, Hogan BL, Wright CV. PDX-1 is required for pancreatic outgrowth and differentiation of the rostral duodenum. Development (Cambridge, England). 1996 Mar 1;122(3):983-95.

42 Afelik S, Chen Y, Pieler T. Combined ectopic expression of Pdx1 and Ptf1a/p48 results in the stable conversion of posterior endoderm into endocrine and exocrine pancreatic tissue. Genes & development. 2006 Jun 1;20(11):1441-6.

43 Burlison JS, Long Q, Fujitani Y, Wright CVE, Magnuson MA. Pdx-1 and Ptf1a concurrently determine fate specification of pancreatic multipotent progenitor cells. Developmental biology. 2008 Apr 1;316(1):74-86.

44 Lioubinski O, Müller M, Wegner M, Sander M. Expression of Sox transcription factors in the developing mouse pancreas. Developmental dynamics : an official publication

of the American Association of Anatomists. 2003 Jul 1;227(3):402-8.

45 Seymour PA, Freude KK, Tran MN, Mayes EE, Jensen J, Kist R, Scherer G, Sander M. SOX9 is required for maintenance of the pancreatic progenitor cell pool. Proceedings of the National Academy of Sciences of the United States of America. 2007 Feb 6;104(6):1865-70.

46 Jensen J. Gene regulatory factors in pancreatic development. Developmental Dynamics. 2004 Jan 1;229(1):176-200.

47 Haumaitre C, Barbacci E, Jenny M, Ott MO, Gradwohl G, Cereghini S. Lack of TCF2/vHNF1 in mice leads to pancreas agenesis. Proceedings of the National Academy of Sciences of the United States of America. 2005 Feb 1;102(5):1490-5.

48 Hogan BLM, Kolodziej PA. Organogenesis: molecular mechanisms of tubulogenesis. Nature reviews Genetics. 2002 Jul 1;3(7):513-23.

49 Lu P, Werb Z. Patterning mechanisms of branched organs. Science (New York, NY). 2008 Dec 5;322(5907):1506-9.

50 Affolter M, Zeller R, Caussinus E. Tissue remodelling through branching morphogenesis. Nature reviews Molecular cell biology. 2009 Dec 1;10(12):831-42.

51 Daley WP, Kohn JM, Larsen M. A focal adhesion protein-based mechanochemical checkpoint regulates cleft progression during branching morphogenesis. Developmental dynamics : an official publication of the American Association of Anatomists. 2011 Sep 1;240(9):2069-83.

52 Wan X, Li Z, Lubkin SR. Mechanics of mesenchymal contribution to clefting force in branching morphogenesis. Biomechanics and Modeling in Mechanobiology. 2008 Oct 28;7(5):417-426.

53 Bryant DM, Mostov KE. From cells to organs: building polarized tissue. Nature reviews Molecular cell biology. 2008 Nov 1;9(11):887-901.

54 Andrew DJ, Ewald AJ. Morphogenesis of epithelial tubes: Insights into tube formation, elongation, and elaboration. Developmental biology. 2010 May 1;341(1):34-55.

55 Metzger RJ, Klein OD, Martin GR, Krasnow MA. The branching programme of mouse lung development. Nature. 2008 Jun 5;453(7196):745-50.

56 Watanabe T, Constantini F. Real-time analysis of ureteric bud branching morphogenesis in vitro. Developmental biology. 2004 Jan 1;271.

57 Onodera T, Sakai T, Hsu JCf, Matsumoto K, Chiorini JA, Yamada KM. Btbd7 regulates epithelial cell dynamics and branching morphogenesis. Science (New York, NY). 2010 Jul 30;329(5991):562-5.

58 McNeill H. Planar cell polarity and the kidney. Journal of the American Society of Nephrology : JASN. 2009 Oct 1;20(10):2104-11.

59 Xu K, Cleaver O. Tubulogenesis during blood vessel formation. Seminars in cell & developmental biology. 2011 May 20.

60 Bagnat M, Cheung ID, Mostov KE, Stainier DYR. Genetic control of single lumen formation in the zebrafish gut. Nature cell biology. 2007 Aug 1;9(8):954-60.

61 Lubkin SR. Branched organs: mechanics of morphogenesis by multiple mechanisms. Current topics in developmental biology. 2008 Jan 1;81:249-68.

62 Sawyer JM, Harrell JR, Shemer G, Sullivan-Brown J, Roh-Johnson M, Goldstein B. Apical constriction: A cell shape change that can drive morphogenesis. Developmental biology. 2010 May 1;341(1):5-19.

63 Wang Q, Uhlirova M, Bohmann D. Spatial restriction of FGF signaling by a matrix metalloprotease controls branching morphogenesis. Developmental cell. 2010 Jan 19;18(1):157-64.

64 Puklin-Faucher E, Sheetz MP. The mechanical integrin cycle. 2009 Jan 15:179-86.

65 Harburger DS, Calderwood DA. Integrin signalling at a glance. Journal of cell science. 2009 Jan 15;122(Pt 2):159-63.

66 Machesky LM, Hall A. Role of actin polymerization and adhesion to extracellular matrix in Rac- and Rho-induced cytoskeletal reorganization. The Journal of Cell Biology. 1997 Aug 25;138(4):913-26.

67 Pozzi A, Zent R. Extracellular matrix receptors in branched organs. Current opinion in cell biology. 2011 Oct 1;23(5):547-53.

68 Puri S, Hebrok M. Dynamics of embryonic pancreas development using real-time imaging. 2007 Jun 1:82-93.

69 Kesavan G, Sand FW, Greiner TU, Johansson JK, Kobberup S, Wu X, Brakebusch C, Semb H. Cdc42-mediated tubulogenesis controls cell specification. 2009 Nov 13:791-801.

70 Zallen JA, Blankenship JT. Multicellular dynamics during epithelial elongation. Seminars in cell & developmental biology. 2008 Jun 1;19(3):263-70.

71 Petzold KM, Naumann H, Spagnoli FM. Rho signaling restriction by the RhoGAP Stard13 integrates growth and morphogenesis in the pancreas. DEVELOP_2012_082701v1.

72 Harris TJC, Tepass U. Adherens junctions: from molecules to morphogenesis. Nature reviews Molecular cell biology. 2010 Jul 1;11(7):502-14.

73 De Arcangelis A, Mark M, Kreidberg J, Sorokin L, Georges-Labouesse E. Synergistic activities of alpha3 and alpha6 integrins are required during apical ectodermal ridge formation and organogenesis in the mouse. Development (Cambridge, England). 1999 Sep 1;126(17):3957-68.

74 Jiang FX, Harrison LC. Extracellular signals and pancreatic beta-cell development: a brief review. 2002 Dec 1:763-70.

75 Bombardelli L, Carpenter ES, Wu AP, Alston N, DelGiorno KE, Crawford HC. Pancreas-specific ablation of beta1 integrin induces tissue degeneration by disrupting acinar cell polarity. Gastroenterology. 2010 Jun 1;138(7):2531-40, 2540.e1-4.

76 Van Aelst L, Symons M. Role of Rho family GTPases in epithelial morphogenesis. Genes & development. 2002 May 1;16(9):1032-54.

77 Etienne-Manneville S, Hall A. Rho GTPases in cell biology. 2002 Dec 12:629-35.

78 Greiner TU, Kesavan G, Ståhlberg A, Semb H. Rac1 regulates pancreatic islet morphogenesis. BMC developmental biology. 2009 Jan 1;9:2.

79 Tcherkezian J, Lamarche-Vane N. Current knowledge of the large RhoGAP family of proteins. Biology of the cell / under the auspices of the European Cell Biology Organization. 2007 Feb 1;99(2):67-86.

80 Soriano P. Generalized lacZ expression with the ROSA26 Cre reporter strain. Nature genetics. 1999 Jan 1;21(1):70-1.

81 Alpy F, Tomasetto C. Give lipids a START: the StAR-related lipid transfer (START) domain in mammals. Journal of cell science. 2005 Jul 1;118(Pt 13):2791-801.

82 Xu K, Chong DC, Rankin SA, Zorn AM, Cleaver O. Rasip1 is required for endothelial cell motility, angiogenesis and vessel formation. Developmental biology. 2009 May 15;329(2):269-79.

83 Spagnoli FM, Brivanlou AH. The RNA-binding protein, Vg1RBP, is required for pancreatic fate specification. Developmental biology. 2006 Apr 15;292(2):442-56.

84 Ng DCH, Chan SF, Kok KH, Yam JWP, Ching YP, Ng IOL, Jin DY. Mitochondrial targeting of growth suppressor protein DLC2 through the START domain. FEBS letters. 2006 Jan 9;580(1):191-8.

85 Leung THY, Ching YP, Yam JWP, Wong CM, Yau TO, Jin DY, Ng IOL. Deleted in liver cancer 2 (DLC2) suppresses cell transformation by means of inhibition of RhoA activity. 2005 Oct 18:15207-12.

86 Xue W, Krasnitz A, Lucito R, Sordella R, Vanaelst L, Cordon-Cardo C, Singer S, Kuehnel F, Wigler M, Powers S, et al. DLC1 is a chromosome 8p tumor suppressor whose loss promotes hepatocellular carcinoma. Genes & development. 2008 Jun 1;22(11):1439-44.

87 Yau TO, Leung THY, Lam S, Cheung OF, Tung EKK, Khong PL, Lam A, Chung S, Ng IOL. Deleted in liver cancer 2 (DLC2) was dispensable for development and its deficiency did not aggravate hepatocarcinogenesis. PloS one. 2009 Jan 1;4(8):e6566.

88 Ching YP, Wong CM, Chan SF, Leung THY, Ng DCH, Jin DY, Ng IOL. Deleted in liver cancer (DLC) 2 encodes a RhoGAP protein with growth suppressor function and is underexpressed in hepatocellular carcinoma. The Journal of biological chemistry. 2003 Mar 21;278(12):10824-30.

89 Nagaraja GM, Kandpal RP. Chromosome 13q12 encoded Rho GTPase activating protein suppresses growth of breast carcinoma cells, and yeast two-hybrid screen shows its interaction with several proteins. Biochemical and biophysical research communications. 2004 Jan 16;313(3):654-65.

90 Kawai K, Seike Ji, Iino T, Kiyota M, Iwamae Y, Nishitani H, Yagisawa H. START-GAP2/DLC2 is localized in focal adhesions via its N-terminal region. 2009 Mar 20:736-41.

91 Kawai K, Iwamae Y, Yamaga M, Kiyota M, Ishii H, Hirata H, Homma Y, Yagisawa H. Focal adhesion-localization of START-GAP1/DLC1 is essential for cell motility and morphology. Genes to cells : devoted to molecular & cellular mechanisms. 2009 Feb 1;14(2):227-41.

92 Kim CA, Bowie JU. SAM domains: uniform structure, diversity of function. Trends in biochemical sciences. 2003 Dec 1;28(12):625-8.

93 Schultz J, Ponting CP, Hofmann K, Bork P. SAM as a protein interaction domain involved in developmental regulation. Protein science : a publication of the Protein Society. 1997 Jan 1;6(1):249-53.

94 Barrera FN, Poveda JA, González-Ros JM, Neira JL. Binding of the C-terminal sterile alpha motif (SAM) domain of human p73 to lipid membranes. The Journal of biological chemistry. 2003 Nov 21;278(47):46878-85.

95 Thorsell AG, Lee WH, Persson C, Siponen MI, Nilsson M, Busam RD, Kotenyova T, Schüler H, Lehtiö L. Comparative Structural Analysis of Lipid Binding START Domains. PloS one. 2011 Jan 1;6(6):e19521.

96 Ligeti E, Dagher MC, Hernandez SE, Koleske AJ, Settleman J. Phospholipids can switch the GTPase substrate preference of a GTPase-activating protein. The Journal of biological chemistry. 2004 Feb 13;279(7):5055-8.

97 Schwenk F, Baron U, Rajewsky K. A cre-transgenic mouse strain for the ubiquitous deletion of loxP-flanked gene segments including deletion in germ cells. Nucleic acids research. 1995 Dec 25;23(24):5080-1.

98 Lammert E, Brown J, Melton DA. Notch gene expression during pancreatic organogenesis. Mechanisms of development. 2000 Jun 1;94(1-2):199-203.

99 Blanpain C, Fuchs E. p63: revving up epithelial stem-cell potential. Nature cell biology. 2007 Jul 1;9(7):731-3.

100 Kopinke D, Brailsford M, Shea JE, Leavitt R, Scaife CL, Murtaugh LC. Lineage tracing reveals the dynamic contribution of Hes1+ cells to the developing and adult pancreas. Development (Cambridge, England). 2011 Feb 1;138(3):431-41.

101 Barbieri CE, Pietenpol JA. p63 and epithelial biology. Experimental cell research. 2006 Apr 1;312(6):695-706.

102 Senoo M, Pinto F, Crum CP, McKeon F. p63 Is essential for the proliferative potential of stem cells in stratified epithelia. Cell. 2007 May 4;129(3):523-36.

103 Mills AA, Zheng B, Wang XJ, Vogel H, Roop DR, Bradley A. p63 is a p53 homologue required for limb and epidermal morphogenesis. Nature. 1999 Apr 22;398(6729):708-13.

104 Yang A, Schweitzer R, Sun D, Kaghad M, Walker N, Bronson RT, Tabin C, Sharpe A, Caput D, Crum C, et al. p63 is essential for regenerative proliferation in limb, craniofacial and epithelial development. Nature. 1999 Apr 22;398(6729):714-8.

105 Koster MI, Kim S, Mills AA, DeMayo FJ, Roop DR. p63 is the molecular switch for initiation of an epithelial stratification program. Genes & development. 2004 Jan 15;18(2):126-31.

106 Carroll DK, Carroll JS, Leong CO, Cheng F, Brown M, Mills AA, Brugge JS, Ellisen LW. p63 regulates an adhesion programme and cell survival in epithelial cells. Nature cell biology. 2006 Jun 1;8(6):551-61.

107 Basturk O, Khanani F, Sarkar F, Levi E, Cheng JD, Adsay NV. DeltaNp63 expression in pancreas and pancreatic neoplasia. Modern pathology : an official journal of the

United States and Canadian Academy of Pathology, Inc. 2005 Sep 1;18(9):1193-8.

108 Casanova ML, Bravo A, Ramírez A, Morreale de Escobar G, Were F, Merlino G, Vidal M, Jorcano JL. Exocrine pancreatic disorders in transsgenic mice expressing human keratin 8. The Journal of clinical investigation. 1999 Jun 1;103(11):1587-95.

109 Magenheim J, Ilovich O, Lazarus A, Klochendler A, Ziv O, Werman R, Hija A, Cleaver O, Mishani E, Keshet E, et al. Blood vessels restrain pancreas branching, differentiation and growth. Development (Cambridge, England). 2011 Nov 1;138(21):4743-52.

110 Pierreux CE, Cordi S, Hick AC, Achouri Y, Ruiz de Almodovar C, Prévot PP, Courtoy PJ, Carmeliet P, Lemaigre FP. Epithelial: Endothelial cross-talk regulates exocrine differentiation in developing pancreas. Developmental biology. 2010 Nov 1;347(1):216-27.

111 Lammert E, Cleaver O, Melton D. Role of endothelial cells in early pancreas and liver development. Mechanisms of development. 2003 Jan 1;120(1):59-64.

112 Lammert E, Gu G, McLaughlin M, Brown D, Brekken R, Murtaugh LC, Gerber HP, Ferrara N, Melton DA. Role of VEGF-A in vascularization of pancreatic islets. Current biology : CB. 2003 Jun 17;13(12):1070-4.

113 Petzold K, Spagnoli F. A system for ex vivo culturing of embryonic pancreas. Journal of visualized experiments. Journal of Visualized Experiments. 2012 Aug 27;(66),e3979.

114 Malliri A, Klooster J, Olivio C. Determination of the activity of Rho-like GTPases in cells. 2002 Jan 1.

115 Cascone I, Audero E, Giraudo E, Napione L, Maniero F, Philips MR, Collard JG, Serini G, Bussolino F. Tie-2-dependent activation of RhoA and Rac1 participates in endothelial cell motility triggered by angiopoietin-1. Blood. 2003 Oct 1;102(7):2482-90.

116 Bhushan A, Itoh N, Kato S, Thiery JP, Czernichow P, Bellusci S, Scharfmann R. Fgf10 is essential for maintaining the proliferative capacity of epithelial progenitor cells during early pancreatic organogenesis. Development (Cambridge, England). 2001 Dec 1;128(24):5109-17.

117 Corson LB, Yamanaka Y, Lai KMV, Rossant J. Spatial and temporal patterns of ERK signaling during mouse embryogenesis. Development (Cambridge, England). 2003 Oct 1;130(19):4527-37.

118 Bain J, Plater L, Elliott M, Shpiro N, Hastie CJ, McLauchlan H, Klevernic I, Arthur JSC, Alessi DR, Cohen P. The selectivity of protein kinase inhibitors: a further update. The Biochemical journal. 2007 Dec 15;408(3):297-315.

119 Descot A, Hoffmann R, Shaposhnikov D, Reschke M, Ullrich A, Posern G. Negative Regulation of the EGFR-MAPK Cascade by Actin-MAL-Mediated Mig6/Errfi-1 Induction. 2009 Aug 14:291-304.

120 Posern G, Treisman R. Actin' together: serum response factor, its cofactors and the link to signal transduction. 2006 Nov 1:588-96.

121 Ferby I, Reschke M, Kudlacek O, Knyazev P, Pantè G, Amann K, Sommergruber W, Kraut N, Ullrich A, Fässler R, et al. Mig6 is a negative regulator of EGF receptor-mediated skin morphogenesis and tumor formation. 2006 May 1:568-73.

122 Dupont S, Morsut L, Aragona M, Enzo E, Giulitti S, Cordenonsi M, Zanconato F, Le Digabel J, Forcato M, Bicciato S, et al. Role of YAP/TAZ in mechanotransduction. 2011 Jun 9:179-83.

123 Wada KI, Itoga K, Okano T, Yonemura S, Sasaki H. Hippo pathway regulation by cell morphology and stress fibers. Development (Cambridge, England). 2011 Sep 1;138(18):3907-14.

124 Durkin ME, Avner MR, Huh CG, Yuan BZ, Thorgeirsson SS, Popescu NC. DLC-1, a Rho GTPase-activating protein with tumor suppressor function, is essential for embryonic development. FEBS letters. 2005 Feb 14;579(5):1191-6.

125 Iden S, Collard JG. Crosstalk between small GTPases and polarity proteins in cell polarization. Nature reviews Molecular cell biology. 2008 Nov 1;9(11):846-59.

126 Yamada S, Nelson WJ. Localized zones of Rho and Rac activities drive initiation and expansion of epithelial cell-cell adhesion. The Journal of Cell Biology. 2007 Jul 30;178(3):517-27.

127 Yu W, Shewan AM, Brakeman P, Eastburn DJ, Datta A, Bryant DM, Fan QW, Weiss WA, Zegers MMP, Mostov KE. Involvement of RhoA, ROCK I and myosin II in inverted orientation of epithelial polarity. EMBO reports. 2008 Sep 1;9(9):923-9.

128 St Johnston D, Ahringer J. Cell polarity in eggs and epithelia: parallels and diversity. Cell. 2010 May 28;141(5):757-74.

129 Brodu V, Casanova J. The RhoGAP crossveinless-c links trachealess and EGFR signaling to cell shape remodeling in Drosophila tracheal invagination. Genes & development. 2006 Jul 1;20(13):1817-28.

130 Denholm B, Brown S, Ray RP, Ruiz-Gómez M, Skaer H, Hombría JCG. crossveinless-c is a RhoGAP required for actin reorganisation during morphogenesis. Development (Cambridge, England). 2005 May 1;132(10):2389-400.

131 Nelson W. Remodeling epithelial cell organization: Transitions between Front–Rear and Apical–Basal polarity. Cold Spring Harbor Perspectives in Biology. 2009 Jan 1.

132 Runswick SK, O'Hare MJ, Jones L, Streuli CH, Garrod DR. Desmosomal adhesion regulates epithelial morphogenesis and cell positioning. Nature cell biology. 2001 Sep 1;3(9):823-30.

133 Sahai E, Marshall CJ. RHO-GTPases and cancer. Nature reviews Cancer. 2002 Feb 1;2(2):133-42.

134 Fuchs E, Tumbar T, Guasch G. Socializing with the neighbors: stem cells and their niche. Cell. 2004 Mar 19;116(6):769-78.

135 Rawlins EL, Clark CP, Xue Y, Hogan BLM. The Id2+ distal tip lung epithelium contains individual multipotent embryonic progenitor cells. Development (Cambridge, England). 2009 Nov 1;136(22):3741-5.

136 Landsman L, Nijagal A, Whitchurch TJ, Vanderlaan RL, Zimmer WE, Mackenzie TC, Hebrok M. Pancreatic mesenchyme regulates epithelial organogenesis

throughout development. PLoS biology. 2011 Sep 1;9(9):e1001143.

137 Rutter WJ, Pictet RL, Morris PW. Toward molecular mechanisms of developmental processes. Annual review of biochemistry. 1973 Jan 1;42:601-46.

138 Legate KR, Wickström SA, Fässler R. Genetic and cell biological analysis of integrin outside-in signaling. Genes & development. 2009 Feb 15;23(4):397-418.

139 Li J, Wang J, Jiao H, Liao J, Xu X. Cytokinesis and cancer: Polo loves ROCK'n' Rho(A). Journal of Genetics and Genomics. 2010;37:159-172.

140 Piekney A, Werner M, Glotzer M. Cytokinesis: welcome to the Rho zone. TRENDS in Cell Biology. 2005;15(12):651-658.

141 Srinivasan L, Sasaki Y, Calado DP, Zhang B, Paik JH, DePinho RA, Kutok JL, Kearney JF, Otipoby KL, Rajewsky K. PI3 kinase signals BCR-dependent mature B cell survival. Cell. 2009 Oct 30;139(3):573-86.

142 Aman A, Piotrowski T. Cell migration during morphogenesis. Developmental biology. 2010 May 1;341(1):20-33.

143 Wansleeben C, Meijlink F. The planar cell polarity pathway in vertebrate development. Developmental dynamics : an official publication of the American Association of Anatomists. 2011 Mar 1;240(3):616-26.

144 Muzumdar MD, Tasic B, Miyamichi K, Li L, Luo L. A global double-fluorescent Cre reporter mouse. Genesis (New York, NY : 2000). 2007 Sep 1;45(9):593-605.

145 Valenzuela DM, Murphy AJ, Frendewey D, Gale NW, Economides AN, Auerbach W, Poueymirou WT, Adams NC. High-throughput engineering of the mouse genome coupled with high-resolution expression analysis. Nature Biotechnology. 2003 Jan 1.

146 Rodríguez C, Buchholz F, Galloway… J. High-efficiency deleter mice show that FLPe is an alternative to Cre-loxP. Nature genetics. 2000 Jan 1.

147 Zambrowicz BP, Imamoto A, Fiering S, Herzenberg LA, Kerr WG, Soriano P. Disruption of overlapping transcripts in the ROSA beta geo 26 gene trap strain leads to widespread expression of beta-galactosidase in mouse embryos and hematopoietic cells. Proceedings of the National Academy of Sciences of the United States of America. 1997 Apr 15;94(8):3789-94.

Selbstständigkeitserklärung

Hiermit erkläre ich, dass ich die vorliegende Arbeit selbstständing und nur unter Verwendung der angegebenen Hilfsmittel angefertigt habe. Diese Arbeit wurde in gleicher oder ähnlicher Form nicht in einer anderen Prüfungsbehörde vorgelegt. Die Promotionsordnung der Mathematisch-Naturwissenschaftlichen Fakultät I der Humboldt-Universität zu Berlin vom 06.07.2009 habe ich gelesen und akzeptiert.

Datum und Unterschrift